ORIGINAL ARTICLE

Engineering nanostructures of CuO-based photocatalysts for water treatment: Current progress and future challenges

Pankaj Raizada [a,b,*], **Anita Sudhaik** [a], **Shilpa Patial** [a], **Vasudha Hasija** [a], **Aftab Aslam Parwaz Khan** [c,d], **Pardeep Singh** [a,b], **Sourav Gautam** [e], **Manpreet Kaur** [e], **Van-Huy Nguyen** [f,*]

[a] School of Chemistry, Faculty of Basic Sciences, Shoolini University, Solan, HP 173229, India
[b] Himalayan Centre for Excellence in Nanotechnology, Shoolini University, Solan, HP 173229, India
[c] Center of Excellence for Advanced Materials Research, King Abdulaziz University, P.O. Box 80203, Jeddah 21589, Saudi Arabia
[d] Chemistry Department, Faculty of Science, King Abdulaziz University, P.O. Box 80203, Jeddah 21589, Saudi Arabia
[e] Department of Chemistry, School of Basic and Applied Sciences, Maharaj Agrasen University, H.P. 174103, India
[f] Institute of Research and Development, Duy Tan University, Da Nang 550000, Viet Nam

Abstract Nowadays, increasing extortions regarding environmental problems and energy scarcity have stuck the development and endurance of human society. The issue of inorganic and organic pollutants that exist in water from agricultural, domestic, and industrial activities has directed the development of advanced technologies to address the challenges of water scarcity efficiently. To solve this major issue, various scientists and researchers are looking for novel and effective technologies that can efficiently remove pollutants from wastewater. Nanoscale metal oxide materials have been proposed due to their distinctive size, physical and chemical properties along with promising applications. Cupric Oxide (CuO) is one of the most commonly used benchmark photocatalysts in photodegradation owing to the fact that they are cost-effective, non-toxic, and more efficient in absorption across a significant fraction of solar spectrum. In this review, we have summarized synthetic strategies of CuO fabrication, modification methods with applications for water treatment purposes. Moreover, an elaborative discussion on feasible strategies includes; binary and ternary heterojunction formation, Z-scheme based photocatalytic system, incorporation of rare earth/transition metal ions as dopants, and carbonaceous materials serving as a support system.

* Corresponding authors at: Duy Tan University, Da Nang 550000, Viet Nam (Van-Huy Nguyen); Shoolini University, Solan, HP 173229, India (Pankaj Raizada).
  E-mail addresses: pankajchem1@gmail.com (P. Raizada), nguyenvanhuy20@duytan.com.vn (V.-H. Nguyen).

The mechanistic insight inferring photo-induced charge separation and transfer, the functional reactive radical species involved in a photocatalytic reaction, have been successfully featured and examined. Finally, a conclusive remark regarding current studies and unresolved challenges related to CuO are put forth for future perspectives.

1. Introduction

In last few years, momentous efforts have been made to degrade micropollutants, containing persistent organic and inorganic pollutants, endocrine-disrupting chemicals, pharmaceuticals, etc. due to their low concentration but a high risk that is causing extensive damage to environments (Raizada et al., 2019a; Dutta et al., 2019a, 2019b). Water is an essential source of livelihood, but currently, the release of toxic non-biodegradable inorganic and organic compounds pollutants in water bodies has caused a scarcity of drinking water. It has become a danger to human health, ecological balance, and the development of commercial civilization with the development of industries (Brillas, 2014; Singh et al., 2019a). Almost two million tons of sewage, agricultural and industrial wastes are constantly released into water resulting in severe health problems and deaths of almost 14,000 humans every day (Singh et al., 2019b; Trujillo-Reyes et al., 2014). As a result, there is an urgent need to control water pollution; hence, numerous treatments have been introduced in progression (Raizada et al., 2017a, 2017b; Kumar et al., 2019a, 2019b). Numerous remediation technologies have been developed for the removal of contaminants, but efficient and economical wastewater treatment is still a challenge as its processes consume loads of energy, resulting in high treatment costs (Chandel et al., 2020; Hasija et al., 2020). Since past years many conventional techniques such as flocculation, coagulation, reverse osmosis, ion-exchange, adsorption, precipitation, membrane-filtration, chlorination, neutralization, photoelectrochemistry, sedimentation, etc., have been employed (Serpone and Emeline, 2012; Raizada et al., 2019b; Singh et al., 2014, 2019). These traditional techniques have some disadvantages, for instance, flocculation and coagulation used to remove insoluble compounds from water, need additional chemicals that could be undoubtedly toxic (Hoffmann et al., 1995; Sharma et al., 2019b). Similarly, membrane filtration and reverse osmosis eliminates the excess of anions and cations, but do not tend to remove other types of pollutants like solvents (phenolic and halogenated compounds, benzene, and pesticides) and organic pollutants (Konstantinou and Albanis, 2004; Raizada et al., 2019c). It is worth noting that methods mentioned above are limited by their high operating costs low energy-efficiency and sophisticated types of equipment requirement; therefore, development of novel techniques are immediately required which should be low cost, environment friendly and can efficiently remove pollutants from wastewater (Hasija et al., 2019b; Bouzaida et al., 2004).

Various studies have shown that advanced oxidation processes (AOPs) are efficient in the oxidation of several organic and inorganic pollutants coming from industrial effluents (Glaze, 1987; Raizada et al., 2019d). AOPs applied for water remediation are classified into different categories such as (i) hydroxyl radical based AOPs, (ii) UV/H_2O_2 (iii) $O_3/H_2O_2/UV$ (iv) $TiO_2/UV/H_2O_2$ photocatalysis, (v) Fenton (Fe^{2+}/H_2O_2) (vi) Photo-Fenton ($Fe^{2+}/UV/H_2O_2$) (vii) Sono-Fenton ($Fe^{2+}/US/H_2O_2$) (Deng et al., 2015; Sharma et al., 2019a). Through AOPs, in-situ production of energetic oxidizing agents, including hydroxyl radicals ($^{\cdot}OH$), superoxide anion radical ($^{\cdot}O_2^-$), and photoinduced charge carriers i.e., electrons and holes (e^-/h^+), caused effective degradation and mineralization of pollutants (Singh et al., 2013a, 2013b; Herrmann, 1999). With the growing demand for pollutant removal and energy concerns, photocatalysis for environmental treatment has received attention (Do et al., 2020; Li et al., 2018; Lu et al., 2016; Molinari et al., 2002; Nguyen et al., 2020a, 2020b, 2020c; Vu et al., 2020; Yu et al., 2016, 2017). It provides a good replacement for energy in-depth treatment methods making use of pollution-free and renewable solar energy. Photocatalysis is a process in which pollutants are oxidized into CO_2, H_2O, and other innocuous constituents. It permits one to utilize light for the acceleration of catalytic reactions and has acclaimed widely as the utmost favorable technique (Raizada et al., 2020). Implementation of process engineering strategies into photocatalysis pointed out that heterogeneous photocatalysis is most prominent due to higher stability, facile separation of products, and easier recyclability of the photocatalyst. Also, it involves photoinduced chemical reaction on the surface of semiconductor materials (photocatalyst) upon exposure to solar light (Shandilya et al., 2018a, 2018b; Sudhaik et al., 2018a). Photocatalyst with light exposure greater or equal to the energy of its bandgap causes electrons transference from the valence band (VB) to the conduction band (CB) leaving positive holes (h^+) in VB whereas, CB band edges accommodate negatives electrons without decomposing semiconductor (Patial et al., in press; Ameta et al., 2013). The photocatalytic mechanism proceeds reaction via photogenerated holes in VB by the oxidation process to generate $^{\cdot}OH$, and photogenerated electrons involve in the reduction process to generate hyperoxide or superoxide radicals (H_2O_2, $O_2^{-\cdot}/HO_2^{\cdot}$) (Fig. 1a).

Generally, semiconductors are known to be the most powerful photocatalysts because of their apt bandgap energies and distinct electronic configuration with occupied VB and unoccupied CB (Singh et al., 2019c). Semiconductors having to distinguish electronic, light absorption, charge transmission properties, and porous structure delivered anticipated activities for photocatalytic removal of various organic pollutants (Shandilya et al., 2019). Many semiconductors, i.e., TiO_2, $g-C_3N_4$, Fe_2O_3, CdS, Cu_2O and ZnO etc. (Sudhaik et al., 2018b), which are designed for environmental pollution mitigation and H_2 production from water splitting, owing to their unique, attractive properties. The mechanism of semiconductor-based photocatalysis (representing semiconductor photocatalyst with PC) is explained by following reaction steps:
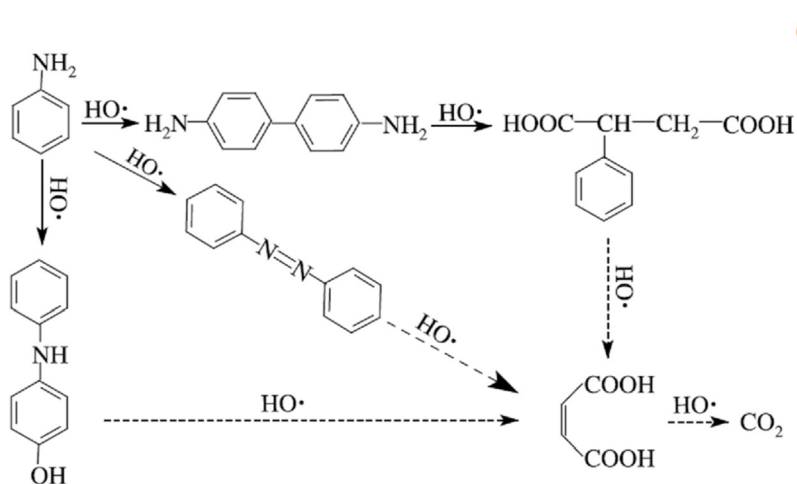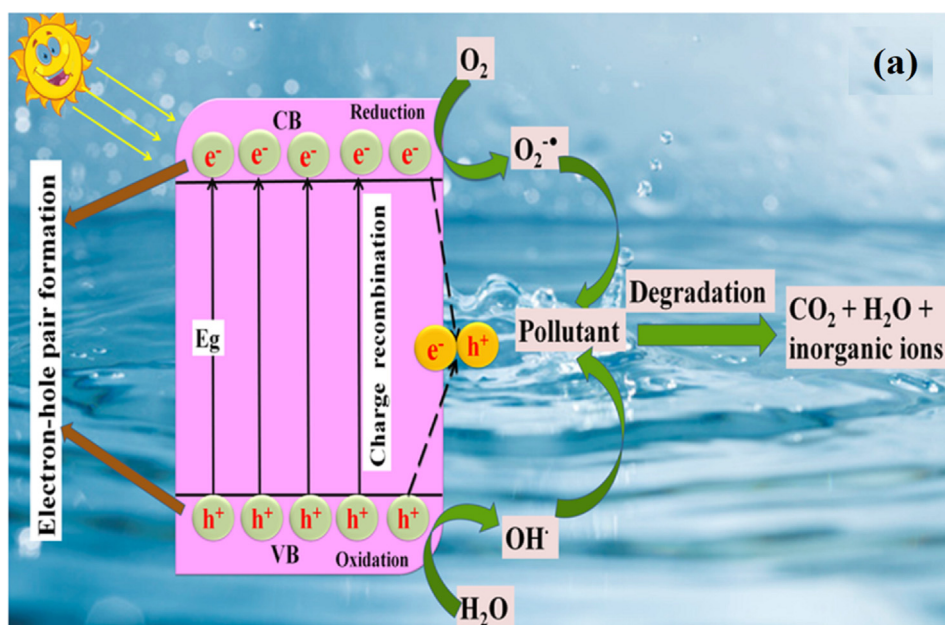
Fig. 1 (a) Mechanistic view of semiconductor photocatalyst for photodegradation in water, (b) Proposed reaction pathways for aniline degradation (Reprinted with permission from Ref. Li et al. (2003) and copyright with license Id. 4843541478931).

i. Charge-carrier formation:

$$PC + hv \rightarrow h_{VB}^+ + e_{CB}^- \qquad (1)$$
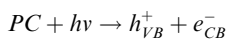
ii. Charge-carrier trapping:

$$h_{VB}^+ + PC\ (OH) \rightarrow \{PC\ OH\}^+ \qquad (2)$$
$$e_{CB}^- + PC\ (OH) \rightarrow \{PC\ OH\} \qquad (3)$$
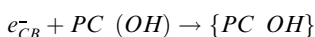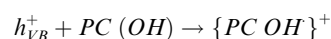
iii. Recombination of Charge-carrier:

$$h_{VB}^+ + PC\ (OH) \rightarrow \{PC\ OH\} + heat \qquad (4)$$
$$e_{CB}^- + \{PC\ OH\}^+ \rightarrow \{PC\ OH\} + heat \qquad (5)$$
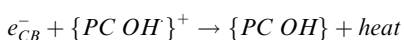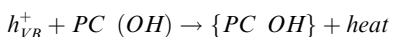
iv. Charge stimulation at the interface:

$$\{PC\ OH\} + Red. \rightarrow \{PC\ OH\} + Red.^{+} \qquad (6)$$
$$e_{CB}^- + O_X \rightarrow \{PCOH\} + O_X^- \qquad (7)$$
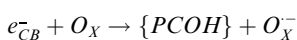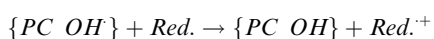
Here Ox and Red denote oxidant and reductant, respectively.

v. Metal ions reduced by e_{CB}^-, if present:

$$ne_{CB}^- + PC^{n+} \rightarrow PC^0 \qquad (8)$$
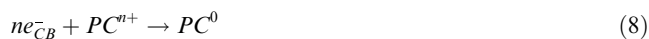
This fundamental mechanism effectively degrades persistent inorganic/organic pollutants in wastewater (Shandilya et al., 2018a, 2018b; Dutta et al., 2019a, 2019b). However, the only drawback associated with semiconductor photocatalyst is its corrosive nature, which could reduce photocatalysis efficacy. Photocatalysis in-situ generation is functional *via* reactive oxidant species (ROS) like ·OH, superoxide (·O_2^-), H_2O_2 etc. (Hasija et al., 2019a). ·OH radicals, the second most energetic high standard reduction potential after fluorine (E° = 3.0 V/SHE) is ·OH possessing E° (·OH/H_2O) = 2.80 V/SHE causing non-selective oxidation with most organics giving innocuous products (such as H_2O and CO_2) (Singh et al., 2018; Glaze, 1987).

Recently, transition metal oxides (TMOs) such as TiO_2, ZnO, MnO_2, SnO_2, CdS, WO_3, CuO etc., has gained significant attention from research communal due to their astonishing physical and chemical properties (Kabra et al., 2004; Suri et al., 2012). Titanium dioxide TiO_2 has been considered as one of the most noticeable photocatalysts since 1972, owing to low price, non-toxic nature, high activation, long-term stability, and easy availability (Fujishima and Honda, 1972; Sharma and Lee, 2016a). It is the most commonly used photocatalysts, but its bandgap (3.0–3.2 eV) is too wide to engross sunlight proficiently (Sharma and Lee, 2016b, 2017a). Another metal oxide, ZnO, is a well-known and well-discovered semiconductor with excellent chemical stability, biocompatibility, unique electronic structure, and low production cost (Sharma and Lee, 2017b, 2016c). It has been broadly used in the various energy conversion process as well as and in photocatalytic fields (Ong et al., 2018). However, it is also associated with some limitations such as wide bandgap, high photocorrosion when subjected to the irradiation, dissolved at acidic and alkaline solutions, and absorption in the UV region (Liu et al., 2013). Correspondingly, the development of visible-light-driven photocatalysts is highly required for the robust harvesting of light energy from the sun or any artificial visible-light sources. Therefore, numerous visible-light-driven novel nanomaterials (metal oxides) have been synthesized as photocatalysts having low bandgap to harvest maximum solar light (visible light) such as CuO (Liu et al., 2013), WO_3 (Hasija et al., 2019c), MnO_2 (Chen et al., 2012), etc. During the past 20 years, variant transition metal oxides (TMOs) materials have been studied as an efficient photocatalyst for degradation and in various other realms (Raizada et al., 2016). These metal oxides possess superior photodegradation activity under visible light irradiation.

1.1. CuO as photocatalyst

Among all metal oxides, cupric oxide (CuO) has been a hot research topic due to its remarkable properties as a p-type semiconductor with constricted band gap (1.2–2.0 eV) and as a basis of several high-temperature superconductors and giant magnetoresistance materials (Anandan and Yang, 2007; Li et al., 2012). CuO monoclinic crystal structure exhibits excellent physical and chemical properties such as large surface areas, proper redox potential, good electrochemical activity superthermal conductivity, and excellent stability in solutions (Narayanan and El-Sayed, 2005; Zhang et al., 2016). CuO constitutes of 3d and O 2p shell occupied by CB and VB edges with lower bandgap resulting in maximum ROS generation and maximum absorption of visible light even up to infrared region (Xu and Schoonen, 2000; Sun et al., 2019). CuO photocatalyst with 1.7 eV bandgap has 0.46 V and 2.16 V of CB and VB potential, respectively, which is more than standard redox potential as well as appropriate for the release of ˙OH and ˙O_2^- radicals, required for photodegradation (Kumar et al., 2014).

1.1.1. Pathways of pollutant removal reaction using CuO based photocatalyst

In the photodegradation process, when CuO based photocatalysts are placed under solar light, the generation of some electron-pairs takes place. In neutral/alkaline pH, released electrons reacted with O_2, which behaves as the final recipient of electrons, and O_2 was converted to O_2^- radicals (Ahmed et al., 2011) (Eqs. (9)–(16)). Norzaee et al. (2017) proposed a possible mechanism of aniline degradation by ˙OH and O_2^- as shown in Fig. 1b. From the Eqs. (9)–(16), it can be clearly witnessed that generated O_2^- and ˙OH radicals reacted with aniline pollutants and degraded it into the nontoxic product. Accordingly, aniline was degraded into intermediate compounds such as dianiline, 4-anilino phenol, and azobenzol. After that, the benzene ring of generated intermediate products was deboned by ˙OH radicals, and some low molecular weight compounds such as phenylsuccinic acid, maleic acid, and other organic compounds were generated (Li et al., 2003). Lastly, the latter compounds were degraded into nontoxic products (CO_2 and H_2O).

$$Photocatalyst + hv \rightarrow e_{CB}^- + h_{vB}^+ \tag{9}$$

$$H_2O + h_{vB}^+ \rightarrow OH^. + H^+ \tag{10}$$

$$h_{vB}^+ + OH^- \rightarrow OH^. \tag{11}$$

$$O_2 + e_{CB}^- \rightarrow O_2^{-.} \tag{12}$$

$$O_2^{-.} + H^+ \rightarrow HO_2^. \tag{13}$$

$$2HO_2^. \rightarrow O_2 + H_2O_2 \tag{14}$$

$$H_2O_2 \rightarrow 2OH^. \tag{15}$$

$$H_2O_2 + e^- \rightarrow OH^. + OH^- \tag{16}$$
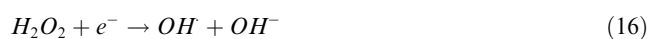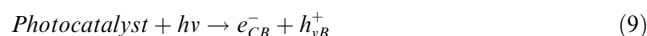
CuO has attracted considerable attention due to its favourable applications in different areas such as photocatalysis, catalysis, electrochemistry, sensors/biosensors, energy storage, antifouling coatings, and biocidal agents (Verma and Kumar, 2019). Besides this, CuO nanoparticles have revealed their application in pharmacological activity, especially in antitumor therapy. Furthermore, physical parameters such as shape, size, structure, and composition which could influence CuO nanostructure can be controlled, and by controlling these parameters, the photocatalytic activities of CuO can be modified to achieve efficient degradation of contaminants (Gusain and Khatri, 2013; Bhaduri and Kajal, 2019). Thus, CuO metal oxide has been proved to be an effective visible range active photocatalyst for photodegradation of contaminants without the addition of H_2O_2 (Hoffmann et al., 1995). Until now, variant advancement in CuO metal oxide photocatalysis for pollutant degradations has been growing over the last 20 years. However, only a few scattered reviews have been published in the literature on the application of CuO in photocatalysis (Zhang et al., 2014; Tran and Nguyen, 2014). Several other reviews have tended to focus on the synthesis and characterization of CuO NPs and their potential applications. To get the idea about overall published research reports, we access the "Scopus" site. From the "Scopus" database, the numbers of reports are 513, 346, and 229 by using keywords "CuO + photocatalyst", "CuO + photodegradation" and "CuO + water splitting", respectively. Overall reports on CuO as photocatalyst for photodegradation from 1996 to 2020 have been illustrated in (Fig. 2a). The given pie chart illustrates diverse photoactive applications of CuO metal oxide-based photocatalyst and the percentage of variant advancement for CuO (Fig. 2b).

CuO has many excellent physical and chemical properties such as high thermal/electrical conductivity, high mechanical strength, high-temperature durability, large surface areas, proper redox potential, good electrochemical activity and excellent stability in solutions which make it an efficient candidate in various fields. Most of the review articles have focused on 1D CuO nanostructures only (Li et al., 2012; Filipič and Cvelbar, 2012), and limited reports have described synthesis techniques implemented for CuO nanocomposite formation with the incorporation of their associated applications (Anandan and Yang, 2007). Till now, very few review articles have been published on the organized introduction of recent advancements in various CuO nanostructures to improve its properties. This article offers a comprehensive review of systemic discussion on the structural and fundamental properties of CuO with its potential applications. The review begins with a description of commonly used different synthetic strategies in consort with the synthesis process. For each synthetic method, several published research articles based on CuO have been cited, and their synthesis route has been conferred. In the same way, diverse modification techniques such as binary and ternary heterojunction formation, Z-scheme based photocatalytic system, incorporation of rare earth/transition metal ions as dopants, and coupling with carbonaceous materials (support system) have been elaborately discussed with its promising applications in wastewater treatment purposes. In the abovementioned different modification techniques, various nanocomposite formations of CuO photocatalysts with other photocatalysts have been discussed. We have focussed on distinct engineering strategies to increase the photocatalytic activity of CuO in pollutant degradation as well as we have also discussed how these strategies affect photocatalytic activities of these photocatalyst systems. We have briefly reported the preparation of CuO NPs and modification to overcome limitations of CuO by binary and ternary heterojunction formation, Z-scheme based photocatalyst, and carbonaceous supported materials. Recent developments in the applications of various

CuO nanostructures are also reviewed. This present discussion will be helpful for promising selections of photocatalysts on the basis of their presented interesting properties and applications. In particular, focus on the fundamental properties and various heterostructure forms of CuO along with perspectives will be beneficial in terms of future research on the development of CuO nanostructures.

1.2. Optical, electrical and structural properties of CuO

The bandgap of semiconducting material plays an essential role in exploring optical properties. Optical properties of CuO photocatalysts in the absorption region are mainly conquered by the absorption edge well-defined by bandgap. CuO nanomaterials exhibit a remarkable property as control of potential energy levels of CBs and VBs along with bandgap through altering the size and shape of CuO. Nanostructured CuO band gap is blue-shifted than bulk CuO i.e. lower bandgap with reported values usually ranging from 1.2 eV to 2.1 eV (Zhang et al., 2014). Some other studies have also stated a wider bandgap of CuO up to 4.13 eV and 3.02 eV for 10 nm quantum dots and well-arranged CuO nanoplatelets, respectively (Yang et al., 2011). Consequently, CuO photocatalyst shows strong absorption in the visible spectrum with a little transparency for wider bandgap nanostructured samples of CuO exhibiting absorption in the UV region. Prominently, CuO photocatalyst optical properties are intensely reliant on sample preparation as well as the techniques used for measurement with test temperature. Raman spectroscopy is a characterization technique used to explore the optical properties of nanoscale materials due to its sensitive examination to native atomic arrangements and vibrations of nanomaterials. CuO has a monoclinic structure with the C_{2h}^6 of space group and displays three acoustic modes (Au + 2Bu), six IR-active approaches (3Au + 3Bu), and three Raman-active modes (Ag + 2Bg) (Sathiya et al., 2017). Some structural properties, such as grain size, grain boundary, film thickness, specific
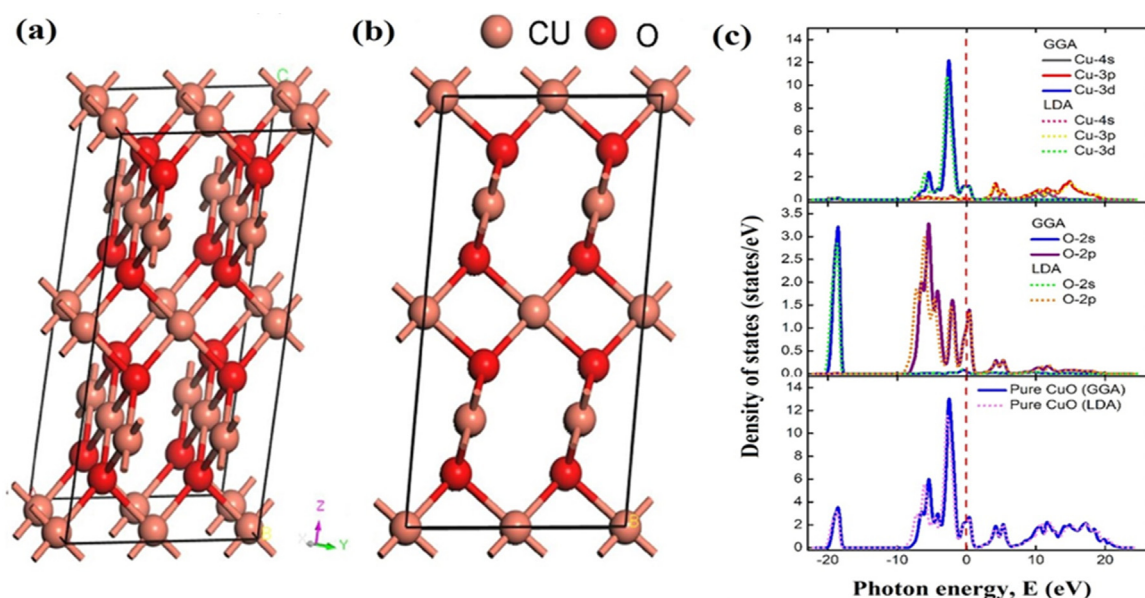
Fig. 2 Crystal structure of CuO (a) three dimensional and (b) two dimensional CuO and (c) partial and total density of states of CuO supercell. (Reprinted with permission from Ref. Nesa et al. (2020) and copyright with license Id. 4771831232359).
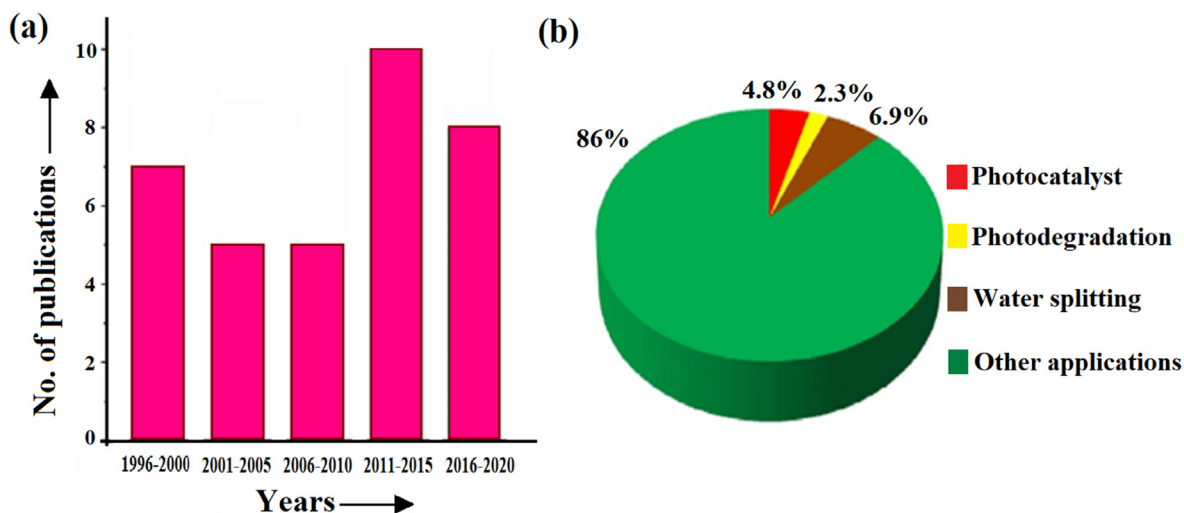
Fig. 3 Based on Scopus database with search terms: ("7930" accessed on February 15, 2020) (a) Bar graph showing overall publications from 1996 to 2020, (b) pie chart showing percentage of sharing by variant photoactive application.

phase, and dopants, remarkably affect the electrical conductivity of the material (Nair et al., 1999). For this, synthesis methods, as well as growth mechanisms, play a significant role and have a strong effect on the electrical properties of CuO. For example, in previous results, it was reported that CuO film synthesized from acetate and sintered at 300–600 °C through a chemical solution deposition technique possessed superior electrical conductivity, i.e., 10^{-2} S/cm to 10^{-3} S/cm. Similarly, film conductivities of CuO nanoparticles synthesized by Cu 2-ethylhexanoate and naphthenate were 10^{-6} to 10^{-4} and 2×10^{-3} to 10^{-5} S/cm, respectively (Zhang et al., 2014). From previous results, it was also observed that the conductivity of doped CuO film rises on doping with Li^{+} and diminished on doping with Al^{3+}.

CuO has been studied thoroughly for decades to fetch a deeper understanding of the physical aspects of CuO metal oxides materials, which includes crystal structure, electronic, optical, and magnetic properties. CuO is considered as prototype material with tenorite monoclinic crystallographic structure possesses low symmetry (C_{2h}^{6}) having general formula units/unit cell Cudennec and Lecerf, 2003). In 1933, Tunnel and co-workers reported the first original crystal structure of CuO and were modified by the X-ray single-crystal method (Åsbrink and Norrby, 1970). For magnetic structure, Cu atom has four coordination number, i.e., four O atoms are linked to Cu in a (1 1 0) plane of square planar configuration, and each O atom is encircled by four Cu in slightly distorted tetrahedron form (Ray, 2001; Tahir and Tougaard, 2012). As 1D nanostructure materials exhibit more grain boundaries and exposed active crystal planes, which leads to the large surface to volume ratios resulting in improved photocatalysis activity (Kum et al., 2013; Zhang et al., 2014). As filled VB and empty CB characterized its electronic properties, the presence of H_2O_2 plays a prominent role in the photocatalysis process. In the absence of H_2O_2, CuO photocatalyst is incapable of generating a good amount of ·OH species which have high oxidation power to degrade organic pollutant. Green's function and coulomb's potential (GW) approximation, advanced techniques, have been used to determine the electronic structure of CuO which enables prediction of the density of states (DOS) and

bandgap of semiconductor without any electron correlation (Wu et al., 2006; Ekuma et al., 2014). Ahmed et al. explicated a comparison of both the above studies, i.e. (DFT + U) and (GW) to determine electronic and optical studies of monoclinic CuO (Ahmad et al.,2016). They explored that DFT + U and GW approximation is adequately reliable to examine CuO nanomaterial properties. Nesa et al. reported structural properties of CuO via DFT based first-principles calculations and explored crystal structure of bare CuO in three and two dimensional as presented in (Fig. 3a) (Nesa et al., 2020). Similarly, partial and total DOS was also demonstrated through local density approximation (LDA) and generalized gradient approximation (GGA) as shown in (Fig. 3b).

2. Synthetic strategies for CuO nanostructures fabrication

To understand the fundamental significance and applications of nanoscale materials, innovative fabrication techniques play an essential role and have attracted much consideration widely. Different fabrication techniques permit researchers to modify morphology, particle size, size distributions, and composition reaction parameters. Recently, many chemical and physical approaches have been invented for the fabrication of different CuO nanostructures with varied and desired morphologies, sizes, and dimensions. However, despite different synthesis strategies reported to CuO nanoparticles, it is not easy to alter the size and shape of nanoparticle simultaneously (Liu et al., 2016a, 2016b). As there is a requirement of precise control over synthetic strategies during fabrication of nanoparticles with desirable properties, which in order give rise to different copper oxide nanostructures formation with controllable dimensions. Various fabrication strategies, i.e., colloidal synthesis, template synthesis, thermal oxidation, sonochemical and solvothermal techniques have been utilized to form CuO nanostructures with a different shape such as nanowires (Li et al., 2014), nanocubes (Rubilar et al., 2013), nanoribbons (Sun et al., 2015), nanoflowers (Shinde et al., 2015), nano-octahedra (Pal et al., 2013) and nanofilms (Lu et al., 2015) etc. Therefore, to streamline the discussion over

CuO nanoparticles synthesis, we present the most common synthetic strategies which have been divided into three different classes based on involved methods, *i.e.,* electrochemical, chemical, and biogenic methods.

2.1. Electrochemical methods

Electrochemical methods are the most commonly used method to synthesize metal oxides among widely available techniques due to its ease, low-temperature procedure, and viability. Many electrochemical techniques such as nanodisks (Das and Srivastava, 2016), nanorods (Karami and Afshari, 2017), nanosheets (Zhang et al., 2010), nanospheres (Yang et al., 2006), nanoribbons (Wang et al., 2018), nanospindles (Yuan et al., 2007), nanowhiskers, and nanodendrites (Lu et al., 2004) have been reported for the fabrication of CuO nanoparticles with anticipated morphology. The electrochemical synthesis process exhibits anodic dissolution of copper in an alkaline medium (Figueroa et al., 1993). Electrolyte concentration, deposition potential and time, reaction temperature, as well as the presence of additives, are the reaction parameters that play a vital role in morphology analysis and nanoparticle yield. Amongst all these parameters, nanomaterials phase composition is highly reliant on reaction solution temperature because it increases $Cu(OH)_2$ decomposition to CuO nanoparticles (Karami and Afshari, 2017). Das and Srivastava synthesized (CuO) nano-disks by optimized Taguchi's robust design and using copper succinate nano-rods. At first, cylindrical copper succinate rods were synthesized *via* electrochemical method using different concentrations (C_o) of a succinic ion at diverse applied currents (I_{ap}) and pH of reaction solution in a glass electrolyte bath. Then prepared copper succinate nano-rods were thermally treated or calcined in a muffle furnace under a static air atmosphere for five hours at varied temperatures to produce copper oxide nanodisks (Das and Srivastava, 2016). Yuan et al. fabricated CuO nanocrystals having different shapes through a simple and effective electrochemical method at room temperature (Yuan et al., 2007). They used aqueous $NaNO_3$ (200 mL electrolyte) and Cu (sacrificial anode) in a single cell at a constant current approach for limited hours to prepare CuO nanocrystals. The sono-electrochemical method was used by Mancier and his group to prepare copper oxide nanopowders utilizing mechanical energy from sonotrode generated in cavitation in liquid to boost a specific chemical reaction (Mancier et al., 2008). Plasma electrochemistry, a new method with an improved version of the electrodeposition method, has attracted much attention to synthesizing CuO nanoparticles. Released plasma is an electrically neutral medium that has reactive radicals and the potential to synthesize copper oxide nanoparticles. In this method, an electrode is replaced with a gaseous discharge of plasma, which assists CuO nanoparticles formation in the plasma − liquid interaction region (Liu et al., 2016a, 2016b).

2.2. Chemical methods

Chemical methods are other conventional techniques which have been widely used to prepare metallic nanoparticles. CuO nanoparticles have been synthesized through numerous chemical methods such as hydrothermal, (Kumar et al., 2014; Jana et al., 2018), reverse microemulsion (Kumar et al., 2013), solvothermal (Yang et al., 2015), sonochemical (Safarifard and Morsali, 2014), mechanochemical (Ameri et al., 2017), etc. These distinct approaches offer scalable applications and variant advantages such as precise uniformity in the shape and size of the final product, cost-effective, efficient-throughput equipment. Copper oxide nanoparticles are generally prepared by chemical reduction of a copper salt precursor using organic and inorganic reducing agents. After the reduction of precursor, the obtained precipitate was washed and calcined to attain different morphology nanostructure. Copper sulfate, copper nitrate, copper acetate, and copper chloride precursors have been used previously by the researcher for the preparation of CuO nanoparticles. It has been reported that the resultant morphology of CuO nanoparticles can be controlled by altering concentration and counterions of precursor (Siddiqui et al., 2016). Chawla et al. fabricated CuO nanostructures through facile chemical precipitation route utilizing copper acetate, copper nitrate, and copper sulfate (three different precursor salts). Spindle-shaped CuO nanostructures were obtained through different precursors, *i.e.,* copper acetate and copper nitrate varying in the average size of 60 and 32 nm, respectively; however, flower-shaped CuO nanoparticles with an average size of ~16 nm were attained through copper sulfate precursor (Chawla et al., 2017). Similarly, copper sulfate and copper nitrate salts also led to the formation of cubical and spherical CuO nanoparticles, respectively (Bhosale and Bhanage, 2017). Furthermore, precursors concentration and selection of capping agent also affects the CuO nanoparticle morphology as higher salt concentration caused an increase in particle size. However, the replacement of ascorbic acid, adipic acids, fumaric acids, and succinic acids (capping agent) leads to the formation of nanocubes, nanorods, nanowires, and nanobelts (Bhosale et al., 2016). Presently, microwave supported chemical methods have gained much attention for preparation of CuO nanostructures having different morphology such as spherical), tubular and cubical due to rapid kinetics, rapidity, and efficiency (Bhosale et al., 2013). This technique involves mainly two parameters, *i.e.,* irradiation time and power applied must be optimized to attain nanoparticles of anticipated shape and dimension. Another technique, sonochemical method, has been reconnoitered to fabricate CuO nanoparticles comprising the use of ultrasound waves. These ultrasound waves bring out some physical and chemical variations in the system throughout cavitation and create a local area with extreme temperature and pressure conditions, appropriate for nanoparticle synthesis. Using this method, consistently dispersed CuO nanoparticles (5–10 nm) have been prepared by Kumar et al. at room temperature and for better dispersibility embedded in poly(vinyl alcohol) (Vijaya Kumar et al., 2001). Nevertheless, sometimes the high temperature is required to improve crystalline nature as well as the particle size of copper oxide nanostructures (Saravanan and Sivasankar, 2016). Moreover, the hydrothermal method is a solution-based technique where the reaction occurs in water. The method has many advantages such as easy desolvation of variant inorganic salts in water, which gives flexible adjustment to required metal ions, active growth of nanostructure due to strong polarity of water, non-toxic and cost-less nature of water which facilitates performance in large scale and low temperature. Furthermore, different morphologies were obtained by a hydrothermal method such as butterfly-like (Zhang et al., 2009),

honeycomb-like (Liu et al., 2007), dendrite (Zhang et al., 2008) and shrimp structure (Liu et al., 2012), layered-hexagonal discs (Abaker et al., 2011), flower (Liu et al., 2007), self-assembled leaf (Dar et al., 2010) and nanobelt (Dar et al., 2009). Another solution-based method is chemical precipitation technique, which is similar to the hydrothermal method. This technique also gives rise to distinct morphologies such as leaf-like, shuttle-like, dandelion-like shapes nanostructures. Vaseem et al. prepared a flower-like shape of CuO nanostructure using chemical precipitation technique, which has been demonstrated in (Fig. 4) (Vaseem et al., 2008).

2.3. Biological methods

Electrochemical and chemical methods are mostly used conventional methods to prepare metal and metal oxide nanoparticles but, due to expensiveness and usage of harsh chemicals, they are not much efficient. Therefore, environment-friendly biological methods have gained much attention to fabricate nanoparticles due to safe, fast, simple, and ecological possessions without the need for any sophisticated apparatus, controlled atmosphere, and noxious chemicals (Nasrollahzadeh et al., 2016; Sharma et al., 2015). The biological method is advantageous in the field of green chemistry as its main emphasis is on those techniques which involve the least usage of material and energy with minimal wastage during production (Upadhyay and Verma, 2015). Amongst all biological methods, an extract of plants and their parts such as stem, flowers, leaves, and roots appear to be the best precursors owing to easy sampling and low-cost for large-scale fabrication of nanoparticles (Nasrollahzadeh et al., 2015a, 2015b). Other than this plant extraction method, naturally present reducing agents, i.e., carbohydrates, enzymes, unicellular/multicellular microorganisms, and biodegradable polymers, can also be used in the synthesis process. Plant-mediated nanomaterial synthesis is a synthesis process where the use of the reducing agent also performs as a stabilizing agent and thus gets rid of the requirement of any external stabilizers. Since the early 1900s, researchers have explored that plant materials can reduce metal ions (Singh et al., 2017a, 2017b). To synthesize CuO nanoparticles via biological methods numerous plant extracts have been explored comprising Carica papaya (Sankar et al., 2014), Solanum lycopersicum (Vaidehi et al., 2018), Tabernae montana divaricate (Sivaraj et al., 2014), Calotropis gigantea (Sharma et al., 2015), Rheum palmatum L. (Bordbar et al., 2017), Aloe vera (Kerour et al., 2018), Camellia japonica (Maruthupandy et al., 2017), Piper betle (Praburaman et al., 2016), Theobroma cacao L. seeds (Mittal et al., 2013) Tamarix gallica (Nasrollahzadeh et al., 2015a, 2015b), Rauvolfia serpentinia (Lingaraju et al., 2015), etc.

The mechanism of nanoparticle synthesis includes the reduction of precursor salt by one or more reducing agents present in the plant extracts. For the preparation of plant extracts, firstly, plant and/or its parts are boiled and crushed in a solvent (mostly distilled water), and then the supernatant was cautiously collected after centrifugation. Plants mostly have a significant chemical composition of phenolic compounds, quinol, alkaloids, flavonoids, terpenoids, and chlorophyll pigments, which can reduce metal ions. Similarly, a major starch component of a plant also has reducing abilities (Tongsakul et al., 2012). Alishah et al. prepared CuO nanoparticles using starch extracted from Solanum tuberosum. It was confirmed by all the analyses that synthesized nanoparticles were highly stable and spherical, with an average size of about 54 nm (Alishah et al., 2017). Yugandhar et al. synthesized CuO NPs using Syzygium alternifolium stem bark and $CuSO_4 \cdot 5H_2O$ precursor. Through FT-IR analysis, it was confirmed that phenols and primary amines caused the capping and stabilization of nanoparticles. Morphology and rate of nanoparticle synthesis can be
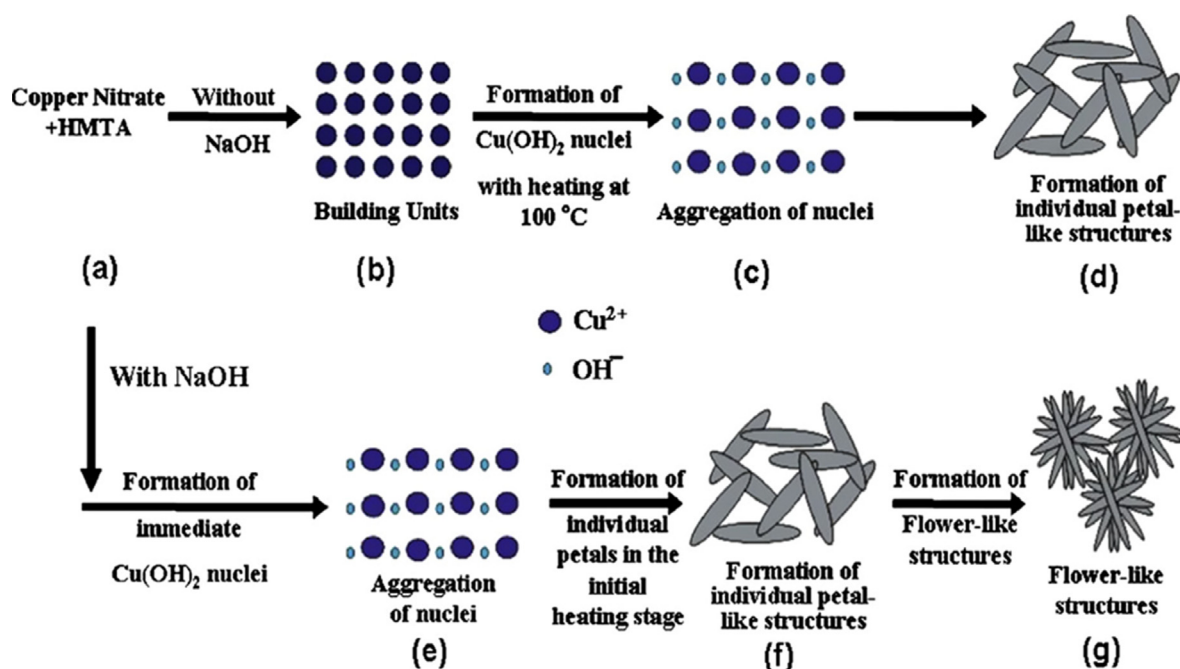
Fig. 4 Schematic developed mechanism view of CuO flower shaped nanostructure formation. (Reprinted with permission from Ref. Vaseem et al. (2008) and copyright with American Chemical Society).

simply controlled by changing pH, temperature, substrate concentration, and exposure time parameters to the precursor (Yugandhar et al., 2017). Furthermore, several microorganisms like bacteria, yeast, fungi, and actinomycetes have also been explored for extracellular/intracellular fabrication of nanoparticles. Cuevas et al. used a white-rot fungus, *Stereum hirsutum*, for the green synthesis of CuO nanoparticles (spherical shaped with a size range of 5–20 nm) in the presence of three different copper salts (CuCl$_2$, CuSO$_4$, and Cu(NO$_3$)$_2$) under varied pH conditions, *i.e.,* 5, 7 and 9 (Cuevas et al., 2015). Honary et al. synthesized and stabilized extracellular fabrication of monodispersed CuO nanoparticles using *Penicillium aurantiogriseum, Penicillium citrinum*, and *Penicillium waksmanii* which have been isolated from soil (Honary et al., 2012). UV–vis and fluorescence spectrum confirmed the existence of some secreted proteins (able to hydrolyze metal precursors into metal oxides extracellularly) from fungi in the culture. Eltarahony et al. performed synchronous biosynthesis of 0D (intracellular) and 1D (extracellular) CuO-NPs *via Proteus mirabilis* 10B first time in 2018 (Eltarahony et al., 2018). Surface plasmon resonance was authenticated by UV–Vis spectroscopy at 275 and 430 nm for intracellular and extracellular CuO-NPs. Surprisingly, extracellular CuO-NPs displayed rod, needle, and wire-shaped nanoparticles with 17–37.5 nm (width) and 112–615 nm (length). Many microorganisms have been employed for the preparation of metallic nanoparticles, but, only a few studies have been stated for CuO nanoparticle preparation.

Besides many unique and excellent properties, CuO is associated with some limitations which have been given as follows:

(i) Low bandgap, so there is the possibility of electron-hole pair recombination
(ii) Photocorrosion of CuO photocatalyst mainly due to an accumulation of photoinduced electrons. To overcome these disadvantages, several modification strategies have been employed. Out of which mainly heterojunction formation leads to enhanced photodegradation.

3. CuO based heterostructure construction for pollutant degradation

Bare CuO TMOs are not so efficient for pollutant degradation due to fast charge recombination; thus, there is a need to enhance its photodegradation efficacy and to make it an efficient photocatalyst. As a consequence, various strategies have been applied to augment photodegradation efficiency, which includes (1) heterojunction construction and (2) Z-scheme heterojunction system, (3) doping with rare earth and transition metals and (4) carbonaceous supported metal oxides.

3.1. Heterostructure formation

Heterojunction formation takes place between two dissimilar semiconductors with suitable bandgap alignment resulting in the enhanced transference of electrons by reducing recombination rates of photogenerated charge carriers. This is the most promising approach for enhanced photocatalytic performance of photocatalysts (Priya et al., 2016; Raizada et al., 2017a, 2017b, 2014a, 2014b). The lower bandgap of CuO TMOs pho-

tocatalyst leads to electron-hole pairs (EHP) recombination, thus possess low photodegradation efficacy. Hence there is the need for heterojunction construction of bare CuO with other photocatalysts to improve its photodegradation efficiency. The conventional heterojunction technique is classified into three different categories, *i.e,* (i) type-I (straddling gap), (ii) type-II (staggered gap), (iii) type-III (broken gap), based on bandgap edges of the composite photocatalyst (Raizada et al., 2020; Sonu et al., 2019; Hasija et al., 2020).

The primary mechanism for photocatalysts heterojunction formation is discussed below:

In type-I heterojunction, VB and CB position of (photosystem) PS-I are lower and more significant than VB and CB of neighboring PS-II, which give rise to migration of photoexcited holes and electrons of PS-I to VB and CB of PS-II that is negative for charge separation.
In the type-II system, VB and CB of PS-I are higher than VB and CB of PS-II, resulting in easy transport of electrons from CB of PS-I to PS-II having reduced reduction potential, simultaneously holes migrate from VB of PS-II to PS-I with reduced oxidation potential leading spatial electron-hole separation.
In type-III heterojunction, migration of charge carriers follow a similar pathway as in type-II, but band edges are further set off, resulting in no transference or separation of EHP (Fig. 5).
Similarly, Z-scheme is also a subset of heterojunction construction used to optimize the drawbacks of lower redox potentials of heterojunction system. Here, electrons/holes were accumulated on distinct PS giving spatial charge carrier separation. This modern approach enables efficient migration of photogenerated charge carriers over short distances to reach active sites on the photocatalyst surface without recombination.

Beyond all three heterojunction systems, type-II heterojunction provides optimum band positions for efficient charge carrier separation leading to enhanced photocatalytic activity. The build-in potential at the interface of semiconductors can enhance the transference and separation of photogenerated EHP. Thus, it is considered as the most prominent composite photocatalytic system among all heterojunctions due to its improved photocatalytic performance *via* reduced EHP recombination, which avails efficient charge carriers for a reactive radical generation.

3.1.1. CuO based Type-II binary heterostructure photocatalyst

The heterojunction of two different semiconductors represents an effective structural design for improving photocatalytic activity. The mixture of variant heterojunction is said to be heterostructure. For photocatalytic activity, two PS employed in heterojunction formation must possess distinct band gaps with lower band energy lying in the visible range. Li and co-workers prepared CuO/CeO$_2$ heterostructure for the degradation of methyl blue (MB) pollutants in high salt wastewater (Li et al., 2019). The synthesized nanocomposite exhibited an absorption range of visible light up to 510 nm, and the calculated bandgap of CuO/CeO$_2$ heterojunction was 2.43 eV, which was confirmed by diffuse reflectance spectroscopy (DRS) results. The photodegradation efficiency of CuO/
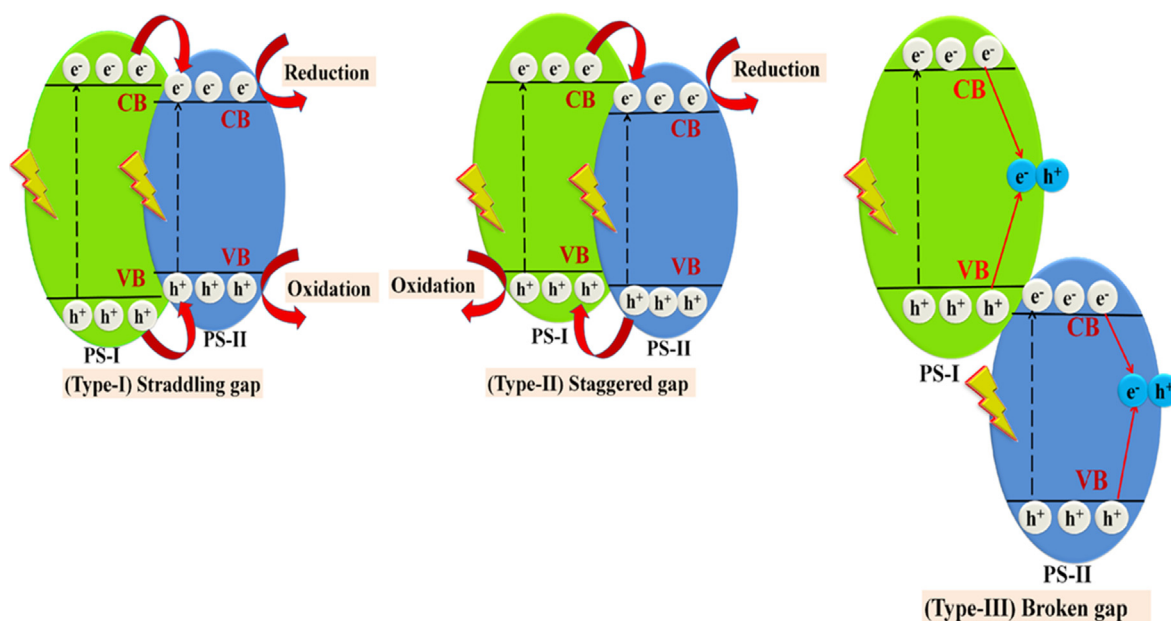
Fig. 5 Schematic heterojunction growth of (a) type-I Straddling gap, (b) type-II Staggered gap and (c) type-III broken gap.

CeO_2 nanocomposite for methyl blue (MB) degradation was enhanced from 18 to 33.74% and was mainly due to the bombardment of ˙OH radical. More than 80% of MB was forcefully removed from wastewater, having 5–80 g/L NaCl in 2.11–9.02 pH range. Nogueira groups prepared $CuBi_2O_4/$ CuO nanocomposites by a solvothermal technique using Bi $(NO_3)_3·5H_2O$ and Cu $(CH_3COO_2).H_2O$ precursors (Nogueira et al., 2019). Photodegradation efficiency of prepared $CuBi_2$- O_4/CuO heterojunctions was evaluated via degrading methylene blue (MB) dye and metronidazole (MTZ) under simulated solar light and visible light illumination, respectively. Field emission scanning electron microscopy (FESEM) results confirmed the formation of $CuBi_2O_4/CuO$ heterostructure in the shape of nanocolumns with a small plate-like
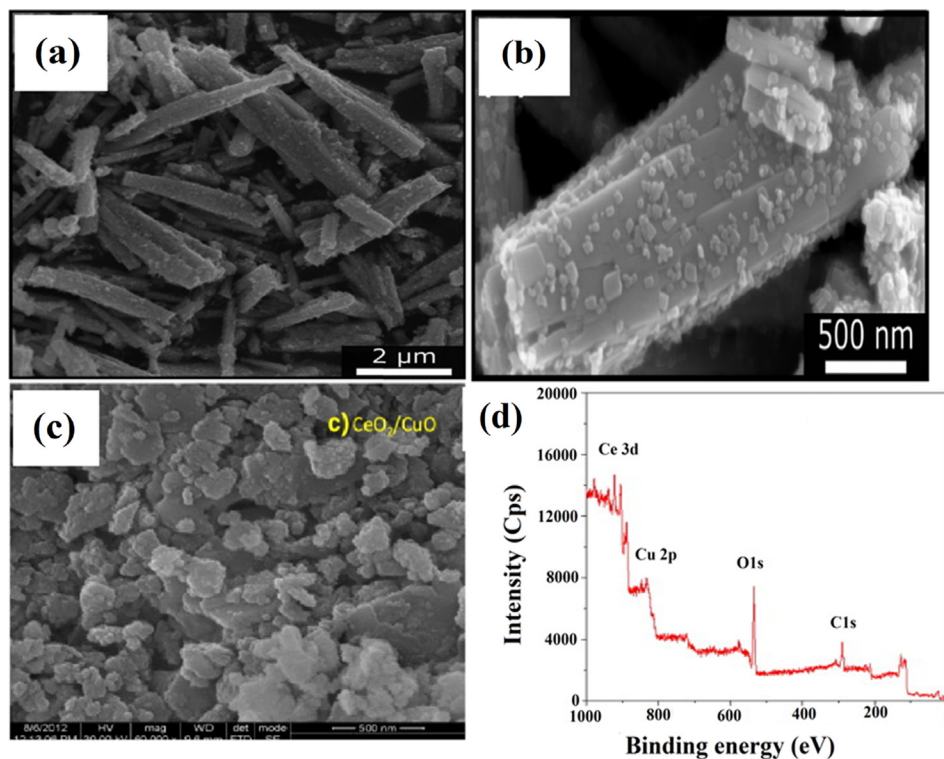
Fig. 6 (a, b) FESEM images of $CuO/CuBi_2O_4$ heterostructure synthesised under solvothermal conditions (120 °C for 12 h), (c) HR-SEM image and (d) XPS spectra of CeO_2/CuO heterojunction. (Reprinted with permission from Ref. Nogueira et al. (2019) and copyright with American Chemical Society).

nanoparticle (diameter as 2 μm) which were consistently dispersed over the surface (Fig. 6a, b). The synthesized heterojunction exhibited excellent photocatalytic activity with 98% and 36% removal of MB degradation and MTZ, respectively, due to effective charge separation under visible light range with 2.1% of apparent quantum yield (AQY) (λ = 540 nm). Similarly, CeO$_2$/V$_2$O5 and CeO$_2$/CuO nanocomposite were prepared using the thermal decomposition technique for effective MB photodegradation (70.1% by CeO$_2$/CuO) under a visible region. X-ray photoelectron spectroscopy (XPS) analysis confirmed the presence of constitutes Ce^{4+}, Cu^{2+}, C, and O

relative oxidation states without any impurities and high-resolution scanning electron microscopy (HR-SEM) results depicted irregular morphology of nanocomposites due to accumulation of small spherical shaped NPs (Fig. 6c, d). For CeO$_2$/CuO nanocomposite, an EHP separation mechanism during the photodegradation process of MB degradation under visible range, as depicted in (Fig. 7). Here, CuO was more activated due to its lower bandgap (1.83 eV), where electrons in CB of CuO undergo reduction reaction and holes in VB of CeO$_2$ experience oxidation reaction, thereby, diminished EHP recombination (Saravanan et al., 2013). Furthermore, Li and
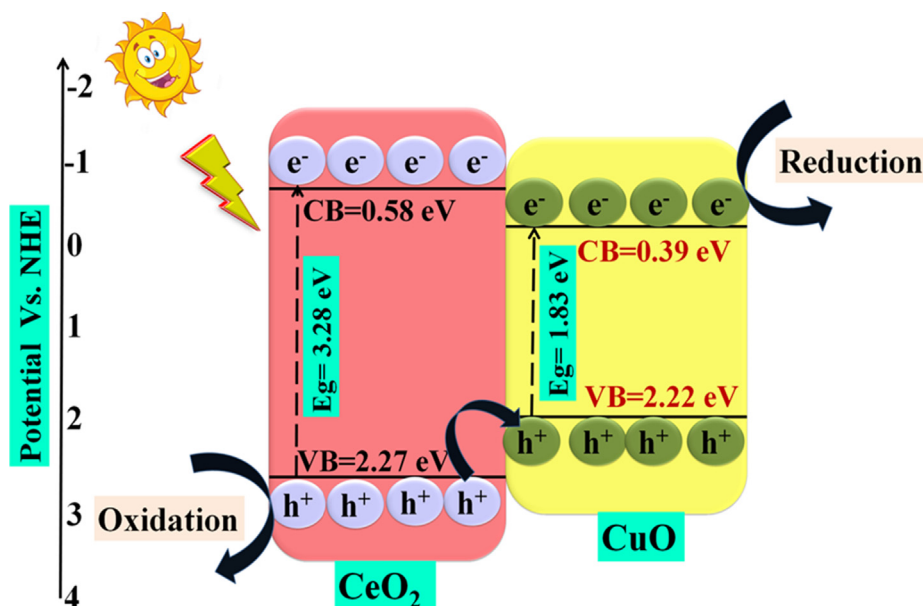
Fig. 7 Schematic growth mechanism showing charge transfer pathway during MB photodegradation of CuO/CeO$_2$ nano-heterostructure (Reprinted with permission from Ref. Saravanan et al. (2013) and copyright with licence Id. 4842450945854).
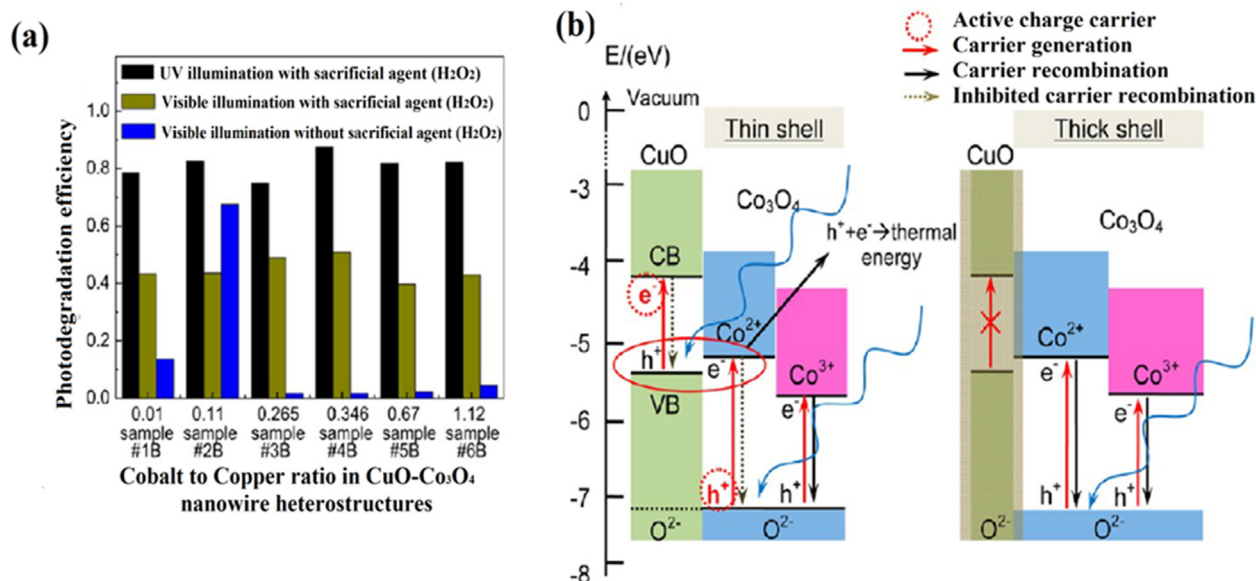
Fig. 8 (a) Comparison of phenol photodegradation efficacy for distinct samples and reactions condition, (b) band gap energies alignment of CuO/Co$_3$O$_4$ nanowire heterojunction and schematic mechanism of electron-hole separation and transference. (Reprinted with permission from Ref. Shi and Chopra (2012) and copyright with American Chemical Society).

co-workers prepared CuO/MoS₂ heterojunction nanoflowers by employing the hydrothermal technique. Through XPS results, they calculated band edges alignment of semiconductor used in heterojunction formation with an energy gap presented by CB (1.7 eV) and VB (0.6 eV) edges between Cu 2p₁/₂ and Mo 3d₂/₃. The synthesized staggered type-II heterojunction of CuO/MoS₂ nanocomposite exhibited enlarged surface area, *i.e.*, 23.5 m²/g and enhanced photocatalytic efficiency for MB which was found to be 95.7% than bare MoS₂ (72.5%) after visible light irradiation for 100 min (Li et al., 2015).

Apart from MB degradation, Rhodamine B (RhB), methyl orange (MO), Congo red (CR) dyes were also used to assess the photodegradation efficiency of CuO heterojunctions. Zeng et al. successfully prepared CuO nanofibres using Cu based coordinated polymer nanofibres and calcined at distinct temperatures (400 °C, 500 °C, 600 °C) by employing L-aspartic acid and Cu(NO₃)₂·3H₂O precursors (Zeng et al., 2018). The CuO nanofibres synthesized at 500 °C possessed excellent photocatalytic activity due to remarkably high photochemical stability and low mass transference limitation, which enable easy accommodation of dye molecules to active sites. Holes are mainly responsible for RhB dye degradation in the presence of H₂O₂ and degraded up to 96% in 160 min under visible-light region. Furthermore, Shi et al. synthesized CuO/Co₃O₄

nanowire heterojunction having well-controlled shape and size in a thermal growth method using the air annealing pathway of Co into CuO nanowire for phenol degradation (Shi and Chopra, 2012). Phenol photodegradation was carried out under UV or visible light irradiation in the presence of H₂O₂ by polycrystalline Co₃O₄ shell on CuO nanowires that displayed 50–90% photodegradation efficiency. Photodegradation results observed with controlled morphology of distinct samples resulting in 87% > 69.6% > 50.8% removal efficiency for UV light with H₂O₂, Vis-light without H₂O₂, and Vis-light irradiation with H₂O₂ as presented in (Fig. 8a). From (Fig. 8b), a thin shell of Co₃O₄ (~5.6 nm) was found better in comparison to thick polycrystalline shell because of CuO nanowire, which became photoactive. The lower bandgap (2.0 eV) of CuO with the introduction of Co₃O₄ NPs possessed better light absorption exhibiting enhanced EHP separation and charges generation at the interface, giving 67.5% removal efficiency in the absence of H₂O₂. Furthermore, Behzadifard et al. reported SmFeO₃/CuOₓ (where x = 5, 8, 10, and 20 wt %) nano-heterostructure synthesized *via* a simple mixing-calcination method (Behzadifard et al., 2018). Fabricated SmFeO₃ and CuO(10 wt%)/SmFeO₃ nanoparticles were spherical with an average grain size of 50 and 30 nm, respectively. 0.15 g of SmFeO₃/CuO(10 wt%) heterostructure
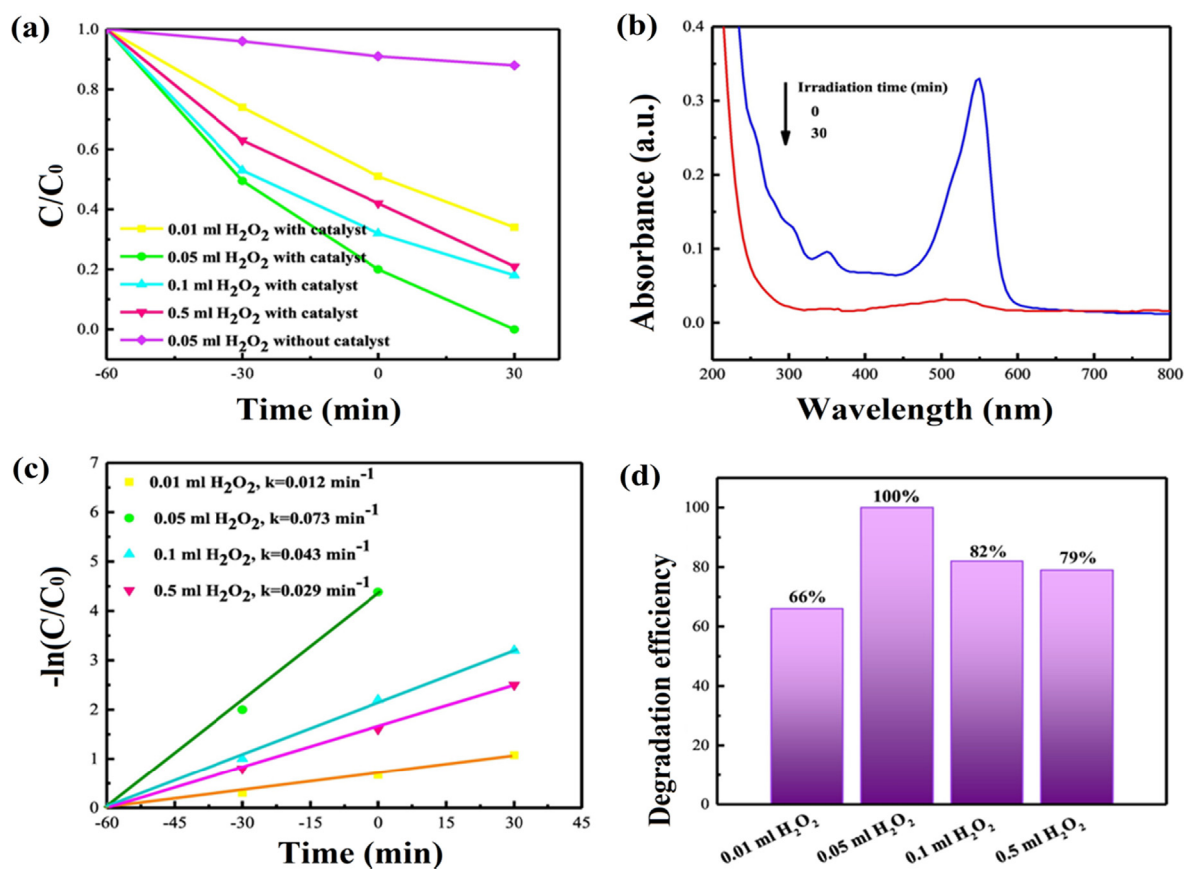
Fig. 9 (a) Photocatalytic degradation of RhB (8 mg/L) in aqueous mixture using H₂O₂ (30 wt%) (pH = 5) with 0.15 mg of SmFeO₃/CuO(10 wt%) nanoheterostructure photocatalyst, (b) Time dependent UV–Vis absorption spectra for the RhB (8 mg/L) photocatalytic degradation via 0.05 mL H₂O₂ (pH = 5) with 0.15 g of the CuO(10 wt%)/SmFeO₃ catalyst, (c) Plots of -ln(C₀/C) versus reaction time for the photocatalytic degradation of RhB (8 mg/L) and (d) degradation efficiency of RhB (8 mg/L) using diverse H₂O₂ (30 wt%) and pH = 5 with 0.15 g of CuO(10 wt%)/SmFeO₃ photocatalyst, respectively. (Reprinted with permission from Ref. Behzadifard et al. (2018) and copyright with License Id. 4771850117484).

(pH = 5) displayed 65% photodegradation of (8 mg/L sample) RhB dye and got increased up to 100% when 0.05 mL of H_2O_2 were added in the reaction under similar reaction conditions (Fig. 9a–d). Besides, $SmFeO_3/CuO(10 wt\%)$ nanocomposite displayed 93 and 85% removal efficiency for 20 mg/L RhB dye and phenol pollutants with 0.05 mL H_2O_2. Sherly et al. successfully prepared ZnO, CuO, and ZnO/CuO heterogeneous structures, i.e., ZnCu, Zn_2Cu, and $ZnCu_2$ via microwave-assisted, one-step and simple technique, respectively (Sherly et al., 2015). The fabricated ZnCu, Zn_2Cu, and $ZnCu_2$ heterostructures were synthesized with different ZnO: CuO molar ratios of 1:1, 2:1, and 1:2 and possessed band gap of 2.98, 2.91 and 2.89 eV, respectively. Among all these samples, Zn_2Cu nano-heterostructure achieved the best photocatalytic performance due to prolonged photoresponsive range and enhanced charge carriers separation rate, confirmed by PL analysis. The Zn_2Cu nano-heterostructure revealed 82% removal efficiency of 2, 4-dichlorophenol under optimum conditions constituting 50 mg/100 mL of catalyst concentration at pH 7 and 240 min irradiation time.

Similarly, bifunctional CuO/Fe_3O_4 heterojunction was fabricated by Sun et al. through a one-step coprecipitation method utilizing ferric chloride, ferrous chloride, and copper chloride as precursors (Sun et al., 2018). Synthesized CuO/Fe_3O_4 nanocomposite was used for the removal of p-arsanilic acid (p-ASA) under visible light irradiation as well as immediately released inorganic arsenic via adsorption from the reaction solution. CuO/Fe_3O_4 nanocomposite exhibited 100% photodegradation of p-arsanilic acid (p-ASA) by the conversion of p-ASA to As (V) within 36 min. Converted As (V) was adsorbed on $CuO-Fe_3O_4$ nanoparticles surface with high efficiency i. e. above 95% at initial pH range from 4 to 7. It was also observed that degradation efficacy got increased simultaneously with the addition of dissolved oxygen in aqueous media because molecular oxygen offers effective electron scavenger, which suppressed charge carrier recombination rates (Fig. 10a). Also, Fourier-transform infrared (FTIR) and XPS spectrum results determined interactions between arsenic and CuO/Fe_3O_4 heterojunction before and after adsorption. In (Fig. 10b), relative peaks of CuO/Fe_3O_4 NPs
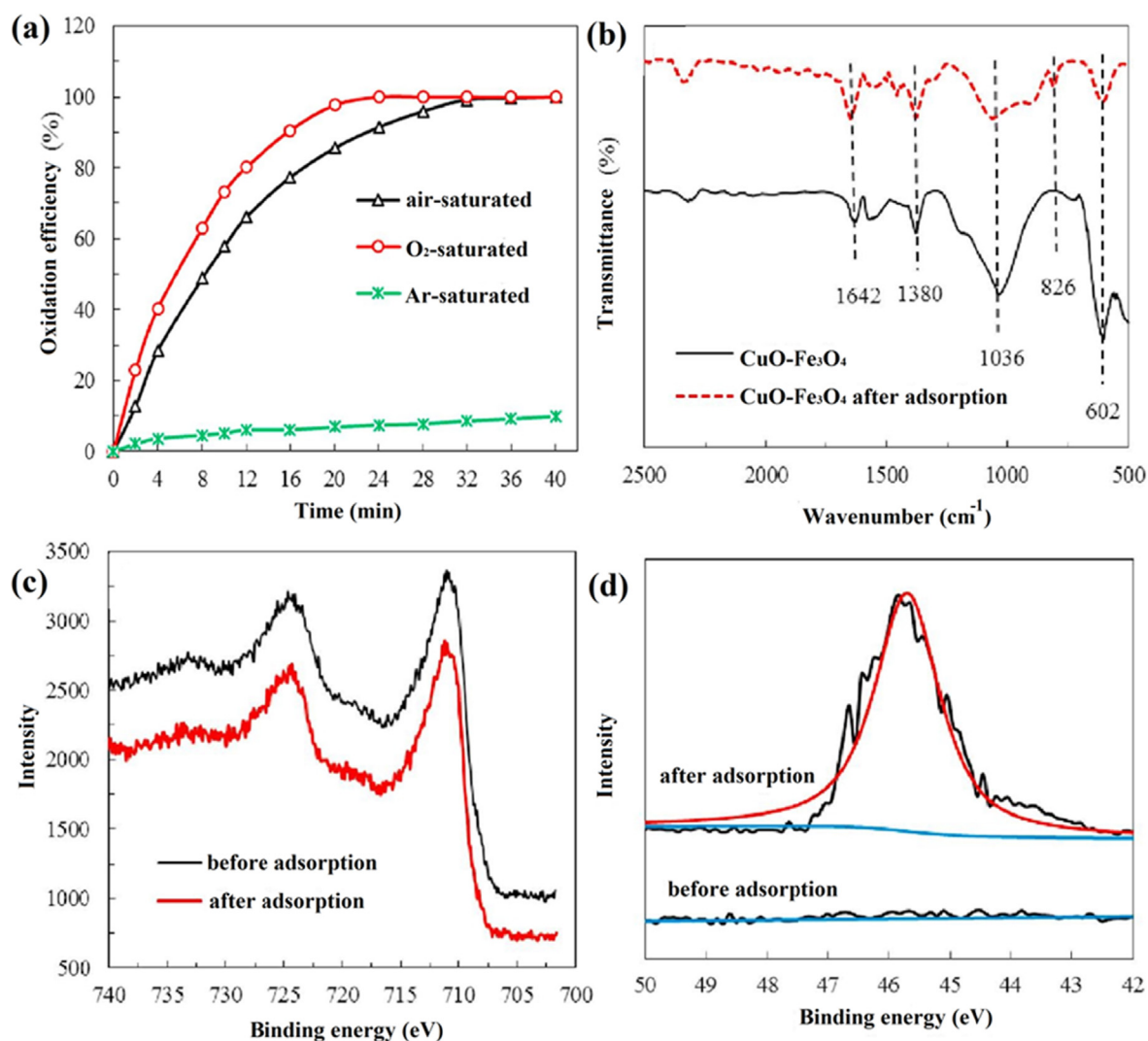
Fig. 10 (a) Effect of different atmospheres conditions on p-ASA photocatalytic degradation by CuO/Fe_3O_4 NPs, (b) FTIR spectrum, (c) Fe 2p and (d) As3d core level photoelectron spectrum of CuO/Fe_3O_4 NPs before and after adsorption. (Reprinted with permission from Ref. Sun et al. (2018) and copyright with License Id. 4771850454409).
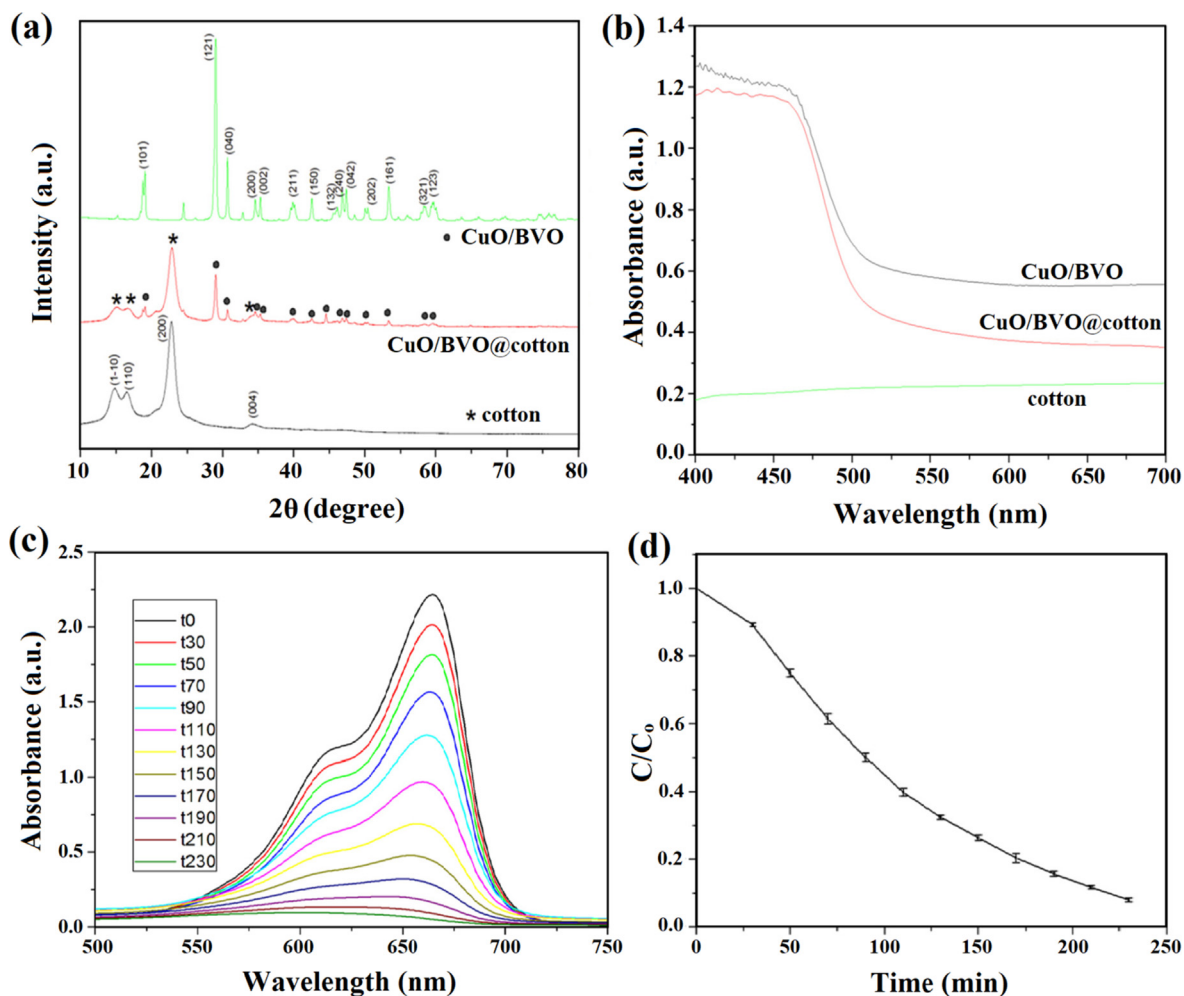
Fig. 11 (a) XRD patterns, (b) UV–Visible light absorption spectra of pure cotton, CuO/BiVO$_4$ and CuO/BiVO$_4$/cotton nanocomposites, (c) UV–visible absorption spectrum of MB aqueous solution at distinct time intervals, and (d) MB photodegradation by CuO/BiVO$_4$ under visible-light region. (Reprinted with permission from Ref. Ran et al. (2019) and copyright with License Id. 4771860722568).
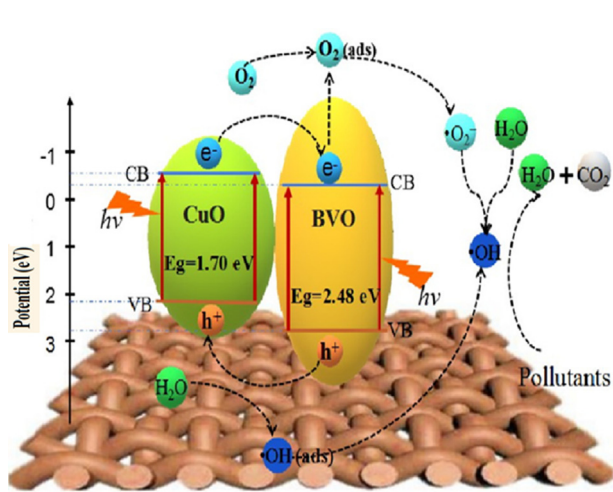
Fig. 12 Schematic mechanism view of CuO/BiVO$_4$ heterostructure under visible-light region. (Reprinted with permission from Ref. Ran et al. (2019) and copyright with License Id. 4771860722568).

displayed peaks at 1642, 1380, 1036, and 826 cm^{-1} indicated adsorption of H$_2$O molecule on heterojunction, stretching vibrations of CO$_3^{2-}$ and Fe-OH and As-O-Fe groups, respectively. Fe 2p and As 3d core levels in between CuO/Fe$_3$O$_4$ NPs and after adsorption were demonstrated in (Fig. 10c). Binding peaks of Fe 2p$_{1/2}$ and Fe 2p$_{3/2}$ were attained at 724.5 and 710.9 eV, respectively, while no changes in peaks were observed after adsorption that indicated sufficient stability in reaction. However, the binding peak of As 3d at 45.6 eV after adsorption revealed easy adsorption of an arsenic product on CuO/Fe$_3$O$_4$ NPs for removal of p-ASA (Fig. 10d). In the photodegradation mechanism of p-ASA with arsenic, adsorption through CuO/Fe$_3$O$_4$ NPs might happen first. After that, the para position of p-ASA was attacked by $\cdot$OH and $\cdot$O$_2^-$ radicals to generate the arsenate, arsenite, and aminophenol compounds. Then, the aminophenol was degraded by the attack of radicals to transform into hydroquinone and benzoquinone. These compounds were further degraded to more straightforward groups (formic, maleic, and formic acid), and under adequate oxidants and treatment time conditions, above formed intermediates, were ultimately

mineralized to NH_4^+, CO_2, and H_2O. In such reaction conditions, arsenite was oxidized to arsenate by free radicals, which was effectively vanished from the adsorption process on CuO and Fe_3O_4 surface. Similarly, Belaissa et al. reported the degradation of amoxicillin antibiotics by novel *p*-CuO/*n*-ZnO heterojunction synthesized *via* the chemical route (Belaissa et al., 2016). The best composition of ZnO/CuO (50:50 wt%) nanocomposite revealed photodegradation > 90% in 4 h under solar light irradiation with (9.95×10^{-3}/min) rate constant at pH ~ 11 due to enhanced charge separation and migration mechanism.

3.1.2. *CuO based Type-II ternary heterostructure photocatalyst*

Coupling of three different semiconductors to form ternary photocatalyst has also achieved great attention in many research fields due to efficient charge separation and bandgap lowering, which lead to enhanced photocatalysis performance. For instance, Ran and co-workers reported CuO/$BiVO_4$ heterostructure with 2.44 eV bandgap attached to cotton fabrics by polydopamine (PDA) templating and denoted as CuO/$BiVO_4$@cotton which was then used for MB degradation (Ran et al., 2019). The synthesized CuO/BVO@cotton nanocomposite possessed multiple applications in highly proficient visible-light-driven photocatalysis, antibacterial activity, and UV protection. Cotton fabrics were utilized to immobilize CuO/$BiVO_4$ nano-heterostructure and were found efficient in the removal of MB dye due to its excellent recyclability and stability. The nanocomposite displayed 97.7% MB removal efficiency in 200 min under visible light illumination, and after five recyclabilities, the removal efficiency was found to be 92.1%. UV–

Visible absorption spectrum confirmed strong absorbance of CuO/$BiVO_4$@cotton heterostructure in Vis-light irradiation (Fig. 11a, b). The photocatalytic performance of CuO/$BiVO_4$@cotton heterostructure was determined by UV–vis absorption showing the absorption peak of MB at 665 nm as displayed in Fig. 11c, d, and decrease in absorbance of residual MB solution were perceived clearly with the upsurge of visible-light irradiation time. Mechanism of CuO/$BiVO_4$ heterostructure revealed the migration of electrons from CB (0.46 eV) of CuO to CB (0.36 eV) of $BiVO_4$ while holes were transported from VB (2.78 eV) of $BiVO_4$ to VB (2.16 eV) of CuO which diminished electron-hole pairs recombination. Correspondingly, holes and electrons on the catalytic surface were abducted by adsorbed $^-OH/H_2O$ and O_2 to yield $^{\cdot}OH$ and $^{\cdot}O_2^-$, respectively (Fig. 12).

Kumaresan et al. prepared ZnO/CuO (ZC_1, ZC_2, and ZC_3) heterostructures with different concentrations of CuO, *i.e.*, 15.7, 31.4 , and 62.8 mg, respectively using zinc acetate dehydrate and NaOH as a precursor (Kumaresan et al., 2020). They explored enhanced degradation efficiency of ZC_3 binary nanocomposites having an optical band gap of 2.9 eV. Thus they coupled ZC_3 binary nanocomposites with reduced graphene oxide (rGO) *via* solid-state reaction technique. Different samples of ZC_3/rGO nanocomposites were prepared with the addition of rGO with 5, 10, 15, and 20 mg concentration and denoted as ZC_3G_5, ZC_3G_{10}, ZC_3G_{15}, and ZC_3G_{20}. FESEM results confirmed the morphology of synthesized ZC_1 nano-heterostructure as nanorods (Fig. 13a), ZC_2 composite of spherical shape (Fig. 13b), and ZC_3, as well as ZC_3G_{15} nano-heterostructure, depicted flower-like
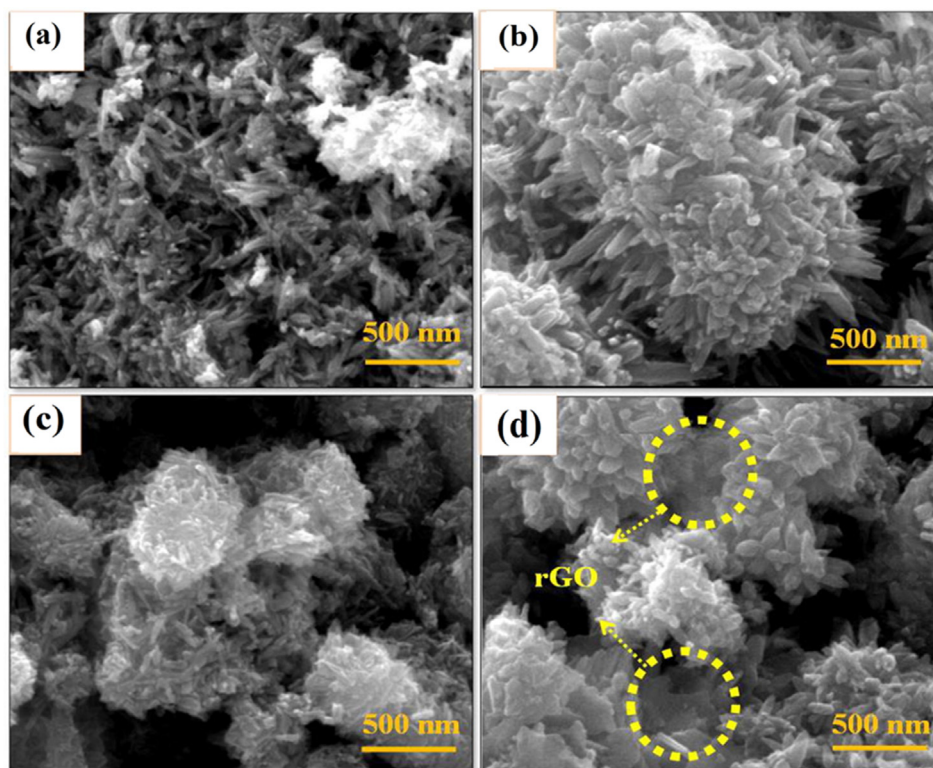
Fig. 13 FESEM images of binary composites (a) ZC_1 (b) ZC_2 (c) ZC_3 and (d) ZC_3G_{15} ternary nanocomposites. (Reprinted with permission from Ref. Kumaresan et al. (2020) and copyright with License Id. 501547730).

morphology (Fig. 13c, d). The optical band gap of ZnO nanoparticles (3.1 eV) was reduced to 2.8 eV in the fabricated (ZnO/CuO)/rGO (ZC_3G_{15}) ternary nanocomposites. Photoluminescence (PL) spectra subsequently showed that ZC_3G_{15} nano heterostructure efficiently promoted electrons and holes separation, thus reducing charge carriers recombination rate (Fig. 14a). Similarly, when the pH value of the RhB dye mixture was increased to 11, degradation efficacy rate reached 99% in 20 min of irradiations, as shown in (Fig. 14b, c).

Similarly, Bai and co-workers prepared TiO_2 nanofibres/ ZnO, nanorods/CuO NPs ternary composite through several stages, firstly TiO_2 via electrospinning, then hydrothermally developed ZnO and finally deposition of CuO NPs (TZC) (Bai et al., 2012). After solar light illumination of 40 min, acid orange was degraded entirely by TiO_2 nanofiber/ZnO nanorod/CuO nanoparticle (TZC) material (ensured increased light absorptivity) whereas 63% and 44% of photodegradation occurred by TiO_2nanofiber/ZnO nanorod (TZ) and TiO_2 nanofibres, respectively. Through XPS results in structural properties and surface chemical configuration were determined, and +2 oxidation states of Ti, Zn, and Cu were confirmed in the form of TiO_2, ZnO, and CuO, respectively, on the surface of TZC material. The enlarged Brunauer Emmett Teller (BET) surface area was obtained as 124.8, 89.8, and 47.6 m^2/g for TZC, TZ, and TiO_2 nanofibres, respectively at 77 K temperature. Consequently, due to the greater surface area, TZC displayed enhanced photocatalytic performance by generating more reactive sites for oxidation reaction and augmented fast mass transference. Besides, other reports also stated the fabrication of ZnO/CuO and Ag_2O/ZnO/CuO nano heterostructure to evaluate photocatalytic activity against acid blue 92 degradations under the visible-light illumination
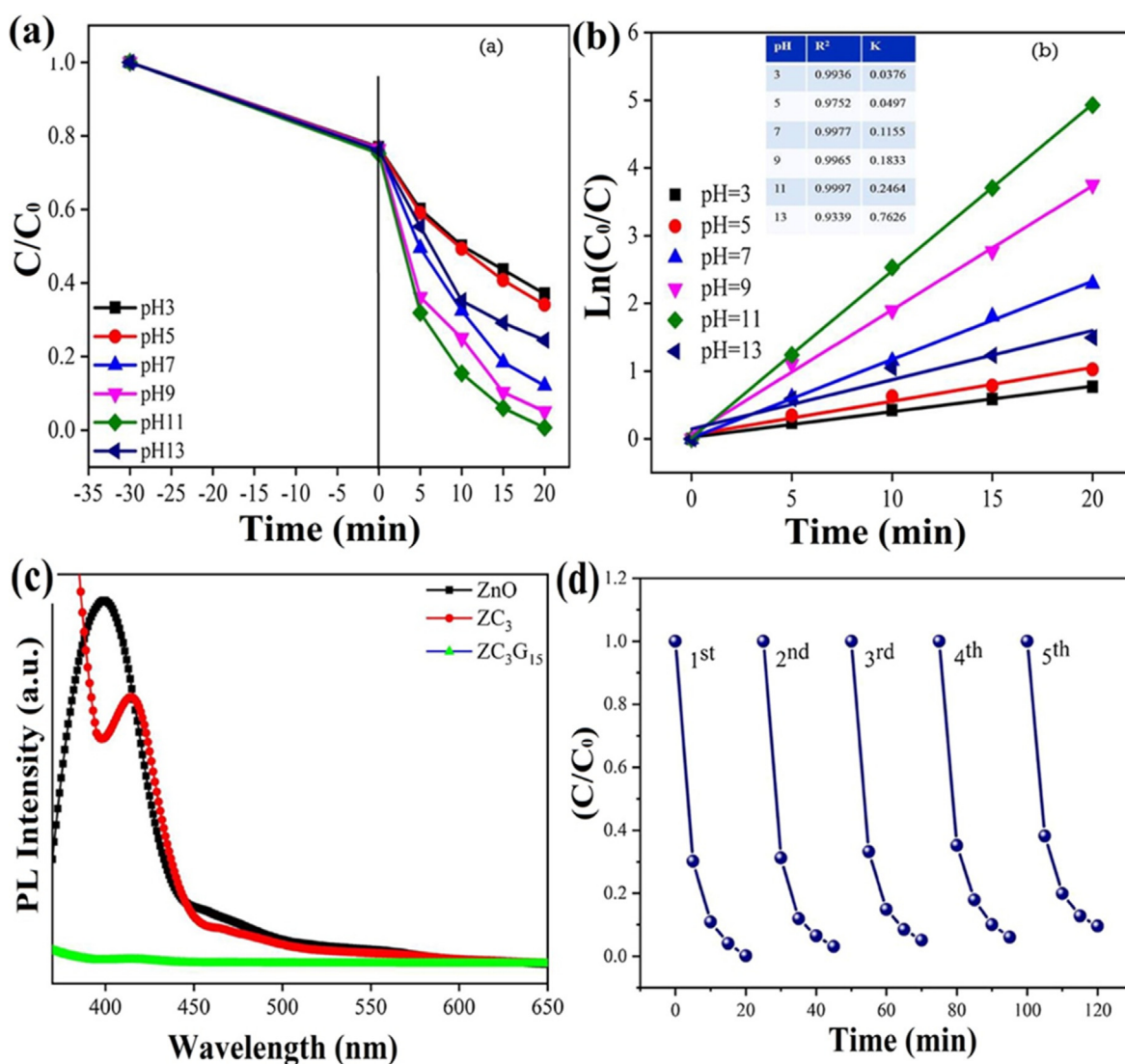
Fig. 14 (a) PL spectrum of ZnO, ZC_3 nanocomposite and ZC_3G_{15} ternary nanocomposites, Effect of different concentration on RhB dye degradation efficiency (b) (C_o/C) versus time plot, (c) Ln (C_o/C) versus time plot for ZC_3G_{15} ternary nanocomposites and (d) recycle test of ZC_3G_{15} ternary nanocomposites against RhB dye. (Reprinted with permission from Ref. Kumaresan et al. (2020) and copyright with License Id. 501547730).

(Salari and Sadeghinia, 2019). CuO/ZnO and Ag$_2$O/ZnO/CuO nanocomposites were fabricated from bimetallic Zn-Cu metal-organic structures *via* temperature-programmed oxidation method. BET surface area of Ag$_2$O/ZnO/CuO (30.8 m^2/g) was higher than ZnO/CuO (26.6 m^2/g) heterostructure, which revealed enhanced adsorption properties. The fabricated ternary nanocomposite exhibited increased photodegradation rate (almost 100% at pH 6.5) with 0.153 min^{-1} rates constant in comparison to binary nanocomposite having a 0.087 min^{-1} rates constant.

Hence, we conclude that type-II heterostructure construction played a critical role in efficient electron-hole pair separation and minimizing the possibility of photogenerated charge carriers recombination; thereby, promoting the photocatalytic performance. However, sometimes band edges alignment or electron trapping (defects or impurity sites) causes charge carriers recombination to some extent and lowered charge separation efficacy. As a result, a modern advanced approach, *i.e.* Z-scheme photocatalyst system, has attracted attention to overcome the limitations of single-component photocatalysts and heterostructures as well as satisfy those requirements above.

3.2. Z-scheme heterojunction photocatalyst system

Z-scheme systems have been classified into three forms, *i.e.,* traditional redox mediator Z-scheme photocatalytic system, all-solid-state (ASS) Z-scheme photocatalytic system and direct Z-scheme photocatalytic system, which have been discussed below:

(i) In traditional redox mediator Z-scheme photocatalytic system, two PS are joined together with an electron mediator such as Fe^{3+}/Fe^{2+}, I$^-$/IO^{3-}, etc. causing electron transference from PS-I to PS-II. Furthermore, electrons from CB of PS are attributed by electron acceptor (A), and holes from VB of second PS are accommodated by electron donor (D), resulting in more significant redox potential participation in reduction and oxidation reaction, respectively.

(ii) In all-solid-state (ASS) Z-scheme photocatalytic system, Z-scheme photocatalyst constructs contact by a trustworthy mediator (such as Ag, Au, etc.) at the interface of two semiconductors.

(iii) Direct Z-scheme photocatalytic system possesses a direct contact between two PS semiconductors without any redox mediator and follows a shorter pathway for migration of photogenerated electrons (Fig. 15).

3.2.1. Traditional electron mediator Z-scheme system

In traditional electron mediator Z-scheme photocatalytic system, reversible redox mediators such as Fe^{3+}/Fe^{2+}, IO$_3^-$/I$^-$ and NO$_3^-$/NO$_2^-$ are primarily served as electron transport chain. This Z-scheme system shows thermodynamically downhill reactions in most cases due to the occurrence of undesirable backward reactions. Also, redox mediators strongly absorb visible light, reducing light absorptivity of semiconductor photocatalyst. Therefore, the Z-scheme system without redox mediators and solid-state mediators are necessary to develop for improved photocatalytic activity.

3.2.2. CuO based ASS Z-scheme heterojunction system

In this heterostructure system, it is necessary to maintain ohmic contact between VB of PS-I and CB of PS-II rather than the Schottky barrier by employing solid mediators (Ag, Au, Ir, etc.) to inhibit EHP recombination. The use of these solid mediators improves chemical stability in aqueous solutions and reduces photocorrosion resistance phenomenon. Plenty of studies have been reported on ASS Z-scheme photocatalytic system for the last few years. Ma et al. reported Ag$_3$PO$_4$/CuO heterostructure representing a combination of Vis-light photocatalyst (Ag$_3$PO$_4$ having bandgap 2.45 eV) and Fenton-like CuO catalysis prepared using ion exchange and hydrothermal technique by regulating the molar ratio of Ag$_3$PO$_4$ to CuO (Ma et al., 2017). Synthesized Ag$_3$PO$_4$/CuO heterostructure performed as a proficient photocatalyst and degraded organic pollutants in the presence of H$_2$O$_2$. FESEM images of Ag$_3$PO$_4$/CuO heterostructure in different molar ratios of Ag$_3$PO$_4$ to CuO were depicted in (Fig. 16a–c). Here, NPs < 10 nm were homogeneously introduced at polyhedrons surface indicated that Ag$^+$ marked variations in CuO microstructure by the annihilation of interaction between CuO NPs. Ag$_3$PO$_4$/CuO heterostructure (1:1 M ratio) not only exhibited the best photocatalytic activity (100% in 20 min) for RhB photodegradation in the presence of H$_2$O$_2$ with higher rate constant of 0.345 min^{-1} but also exhibited strong stability even after five runs of recyclability. The addition of different quenchers (benzoquinone, *tert*-butanol, and EDTA-2Na) inhibited RhB degradation and confirmed the generation of $\cdot$O$_2^-$, $\cdot$OH, and h$^+$ reactive species during photocatalysis reaction (Fig. 16d). Schematic mechanism of RhB degradation through Ag$_3$PO$_4$/CuO heterostructure in the presence of H$_2$O$_2$ was shown in (Fig. 17a). It was clearly interpreted from the mechanism that CB (−0.46 eV) electrons of CuO were suitably more negative to lowered adsorbed O$_2$ into $\cdot$O$_2^-$ species whereas VB (1.1 eV) holes of CuO exhibited no oxidative capability to degrade dye due to low oxidation potential. However, Ag$_3$PO$_4$/CuO heterostructure followed the Z-scheme photocatalysis pathway, where CB electrons of CuO reacted with O$_2$ to give $\cdot$O$_2^-$ radicals, which led to RhB degradation and VB holes of Ag$_3$PO$_4$ directly oxidized RhB and revealed increased electron-hole separation.

Similarly, Rukibuddin and co-workers prepared CuO/Ag$_3$AsO$_4$/GO (graphene oxide) nanocomposite *via* electrostatic employed self-assembled technique (Rakibuddin et al., 2017). CuO/Ag$_3$AsO$_4$/GO ternary composite with bandgap 1.41 eV and BET surface area 170 m^2/g exhibited lower PL emission intensity and greater separation efficacy of photoexcited charge carriers that indicated increased photodegradation activity. Under the vis-light region, phenol degradation was 85% in 20 min using CuO/Ag$_3$AsO$_4$/GO nanocomposite with 1.9 × 10^{-1} rate constant and was found to be highest than CuO/Ag$_3$AsO$_4$ (52% in 20 min) and Ag$_3$AsO$_4$/GO (62% in 20 min) nanocomposite. Also, curcumin functionally deposited CuO/Ag (c-C/Ag) nano heterostructure was proved to be an excellent nanocomposite for MO degradation under vis-light irradiation (Kumar et al., 2019a, 2019b). Here, curcumin (multifunctional conjugated structural chain of 21 carbons) offered photosensitizer in solar cells and proved an active photocatalyst in superoxide generation to yield Vis-light photocatalysis activity. In comparison to bare CuO, c-C/Ag composite (bandgap 1.5 eV) exhibited the best
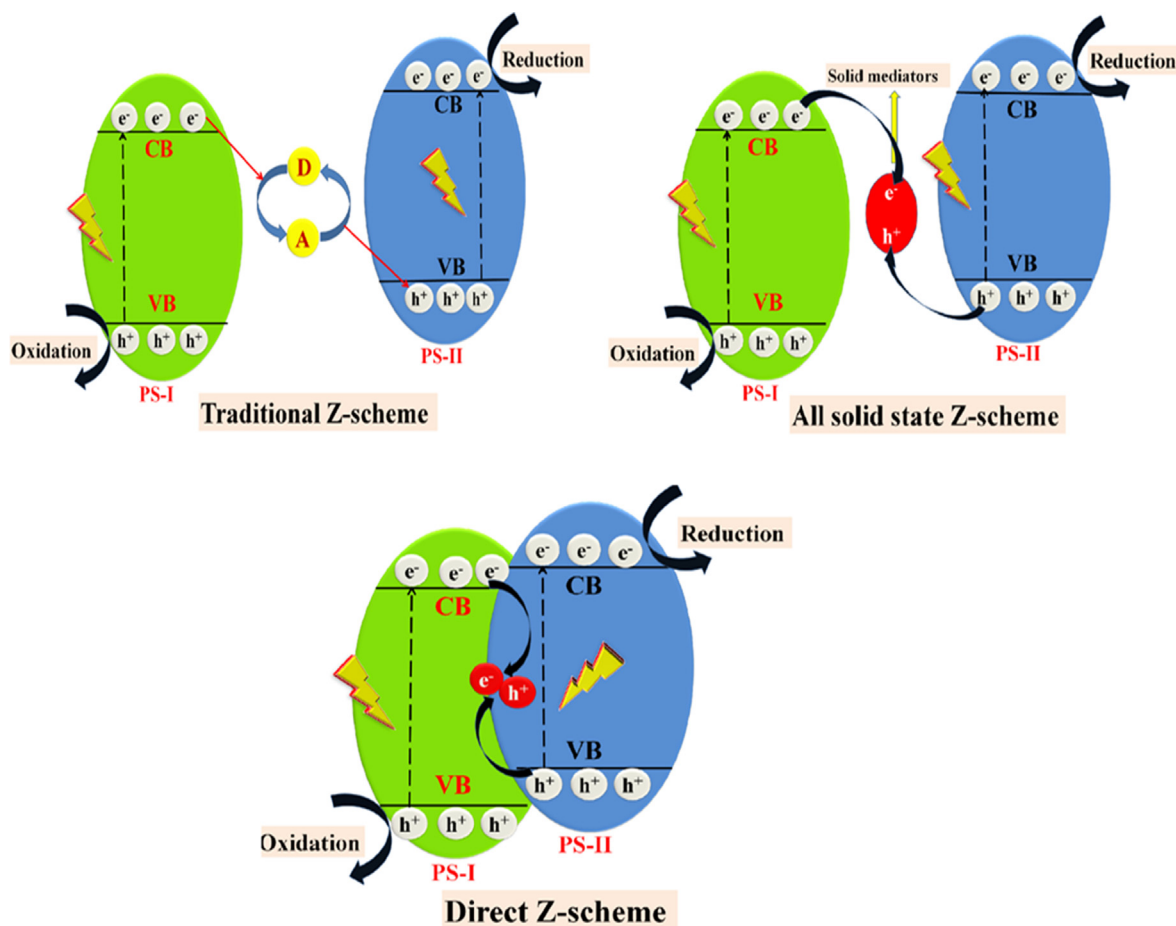
Fig. 15 Schematic mechanism growth of Z-scheme based photocatalysis: (a) traditional Z-scheme system, (b) ASS Z-scheme system and (c) direct Z-scheme system.

photodegradation activity (almost 100% with 0.0157 s^{-1} rates constant) for MO photodegradation. According to bandgap alignment, the proposed Z-scheme mechanism of the photocatalysis pathway, as illustrated in (Fig. 17b). Z-scheme mechanism explored that the Ag group offered bridge for electrons transference from CB of (0.56 eV) CuO to highest occupied molecular orbital (HOMO) of curcumin, *i.e.,* 0.55 eV. Holes in VB (2.06 eV) of CuO, as well as electrons at the lowest occupied molecular orbital (LUMO) of curcumin *i.e.,* −2.09 eV, remained as such to react with the pollutant. Photoexcitation caused the accumulation of holes in VB of CuO and electrons in LUMO of curcumin. These remaining electrons and holes enhanced charge separation, thus augmented photocatalytic degradation, whereas photoexcited electrons in electrons in LUMO of curcumin reacted with adsorbed O_2 to convert it into $\cdot O_2^-$ species. TEM (transmission electron microscopy) results confirmed that high degradation efficiency was mainly due to the correct amount of added Ag group (Fig. 18a–c).

Similarly, Xu et al. successfully synthesized ternary Ag/CuO/ZnO heterojunction nanotubes *via* simple and low-temperature chemical and photochemical deposition methods (Xu et al., 2017). Ag/CuO/ZnO nanotubes possessed distinct hollow shape and size of 1D ZnO nanotubes, which helped to develop blocks for core-shell structural constructions

(Fig. 18d). Selected area electron diffraction (SAED) and high-resolution TEM (HRTEM) analysis depicted Ag/CuO/ZnO core-shell nanotubes where d-spacing of Ag plane (110) at 0.14 nm, CuO plane (111) at 0.23 nm, ZnO plane (100) at 0.28 nm were observed. ZnO nanotubes were acquired as vertically self-assembled with Ag and CuO NPs at the outer and inner surface, respectively (Fig. 18e, f). UV–Visible absorption spectrum revealed ZnO nanorods only responded to UV region (380 nm), whereas ZnO nanotubes extended to the visible region resulting in more significant potential of absorption, which enhanced EHP generation and degradation capability (Fig. 18g). Furthermore, Ag/CuO/ZnO composite nanotubes exhibit enlarged BET surface area (19.85 m^2/g) in comparison to Ag/CuO/ZnO nanorods (1.77 m^2/g) and stability in degradation efficiency remained constant after each cycle whereas decreased from 46% to 5% after twenty recycles in Ag/CuO/ZnO nanorods. In the photodegradation mechanism of Ag/CuO/ZnO nanotubes, under visible light fall on CuO photocatalyst, photoexcited electrons were transferred from VB to CB leaving behind holes in VB. These excited electrons then migrated to CB of ZnO (acted as photoelectronic acceptor), which further adsorbed by O_2 to obtain $\cdot O_2^-$ species whereas holes stimulated in an opposite path which oxidized H_2O into $\cdot OH$ species and reacted with organic pollutant to yield CO_2 and H_2O.
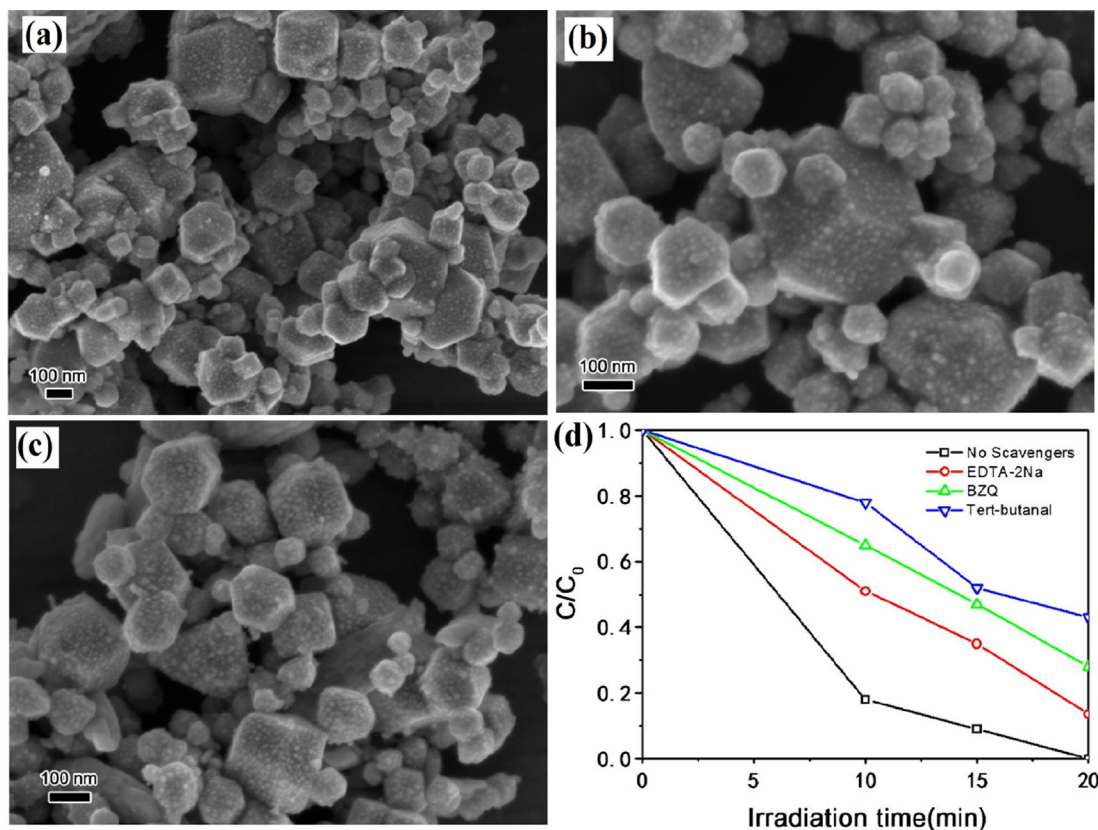
Fig. 16 FESEM image of Ag$_3$O$_4$/CuO composite with different Ag$_3$O$_4$ to CuO molar ratios of (a) 1:1, (b) 0.5:1, (c) 0.33:1 and (d) effect of variant scavengers on photocatalysis activity of Ag$_3$O$_4$/CuO composite with 100 mL of H$_2$O$_2$. (Reprinted with permission from Ref. Ma et al. (2017) and copyright with License Id. 4771870019276).
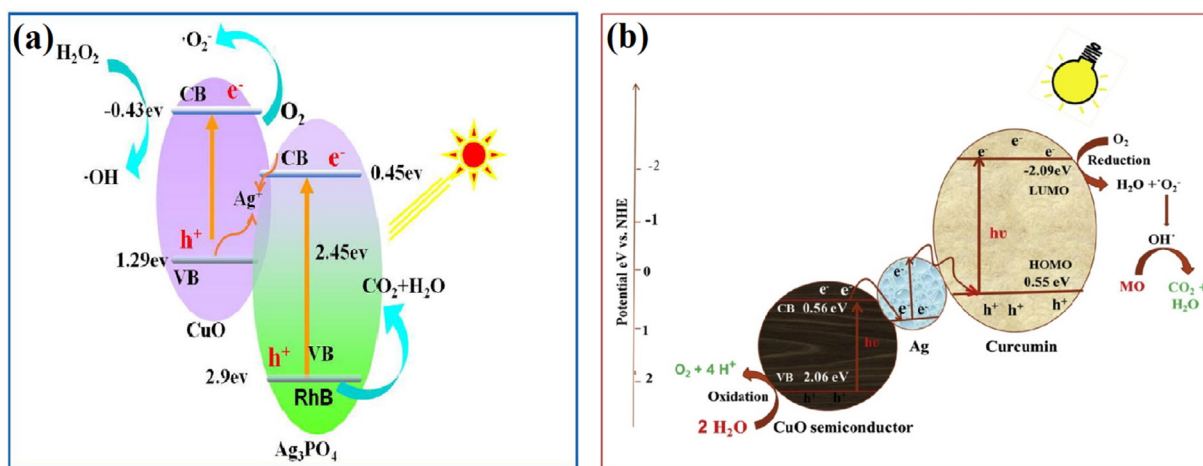
Fig. 17 (a) Schematic mechanism growth of Ag$_3$O$_4$/CuO heterostructure in presence of H$_2$O$_2$ under Visible light region and (b) Z-scheme mechanism of photocatalysis activity indulged in photodegradation of methyl orange. (Reprinted with permission from Ref. Ma et al. (2017), Kumar et al. (2019a, 2019b) and copyright with License Id. 4771870019276, 4774840674530).

3.2.3. CuO based direct Z-scheme heterojunction system

Direct Z-scheme PS possesses feasible EHP stimulation than type-II heterostructure due to higher redox potential and electron transference from CB of one PS to VB of another PS, which is due to electrostatic interaction between EHP. Ruan et al. prepared ZnO/CuO heterostructure for acid orange 7

degradation by employing a microwave-assisted technique using zinc acetate and cupric acetate as a precursor (Ruan et al., 2020). In (Fig. 19a), acid orange 7 degradation was depicted as 64.1%, 80.5%, 56.4% and 47.8% by using ZnO/CuO(0.1) (3.22 eV bandgap), ZnO/CuO(2.0) (3.20 eV bandgap) and ZnO/CuO(5.0) (3.23 eV bandgap) heterostructure
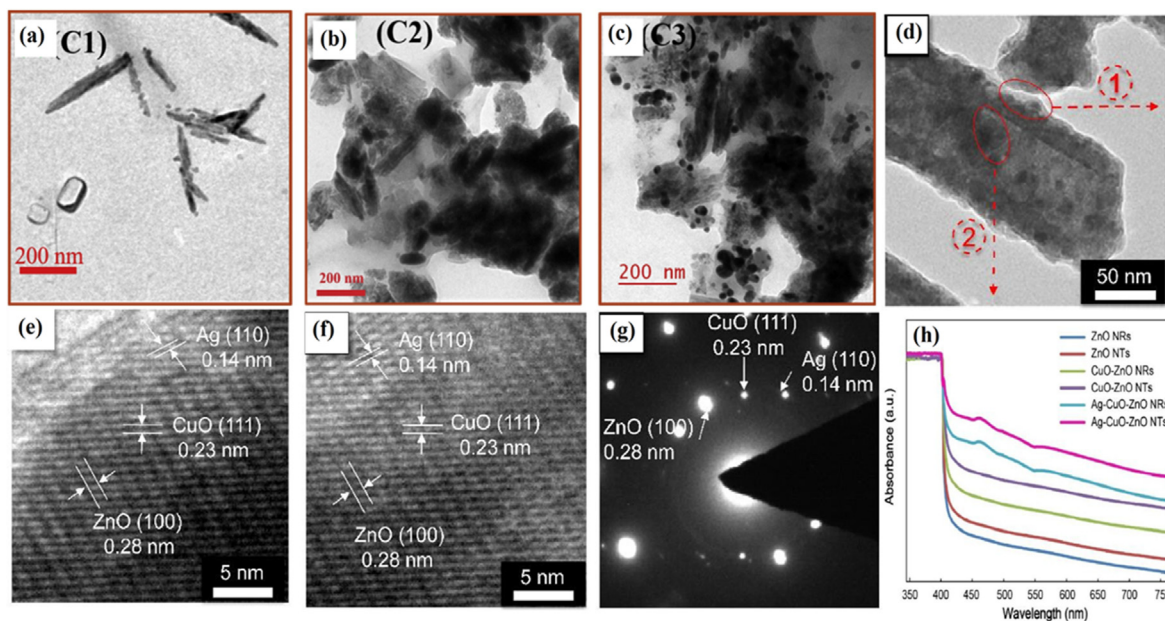
Fig. 18 TEM image of curcumin functionalized CuO/Ag samples with distinct amount of alkaline curcumin *i.e.* (a) 1.95×10^{-4} M, (b) 1×10^{-4} M, (c) 1×10^{-3} M, (d) TEM image of Ag/CuO/ZnO nanotubes composites, (e) HRTEM photos of areas introduced by red circles in (d) in respect of inner and outer surfaces and (f) SAED pattern of nanocomposite mentioned in (d) and (g) UV–Visible spectrum of pure ZnO nanotubes and nanorods, binary (CuO/ZnO) and ternary composite of Ag/CuO/ZnO nanotubes and nanorods. (Reprinted with permission from Ref. Kumar et al. (2019a, 2019b), Xu et al. (2017) and copyright with License Id. 4774840674530 and Royal society of chemistry).
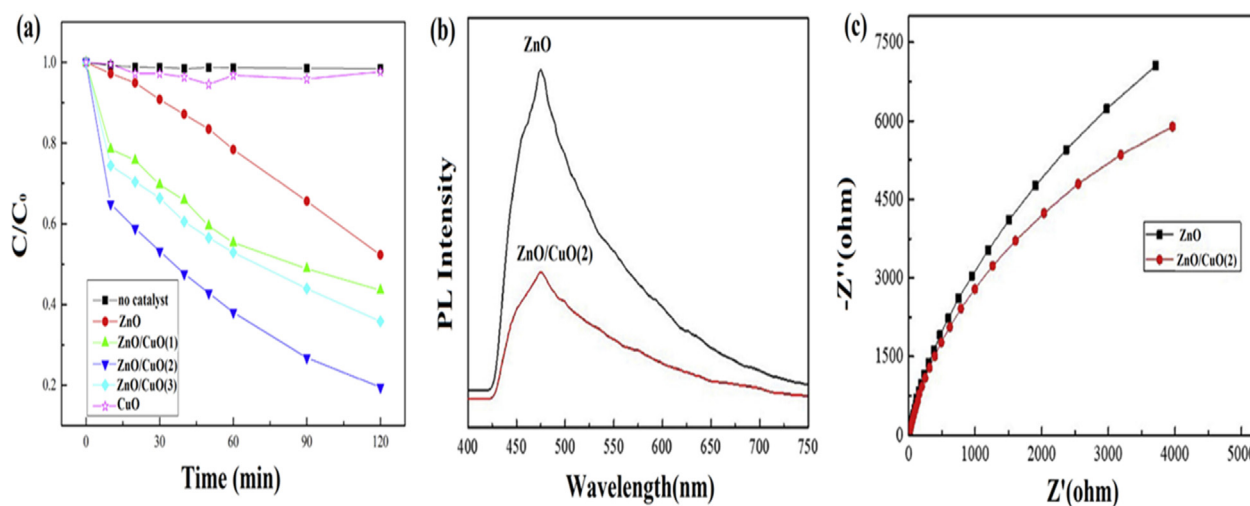
Fig. 19 (a) Degradation of acid orange 7 under solar light irradiation, (b) PL spectrum of ZnO and ZnO/CuO(2) and (c) EIS spectrum of ZnO and ZnO/CuO(2). (Reprinted with permission from Ref. Ruan et al. (2020) and copyright with License Id. 4774850102079.

and bare ZnO, respectively which revealed highest photodegradation efficiency by ZnO/CuO(2.0) nanocomposite. PL and electrochemical impedance spectroscopy (EIS) results confirmed that ZnO/CuO (2.0) quenched excited emission and relative weaker intensity peak (475 nm) (Fig. 19b), as well as lower semicircle arc displayed in (Fig. 19c), indicated fast carriers simulation capability with a lowered rate of electron-hole pair recombination. In the Z-scheme mechanism of ZnO/CuO nanocomposite, photoexcited electrons stimulated from (-0.27 eV) CB of ZnO to (0.49 eV) VB of CuO leaving elec-

trons at CuO CB and holes at ZnO VB which further reacted and lowered recombination at ZnO surface. Due to negative CB potential (-0.92 eV) of CuO, photoexcited electrons reduced adsorbed O_2 into $\cdot O_2^-$ species and simultaneously positive VB potential of ZnO (3.01 eV) oxidized H_2O into $\cdot OH$ species thereby increased photodegradation efficacy (Fig. 20). Similarly, Catano et al. prepared ZnO/CuO nanocomposite by electrochemical deposition method using $Zn(NO_3)_2$ and $CuSO_4$ as precursors for photocatalytic mineralization of methyl orange (Catano et al., 2018). By coupling of CuO
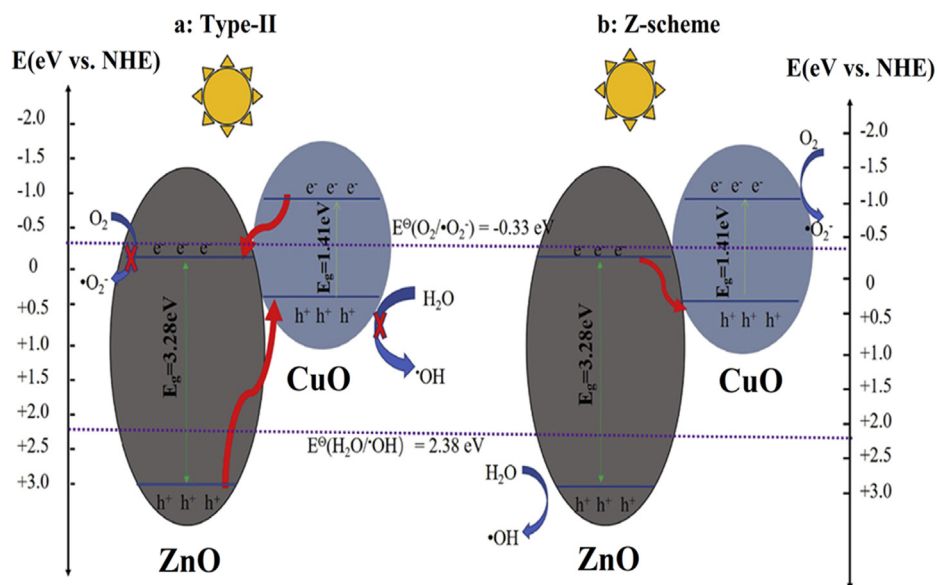
Fig. 20 Z-scheme mechanism growth of ZnO/CuO composite under solar light irradiation. (Reprinted with permission from Ref. Ruan et al. (2020) and copyright with License Id. 4774850102079).

(1.48 eV bandgap) with ZnO (3.22 eV bandgap), more number of EHP were produced, and extension in light absorptivity 464.8 nm was observed. Thus, in the Z-scheme mechanism of ZnO/CuO nanocomposite, photogenerated electrons migration occurred from CB (-0.24 eV) of ZnO to VB (1.02 eV) of CuO due to more negative potential of ZnO CB. Since electrons and holes remained in CB of CuO and VB of ZnO, respectively; thus, holes at VB (2.98 eV) edge of ZnO participated in oxidation reaction by oxidizing methyl orange directly into $\cdot$OH species. Moreover, trapped electrons at CB (-0.46) of CuO reduced adsorbed O_2 into $\cdot O_2^-$ species.

3.3. Doping with rare earth and transition metals

Doping of rare earth and transition metals elements in CuO leads to narrowing in the bandgap, absorption in the visible region gives higher optical activity that facilitates concentration of contaminants molecules at CuO surface, and enhances light sensitivity of CuO NPs. Thus, to enhance charge carrier transference, modification in CuO NPs is done by employing a growth process, *i.e.*, doping strategy, which helps in organic pollutant photodegradation. Incorporation of dopants into pure CuO nanostructure results in greater photodegradation efficiency due to the following aspects:

  i. Improved electrical conduction
  ii. Enlarged surface area
  iii. High dopant concentration increases degradation efficacy
  iv. Temperature variations modify degradation capability
  v. Strong recyclability

The introduction of selective metal (doping of rare earth and transition metals) into CuO NPs creates structural and interstitial defects that changed crystallite size, electronic and optical properties. For example, Shaghaghi and co-workers

fabricated Er-doped CuO NPs through thermal decomposition of Cu (II) Salophen based complexes constituting nitro, Bromo, and chloro functional groups as precursors with 0.2% Er^{3+} for the degradation of Reactive Black 5 dye (RB-5) (Shaghaghi et al., 2020). UV–visible spectrum and PL results depicted similar bandgap energy for both Er-doped CuO and pure CuO, *i.e.*, 3.60 eV. A significant decline in emission intensity (380–480 nm) was observed, which finally vanished after Er^{3+} doping. Electron transmission from CB (0.46 eV) of CuO to Er^{3+} species further reduced to Er^{2+} after interaction with adsorbed O_2, which was converted into $\cdot O_2^-$ species. Produced $\cdot O_2^-$ reactive species further assisted in photodegradation reaction, and the highest percentage of RB-5 dye degradation was attained using Er-doped CuO. Similarly, the enlarged surface area of Er-doped CuO (24.585 m^2/g) than bare CuO (9.1841 m^2/g) resulted in structural conversion from nonporous to mesoporous. Devi et al. prepared Tb doped CuO NPs with a 1.7 eV bandgap *via* the combustion method and annealed at diverse temperature conditions using Cu $(NO_3)_2^-$ $\cdot 3H_2O$ and Tb $(NO_3)_3 \cdot 6H_2O$ as precursors (Devi et al., 2017). The synthesized Tb doped CuO nanoparticles were employed for methylene blue (MB) degradation. DRS results depicted asymmetrical absorption band because of electrons migration to Cu^{2+} group under visible range, while Tb dopants in CuO caused surface defects due to blue shift in the absorption region. BET surface area of Tb doped CuO decreased from 27.793 m^2/g to 15.597 m^2/g for synthesized photocatalysts at 600 °C temperature, which was mainly owed to grain-like structure that lowered pore volume. Thus, photodegradation efficiency of Tb doped CuO NPs was found to be 91% and 94% when annealed at 600 and 800 °C in 120 min, respectively. However, the degradation efficiency decreased from 92% to 84%, with the rise in temperature for pure CuO under the same reaction conditions. Thus, temperature variation and type of dopant species led to a modification in degrading capability. Rodney and his peer group prepared

La-doped CuO NPs employing a solution combustion method using $Cu(NO_3)_2 \cdot 3H_2O$ and $La(NO_3)_3 \cdot 6H_2O$ starting materials in order to scrutinize their structural, morphological and optical possessions (Rodney et al., 2018). UV–visible spectrum confirmed strong absorption for 3%, 2%, and 1% of La-doped CuO at wavelength 662, 619, and 581 nm with relative bandgap energy, i.e., 1.95, 2.01 and 2.07 eV, respectively. However, increased dopants concentration showed a gradual dip in the bandgap, which confirmed redshift in the bandgap. This redshift was mainly attributed to the presence of La in CuO NPs vacancies, which resulted in the generation of dopants energy levels that enhanced optical activity. La-doped CuO nanocomposite exhibited maximum removal efficiency, i.e., 98% in 90 min for MB dye degradation in the presence of H_2O_2.

Apart from rare earth metal ion doping, transition metal ions dopants under visible region also displayed improved photocatalytic performance. Vomacka et al. reported the controlled morphological preparation of Sn doped CuO via solution technique at a lower temperature using $CuSO_4 \cdot 5H_2O$ and $SnCl_2 \cdot 2H_2O$ as a precursor (Vomáčka et al., 2016). An increase in dopant amount led to red-shift in absorption due to dropping in bandgap from 1.33 to 1.18 eV. HR-SEM results revealed different morphologies after Sn doping into bare CuO (plate-like structure) with different constituents (0.1/0.2 5/0.50/0.75/1.0 g) of Sn, which transformed into a rectangular quadric structure and finally to rod-like NPs. BET surface area was increased with the rise in doping amount such as (0.1 g) Sn doped CuO, (0.25 g) Sn doped CuO, (0.50 g) Sn doped CuO, (0.75 g) Sn doped CuO and (1.0 g) Sn doped CuO exhibited 30 26, 27, 75 and 100 m^2/g surface area, respectively compared to bare CuO (36 m^2/g). Also, UV–visible spectra confirmed improved photodegradation of RhB (99% in 2 h) when Sn (0.50 g) dopants concentration raised to 4% in (0.50 g) Sn doped CuO sample with 0.025 min^{-1} rates constant. Similarly, Zn doped copper oxide (Zn-CuO) nanofibers were fabricated by Sethuraman et al. employing the electrospinning technique by utilizing zinc acetate and copper acetate precursors. Further, synthesized Zn doped copper oxide (Zn-CuO) nanofibers were annealed at different temperatures, i.e., 600, 500, and 400 °C, providing different band gaps of 1.98, 1.94 and 1.86 eV, respectively (Sethuraman et al., 2018). Zn doped CuO (500 °C) revealed the highest photodegradation efficiency for 10 ppm of MB degradation almost 100% in 180 min at pH ~ 8 with 0.3319 min^{-1} rates constant.

3.4. Carbonaceous based CuO TMOs photocatalysis

CuO NPs, due to the lower bandgap (1.7 eV) increases the probability of charge carrier recombination rate, which decreases photocatalytic performance in degrading contaminants. To optimize this problem, variant carbonaceous materials such as graphene, graphitic carbon nitride (g-C_3N_4), carbon nanotubes (CNT), etc., have gained attention by reducing EHP recombination rate and enhancing the surface area. Carbonaceous materials as catalysts also offer support for anchoring metal oxides for pollutant adherence (Gautam et al., 2017). Khusnun et al. prepared CuO/CNT photocatalyst by employing electrolysis synthesized technique for photocatalytic degradation of p-chloroaniline (pCA) (Khusnun et al., 2018). TEM results depicted tube-shaped CNT material and a dark-colored

area (20 nm) of CuO NPs while the white line portion mentioned with value 0.242 nm was for CuO (1 1 1) plane as well as blackline portion with 0.4 nm was for CNT (0 0 2) plane (Fig. 21a, b). FTIR results confirmed the adsorption of pCA on the photocatalyst (CuO/CNT) surface through the absorption band (1257 cm^{-1}), which was ascribed to the stretching vibration of the C-N group assisting degradation activity. Removal efficiency of 10 mg/L pCA using 50 wt% CuO/CNT, 10 wt% CuO/CNT, CNT, 90 wt% CuO/CNT and CuO photocatalyst at pH ~ 7 was observed to be 97.0%, 91.8%, 84.7%, 82.1%, and 75.5%, respectively. Thus, 50 wt% CuO/CNT nanocomposite exhibited the highest number of Cu-O-C bonds which enhanced degradation efficiency (97% in 3 h) under visible region at 300 K. Furthermore, Liang et al. reported the preparation of CuO nanosheet via C_3N_4 template technique using copper nitrate, sodium citrate, and benzyl alcohol as chemicals for chlortetracycline degradation (Liang et al., 2017). Small CuO NPs were uniformly arranged on C_3N_4 nanosheets surface (2.75 eV bandgap), as shown in (Fig. 21c, d). Pt spurring on CuO nanosheet increased absorption band edges up to 750 nm, thereby enhanced EHP generation and more visible light absorption. Similarly, reduced emission band from the PL spectrum confirmed effective EHP separation. The highest photodegradation efficacy for chlortetracycline degradation was achieved with Pt/CuO nanosheet catalyst (almost 80% in 1 h) with H_2O_2. Furthermore, Duan and his peer group discussed the fabrication of CuO/g-C_3N_4 nanosheet through the chemical decomposition of melamine nitrate and copper nitrate with NH_4NO_3 (Duan, 2018). TEM and HR-TEM results depicted thin nanosheet morphology of (1.0 wt%) CuO/g-C_3N_4 nanocomposite, where small copper NPs were identified on the g-C_3N_4 surface and displayed characteristic d-spacing at 0.23 nm for CuO (1 1 1) plane. Enlarged surface area (25.97 m^2 g^{-1}) of (1.0 wt%) CuO/g-C_3N_4 photocatalyst with 1.84 eV bandgap and p-n heterostructure construction revealed enhanced charge carrier separation and excellent photodegradation efficacy (94% in 80 min) for the degradation of salicylic acid even after five recyclabilities (Fig. 21e, f).

Wang et al. discussed the preparation of CuO/g-C_3N_4 nanocomposite with supramolecular based Cu-melamine chemicals via a facile and straightforward synthesis method for RhB degradation (Wang et al., 2015). TEM and HR-TEM results of CuO/g-C_3N_4 nanocomposite confirmed nanorods shaped material with 0.158 and 0.324 nm d-spacing, which corresponded to (2 0 2) and (0 0 2) of CuO and g-C_3N_4, respectively. CuO/g-C_3N_4 nanocomposite exhibited a higher BET surface area, i.e., 15.37 m^2/g than bare g-C_3N_4 (5.26 m^2/g). Maximum RhB degradation was shown by CuO/g-C_3N_4 photocatalyst (94% in 20 min) at $\lambda > 400$ nm with strong stability after three recyclability tests whereas only 5 and 12% RhB degradation was exhibited by CuO and g-C_3N_4, respectively. In the Z-scheme proposed mechanism of CuO/g-C_3N_4 nanocomposite, photogenerated electrons were transferred from CB (−0.46 eV) of CuO (1.68 eV bandgap) to VB (1.58 eV) of g-C_3N_4 (2.7 eV bandgap). The photogenerated electrons at g-C_3N_4 surface further reacted with adsorbed oxygen to give $\cdot O_2^-$ species and thus played a significant role in degradation reaction.

Darvishi et al. prepared CuO/graphene heterojunction. via a microwave-irradiation reduction method for MB degradation using CuO and graphite oxide as chemicals (Darvishi
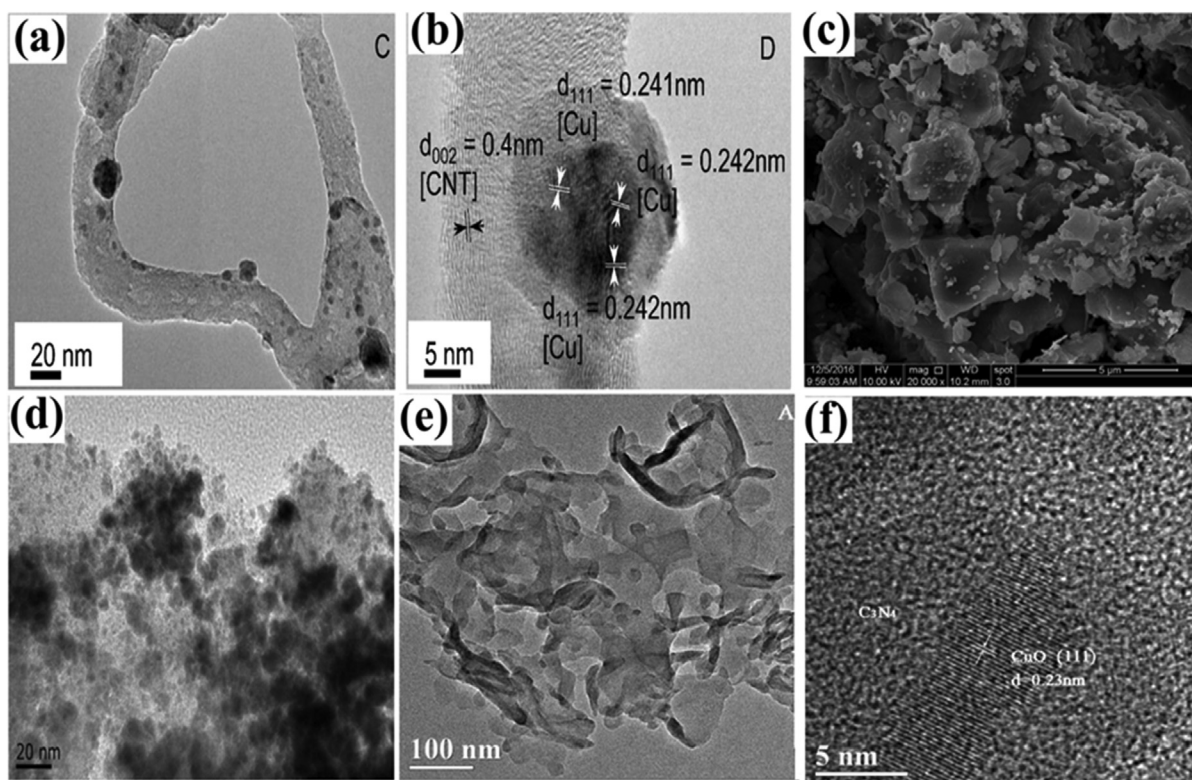
Fig. 21 TEM images of CuO/CNT photocatalyst (a) low magnified, (b) high magnified, (c) SEM image of CuO nanosheet, TEM images of (d) Pt/CuO nanosheet, (e) CuO(1.0)/g-C$_3$N$_4$ and (f) HR-TEM image of CuO(1.0)/g-C$_3$N$_4$. (Reprinted with permission from Ref. Khusnun et al. (2018), Liang et al. (2017), Duan (2018) and copyright with License Id. 4775150310916, 4775150310916, 4775141271177).

et al., 2017). Through the incorporation of graphene into CuO nanostructure, absorption in the UV range got increased as well as redshift in absorption towards higher wavelength was observed while band gap energy decreased to ~1.3 eV from ~1.4 eV. Photocatalytic activity of CuO/graphene nanocomposite containing 30% of graphene (*i.e.*, 3.051×10^{-2} cm^{-1}) exhibited 4.84 times higher of performance in MB degradation (almost 84% in 1 h) than bare CuO (30% in 1 h). Similarly, Arshad et al. prepared CuO/graphene by chemical reaction using CuCl$_2$·2H$_2$O and NaOH as precursors (Arshad et al., 2017). Here, graphene inclusion into CuO promoted photodegradation efficiency without affecting inherent properties. Graphene, due to its electrically conductive nature, increased charge carrier separation and lowered the energy bandgap to 1.39 eV. When exposed to solar light illumination, CuO/-graphene nanocomposite displayed improved (99.44% degradation in 80 min) MB photodegradation efficiency than pure CuO (75% in 80 min) (see Table 1).

4. Current scenario and future aspects

4.1. Current scenario

The mineralization and photodegradation efficacy (technical evaluation), as well as reaction economics (economic evaluation), play a vital role in the selection of the particular type of photocatalyst for a wide range of applications, including heterogeneous photocatalysis. Overall, reaction conditions can be improved by varying reaction parameters, which affects overall treatment costs. The process parameters include the use of non-toxic additives, altering pH conditions, and a low dose of the catalyst by recyclability could achieve significant cost reduction and environmentally friendly. To promote photocatalysis efficiency, photocatalyst should exhibit high surface area, low charge recombination, and extended visible light absorption. Moreover, distinct variant strategies can be employed to enhance photocatalytic performance *via* doping, heterostructures formation etc. Various earth-abundant photocatalyst, including metal sulfides (Lee and Wu, 2017) and metal oxides (Kumaravel et al., 2019) have been widely investigated to enhance photocatalyst performance. However, they exhibit limitations due to photocorrosive nature in comparison to other supported photocatalyst used with CuO. Nonetheless, most photocatalyst utilizes carbon materials (Fu et al., 2018), non-metals and noble metals like Pd (Luna et al., 2017), Ru (Ouyang et al., 2018), Ag (Qin et al., 2016), Rh (Shen et al., 2013), Au (Ma et al., 2019), Ir (Xiao et al., 2017) and Pt (Zhang et al., 2015) but less in commercial use due to their inherent drawbacks of high cost and scarcity. Recently, sufficient efforts have been made to replace noble metals with earth-abundant materials due to their unique properties such as chemical stability, low cost, and non-toxicity. Among variant semiconductor-based photocatalyst (metal oxides), CuO has achieved great attention for photodegradation due to low cost and successful degradation of non-biodegradable and toxic compounds (Table 2).

Table 1 Summary of binary and ternary CuO based heterostructures for photocatalysis of pollutant degradation.

Heterostructure	Synthetic method/Precursor	Light source	Band gap (eV)	pH	Targeted pollutant/ Degraded products	Reactive oxidative species	Degradation efficiency (%)/time	Ref.
CuO/ZnO	Deposition/Zn(CH$_3$COO)$_2$·2H$_2$O and Cu(NO$_3$)$_2$·2.5H$_2$O	Xe lamp (λ > 420 nm)	2.77 (ZnO-3.14 CuO-1.70 eV)	–	Orange II dye	·OH, ·O$_2^-$	41.8%/300 min (ZnO-9.8%)	(Yu et al., 2019)
Chitosan/ZnO/ CuO	Wet impregnation/Zn(CH$_3$COO)$_2$·2H$_2$O and CuSO$_4$·5H$_2$O	100 W high pressure Hg lamp (λ = 290–450 nm)	–	–	Fast green dye	·OH, ·O$_2^-$	91.21%/110 min (Chitosan/ZnO-71.45%)	(Alzahrani, 2018)
TiO$_2$/CuO	Ultrasonic assisted sol–gel/Tetra-n butylorthotitanate and CuSO$_4$·5H$_2$O	50 W LED lamp (λ > 405 nm)	1.5 (TiO$_2$-3.17)	4	Direct red 16	·OH, ·O$_2^-$	100%/120 min	(Zangeneh et al., 2020)
CuO/Li$_3$BO$_3$	Pechini sol–gel/LiSO$_4$·H$_2$O, Cu(NO$_3$)$_2$·3H$_2$O and ethylene glycol	400 W Osram lamp (λ > 340–530 nm)	3.11 (Li$_3$BO$_3$- 3.3)	10	Acid violet 7	·OH, ·O$_2^-$, h$^+$	80%/150 min	(Ranjeh et al., 2020)
CuO/Cu(OH)$_2$	Co-precipitation/CuSO$_4$·5H$_2$O and liquid NH$_3$	Vilber Lourmat Multilamp (λ = 365 nm)	2.39	11	Reactive green 19A/CO$_2$, H$_2$O	·OH, ·O$_2^-$, h$^+$	98%/12 h	(Saratale et al., 2018)
TiO$_2$/CuO	Titanium isopropoxide (TTIP), CuSO$_4$·5H$_2$O and ascorbic acid (C$_6$H$_8$O$_6$)	6 W UV lamp (λ = 462 nm)	2.53 (TiO$_2$-2.95)	6.5	Methyl orange, cyanide/CO$_2$, H$_2$O	·OH	95%/210 min, (TiO$_2$-87%)	(Koohestani and Sadrnezhaad, 2016)
CuO/Cu$_2$O	Wet chemical/Cu$_2$O octahedra, polyvinylpyrrolidone (PVP) and ethylenediamine	300 W Xe lamp	–	–	Methyl orange	·OH,·O$_2^-$	90%/30 min (Cu$_2$O- less than 10% 120 min)	(Jiang et al., 2017)
CuO/TiO$_2$	Impregnation/Cu(NO$_3$)$_2$·3H$_2$O, nano TiO$_2$ and NaCl	300 W Xenon arc lamp	–	–	Methylene blue	·O$_2^-$	99%/5h	(Simamora et al., 2012)
CuO/ZnO	Hydrothermal/ZnO, trimethylamine, CuO and NaOH	Sunlight	–	3.93	Direct Blue 71	·OH	97%/180 min (ZnO-7%)	(Salehi et al., 2017)
Graphene/CuO	Wet chemical/CuCl$_2$·2H$_2$O, graphene nanoplatelets and NaOH	Sunlight	(CuO-1.66 GNPs-1.39)	–	Methylene blue	·OH, ·O$_2^-$, h$^+$	99.44%/80 min	(Arshad et al., 2017)
CuO/BiVO$_4$	Polyol-reduction/Bi(NO$_3$)$_3$·5H$_2$O, Cu(CH$_3$COO)$_2$ and ethylene glycol	100 W Xe lamp (λ = 420 nm)	2.30	7	Bisphenol-A/ CO$_2$, H$_2$O	·OH,·CO$_3^-$	95%/5 min	(Kanigaridou et al., 2017)
CuO/Co$_3$O$_4$	Hydrothermal/cobaltous nitrate, ethylene glycol and urea	500Xe lamp (λ = 325 nm)	–	–	Methylene blue	·OH,·O$_2^-$	56%/180 min (CuO-40%)	(Chen et al., 2015)
CuO/Pb$_2$O$_3$	Wet chemical/Copper nitrate, Lead chloride and ethanol	300 W Xe lamp (λ > 420 nm)	1.28 (Pb$_2$O$_3$-3.0, CuO-1.15)	11	Rose bengal dye/ CO$_2$, H$_2$O	·OH,·O$_2^-$	99%/90 min (Pb$_2$O$_3$-30%, CuO-64%)	(Kamaraj et al., 2018)
CuO/CuCr$_2$O$_4$	Reflux condensation/Cu(NO$_3$)$_2$·3H$_2$O, Cr(NO$_3$)$_2$·9H$_2$O and ammonium hydroxide	300 W Xe lamp	1.23 (CuCr$_2$O$_4$- 1.40)	–	Methyl orange and methylene blue	·OH,·O$_2^-$	97.16%, 98.16%	(Mageshwari et al., 2015)
CuO/Cu$_2$O/Cu	Sonochemical combined thermal synthesis/Copper acetate monohydratye, ammonia	Blue LED lamp	1.42	6	Methylene blue	·OH, ·O$_2^-$, h$^+$	91.91%/90 min (Cu/Cu$_2$O-67%/120 min)	(Mosleh et al., 2018)
Fe$_3$O$_4$/CuO/ rGO	Low temperature hydrothermal/ FeCl$_3$·6H$_2$O, ethylene glycol and Cu(OAc)$_2$	500 W Xe lamp (λ > 420 nm)	1.5 (Fe3O4@CuO-1.87)	10	Methylene blue/ CO$_2$	·OH, ·O$_2^-$, h$^+$	98.7%/150 min (Fe$_3$O$_4$/RGO-27.6%, CuO/RGO-45.7%)	(Ding et al., 2016)

Table 1 (*continued*)

Heterostructure	Synthetic method/Precursor	Light source	Band gap (eV)	pH	Targeted pollutant/ Degraded products	Reactive oxidative species	Degradation efficiency (%)/time	Ref.
ZnAl LDH/g-C₃N₄/CuO NPs	Calcination/Al(NO₃)₂·9H₂O, Zn (NO₃)₂·6H₂O and Cu(OAc)₂·H₂O	125 W UV lamp ($\lambda > 365$ nm)	3.10 (ZnAlLDH/ CuONP-2.50, g-C₃N₄-2.70 eV)	6.5	phenol	·OH, ·O₂⁻	85%/1h (ZnAlLDH/CuONP-63%), ZnAlLDH-5%)	(Mureseanu et al., 2017)
CuO/CuS/Cu	Simple surface oxidation process/Cu mesh, (NH4)₂S₂O₈, NH₃	500 W (a xenon lamp	1.63 (CuS-1.90, CuO-1.40)	–	Methylene blue	·OH	98.6%/40 min (Cu(OH)₂/Cu 90.8%, CuO/Cu-88.1%)	(Wu et al., 2020)
CuO-Fe₃O₄	One-step coprecipitation/FeCl₃·6H₂O, FeCl₂·4H₂O, CuCl₂·2H₂O	300 W Xe lamp	1.69	7.0	(p-arsanilic acid) p-ASA/CO₂, H₂O	·OH, ·O₂⁻	100%/32 min	(Sun et al., 2018)
CuO/WO₃/CdS	Isoelectric point method/Cu (NO₃)₂·3H₂O, NaOH, NaWO₄·2H₂O, Na₂S·9H₂O and CdCl₂·2.5H₂O	300 W xenon lamp	CuO-1.76, WO₃-2.87, CdS-2.33	3.0	Methylene blue/ CO₂, H₂O and inorganic ions	e⁻, h⁺	87.11%/4h, (6.4-fold of CuO/CdS, 2.2-fold of CuO/WO₃ and 1.7-fold of CdS/ WO₃)	(Wang et al., 2019)
Ag₃PO₄/CuO	In- situ precipitation method/Cu (Ac)₂·H₂O, AgNO₃, PVP, NaH₂PO₄·2H₂O, Na₂HPO₄·12H₂O, 125 H₂O₂(30%), Na₃PO₄·12H₂O, and Ethanol	125 W, a UV lamp	Ag₃PO₄-2.45, CuO-1.7	–	Phenol/CO₂, H₂O	·OH, ·O₂⁻	Ag₃PO₄/CuO catalyst exhibits 2-fold of CuO and 1.5-fold of Ag₃PO₄ on the addition of H₂O₂	(Ma et al., 2017)
g-C₃N₄/CuO	Simple liquid phase synthesis process/ Melamine, H₂O₂, Cu(Ac)₂·H₂O and hexamethylenetermine (HMT)	300 W Xe lamp with a UV filter,	–	–	Rhodamine B (RhB)/CO₂, H₂O	·O₂⁻	100%/5 min (g-C₃N₄-28% CuO-30%)	(Hong et al., 2016)

Table 2 Techno-economic analysis of CuO based photocatalyst.

Heterostructure Photocatalyst	Supportive photocatalyst	Earth abundant	Magnetic separations	Recyclability	Visible/Solar Light active photocatalyst	Ref.
CuO/Fe_3O_4	Fe_3O_4	✔	✔	✔	✔	(Sun et al., 2018)
$CuO/BiVO_4$	$BiVO_4$	✔	✔	✗	✔	(Kanigaridou et al., 2017)
CuO/ZnO	ZnO	✔	✔	✗	✔	(Yu et al., 2019)
CuO/TiO_2	TiO_2	✔	✗	✔	✔	(Zangeneh et al., 2020)
CuO/Cu_2O	Cu_2O	✔	✗	✔	✔	(Jiang et al., 2017)
CuO/CuS	CuS	✔	✔	✔	✔	(Wu et al., 2020)
CuO/CdS	CdS	✗	✗	✔	✔	(Wang et al., 2019)
CuO/Ag_3PO_4	Ag_3PO_4	✗	✗	✔	✔	(Ma et al., 2017)
CuO/Ag	Ag	✗	✗	×	✔	(Yang et al., 2014)
CuO/Ag	Ag	✗	✗	✔	✔	(Chang and Guo, 2019)
CuO/CNT	CNT	✗	✗	✗	✔	(Khusnun et al., 2018)
$CuO/graphene$	graphene	✗	✗	✗	✗	(Darvishi et al., 2017)
$CuO/g-C_3N_4$	$g-C_3N_4$	✔	✗	✔	✔	(Ruan et al., 2015)
$CuO/g-C_3N_4$	$g-C_3N_4$	✔	✗	✔	✔	(Hong et al., 2016)
$g-C_3N_4$/layer double hydroxide (LDH)	$g-C_3N_4$	✔	✔	✗	✔	(Mureseanu et al., 2017)

4.2. Future aspects

In this updated review, variant recognized strategies have been systematically mentioned to obtain improved photocatalytic activity of CuO TMOs. Several prominent applications based on CuO heterojunction construction have been enlightened. Although the tailored architecture of CuO nanocomposite have achieved attention as discussed in this review, numerous challenges and future aspects in new direction still needs to be explored;

- CuO NPs exhibits distinct, well-defined morphologies through several synthetic techniques, but the development of mechanism insight responsible for CuO fabrication still needs to be investigated.
- Heterojunction formation provides recombination to a certain extent induced by electron trapping (impurity or defects sites) or emission (band to band) because of inappropriate band edges alignment. Thus, the Z-scheme based photocatalyst mechanism illuminated for enhanced performances is still not elucidated.
- Solar light harvesting range must be extended from visible to the near-infrared region to obtain extensive renewable solar energy for water and environment remediation. This could be done using a composite formation with bare CuO photocatalyst.
- First reports based on doping with rare earth and transition metals have been stated, but their use in a wide range of applications hindered due to cost ineffectiveness. Thus, the researcher must focus on advancements of incorporating other metals and non-metal ions as dopants for better photocatalysis activity.

- A hybrid composite of carbonaceous supported materials with bare CuO for effective photocatalysis performance has not been elucidated. More research progress must be considered to obtain photo corrosion resistivity in an aqueous mixture using CuO with a graphene layer.

5. Conclusions

In summary, it is envisaged that CuO nanostructure with tailored architecture offered practical photocatalysis ability due to efficient (0.46 eV) CB and (2.16 eV) VB potential more than standard redox potential required for photodegradation. Studies to date have shown that bare CuO is less likely to achieve sufficient efficiency and stability in photocatalysis. To enrich photocatalytic performance, construction of heterogeneous systems with other components (like CuO/CeO_2, CuO/MoS_2, CuO/Cu_2O, $ZnO/CuO/TiO_2$, $ZnO/CuO/rGO$ etc.) could combine advantages of distinct components to optimize the drawbacks of single component CuO photocatalyst. A wide range of heterostructure including binary, ternary, and Z-scheme based heterojunction have been explored for enhanced photocatalyst by improving charge separation and transportation, broad light absorption, increasing photocatalytic activity, and prolonging functional life-time. Besides, Z-scheme based nanocomposite formation of bare CuO with other metal oxides (like ZnO) giving distinct morphologies to obtain enlarged BET surface area and chemical stability in the degradation process. Also, incorporation of rare earth and transition metal ions as dopants into pure CuO creates interstitial and structural defects modifying the crystalline size, electronic and optical properties resulting in enhancement of carrier stimulation

enhancing photodegradation of pollutants. Moreover, carbonaceous materials as catalysts offer support for anchoring metal oxides for pollutant adherence. Hybrid composite of g-C_3N_4 with metal oxides, *i.e.,* p-n type heterojunction, leads to enhanced charge carriers separation with strong stability increases degradation efficiency. Therefore, up-to-date research progresses in the photodegradation phenomenon using several strategies that are systemically summarised.

Declaration of Competing Interest

The authors declare that they have no known competing financial interests or personal relationships that could have appeared to influence the work reported in this paper.

References

Abaker, M., Umar, A., Baskoutas, S., Kim, S.H., Hwang, S.W., 2011. Structural and optical properties of CuO layered hexagonal discs synthesized by a low-temperature hydrothermal process. J. Phys. D: Appl. Phys. 15, 155–405 http://iopscience.iop.org/0022-3727/44/15/155405.

Ahmad, F., Agusta, M.K., Dipojono, H.K., 2016. Electronic and optical properties of CuO based on DFT + U and GW approximation. J. Phys. Conf. Ser. 739, (1) 012040.

Ahmed, S., Rasul, M., Brown, R., Hashib, M., 2011. Influence of parameters on the heterogeneous photocatalytic degradation of pesticides and phenolic contaminants in wastewater: a short review. J. Environ. Manage. 92 (3), 311–330. https://doi.org/10.1016/j.jenvman.2010.08.028.

Alishah, H., Pourseyedi, S., Ebrahimipour, S.Y., Mahani, S.E., Rafiei, N., 2017. Green synthesis of starch-mediated CuO nanoparticles: preparation, characterization, antimicrobial activities and in vitro MTT assay against MCF-7 cell line. Rendiconti Lincei 28 (1), 65–71. https://doi.org/10.1007/s12210-016-0574-y.

Alzahrani, E., 2018. Chitosan membrane embedded with ZnO/CuO nanocomposites for the photodegradation of fast green dye under artificial and solar irradiation. J. Anal. Chem. Insights 13. https://doi.org/10.1177/1177390118763361.

Ameri, B., Davarani, S.S.H., Roshani, R., Moazami, H.R., Tadjarodi, A., 2017. A flexible mechanochemical route for the synthesis of copper oxide nanorods/nanoparticles/nanowires for supercapacitor applications: The effect of morphology on the charge storage ability. J. Alloys Compd. 695, 114–123. https://doi.org/10.1016/j.jallcom.2016.10.144.

Ameta, R., Benjamin, S., Ameta, A., Ameta, S.C., 2013. Photocatalytic degradation of organic pollutants: a review. Mater. Sci. Forum. 734, 247–272. https://doi.org/10.37023/ee.6.2.5.

Anandan, S., Yang, S., 2007. Emergent methods to synthesize and characterize semiconductor CuO nanoparticles with various morphologies–an overview. J. Exp. Nanosci. 2 (1–2), 23–56. https://doi.org/10.1080/17458080601094421.

Arshad, A., Iqbal, J., Siddiq, M., Ali, M.U., Ali, A., Shabbir, H., Saleem, M.S., 2017. Solar light triggered catalytic performance of graphene-CuO nanocomposite for waste water treatment. J. Ceram. Int. 43 (14), 10654–10660. https://doi.org/10.1016/j.ceramint.2017.03.165.

Åsbrink, S., Norrby, L.J., 1970. A refinement of the crystal structure of copper (II) oxide with a discussion of some exceptional esd's. Acta Crystallogr., Sect. B: Struct. Sci. Cryst. Eng. Mater. 26 (1), 8–15. https://doi.org/10.1107/S0567740870001838.

Bai, H., Liu, Z., Sun, D.D., 2012. Solar-light-driven photodegradation and antibacterial activity of hierarchical TiO_2/ZnO/CuO material. Chem. Plus. Chem. 77 (10), 941–948. https://doi.org/10.1002/cplu.201200131.

Behzadifard, Z., Shariatinia, Z., Jourshabani, M., 2018. Novel visible light driven CuO/$SmFeO_3$ nanocomposite photocatalysts with enhanced photocatalytic activities for degradation of organic pollutants. J. Mol. Liq. 533–548. https://doi.org/10.1016/j.molliq.2018.04.126.

Belaissa, Y., Nibou, D., Assadi, A.A., Bellal, B., Trari, M., 2016. A new hetero-junction p-CuO/n-ZnO for the removal of amoxicillin by photocatalysis under solar irradiation. J. Taiwan Inst. Chem. E. 68, 254–265. https://doi.org/10.1016/j.jtice.2016.09.002.

Bhaduri, A., Kajal, 2019. Facile synthesis and characterization of cupric oxide (CuO) nanoparticles: Inexpensive and abundant candidate for light harvesting. In: AIP Conference Proceedings, vol. 2093, No. 1. AIP Publishing LLC, p. 020047. https://doi.org/10.1063/1.5097116.

Bhosale, M.A., Bhanage, B.M., 2017. A simple, additive free approach for synthesis of Cu/Cu_2O nanoparticles: effect of precursors in morphology selectivity. J. Cluster Sci. 28 (3), 1215–1224. https://doi.org/10.1007/s10876-016-1124-6.

Bhosale, M.A., Bhatte, K.D., Bhanage, B.M., 2013. A rapid, one pot microwave assisted synthesis of nanosize cuprous oxide. Powder Technol. 235, 516–519. https://doi.org/10.1016/j.powtec.2012.11.006.

Bhosale, M.A., Karekar, S.C., Bhanage, B.M., 2016. Room temperature synthesis of copper oxide nanoparticles: morphological evaluation and their catalytic applications for degradation of dyes and C-N bond formation reaction. Chem. Select 1 (19), 6297–6307. https://doi.org/10.1002/slct.201601484.

Bordbar, M., Sharifi-Zarchi, Z., Khodadadi, B., 2017. Green synthesis of copper oxide nanoparticles/clinoptilolite using Rheum palmatum L. root extract: high catalytic activity for reduction of 4-nitro phenol, rhodamine B, and methylene blue. J. Sol-Gel Sci. Technol. 81 (3), 724–733. https://doi.org/10.1007/s10971-016-4239-1.

Bouzaida, I., Ferronato, C., Chovelon, J.M., Rammah, M.E., Herrmann, J.M., 2004. Heterogeneous photocatalytic degradation of the anthraquinonic dye, Acid Blue 25 (AB25): a kinetic approach. J. Photoch. Photobiol. 168 (1–2), 23–30. https://doi.org/10.1016/j.jphotochem.2004.05.008.

Brillas, E., 2014. A review on the degradation of organic pollutants in waters by UV photoelectro-Fenton and solar photoelectro-Fenton. J. Braz. Chem. 25 (3), 393–417. https://doi.org/10.5935/0103-5053.20130257.

Catano, F.A., Caceres, G., Burgos, A., Schrebler, R.S., 2018. Synthesis and characterization of a ZnO/CuO/Ag composite and its application as a photocatalyst for methyl orange degradation. Int. J. Electrochem. Sci 13, 9242–9256. https://doi.org/10.20964/2018.10.08.

Chandel, N., Sharma, K., Sudhaik, A., Raizada, P., Hosseini-Bandegharaei, A., Thakur, V.K., Singh, P., 2020. Magnetically separable ZnO/$ZnFe_2O_4$ and ZnO/$CoFe_2O_4$ photocatalysts supported onto nitrogen doped graphene for photocatalytic degradation of toxic dyes. Arab. J. Chem. 13, 4324–4340. https://doi.org/10.1016/j.arabjc.2019.08.005.

Chang, Y.C., Guo, J.Y., 2019. Double-sided plasmonic silver nanoparticles decorated copper oxide/zinc oxide heterostructured nanomaces with improving photocatalytic performance. J. Photoch. Photobiol. A 378, 184–191. https://doi.org/10.1016/j.jphotochem.2019.04.036.

Chawla, M., Sharma, V., Randhawa, J.K., 2017. Facile one pot synthesis of CuO nanostructures and their effect on nonenzymatic glucose biosensing. Electrocatalysis 8 (1), 27–35. https://doi.org/10.1007/s12678-016-0337-7.

Chen, R.X., Zhu, S.L., Mao, J., Cui, Z.D., Yang, X.J., Liang, Y.Q., Li, Z.Y., 2015. Synthesis of CuO/Co_3O_4 coaxial heterostructures for efficient and recycling photodegradation. Int. J. Photoenergy 2015. https://doi.org/10.1155/2015/183468.

Chen, Z., Jiao, Z., Pan, D., Li, Z., Wu, M., Shek, C.H., Wu, C.L., Lai, J.K., 2012. Recent advances in manganese oxide nanocrystals:

fabrication, characterization, and microstructure. Chem. Rev. 112 (7), 3833–3855. https://doi.org/10.1021/cr2004508.

Cudennec, Y., Lecerf, A., 2003. The transformation of Cu (OH)$_2$ into CuO, revisited. J. Solid. State Sci. 5 (11–12), 1471–1474. https://doi.org/10.1016/j.solidstatesciences.2003.09.009.

Cuevas, R., Durán, N., Diez, M.C., Tortella, G.R., Rubilar, O., 2015. Extracellular biosynthesis of copper and copper oxide nanoparticles by Stereum hirsutum, a native white-rot fungus from chilean forests. J. Nanomater. 2015. https://doi.org/10.1155/2015/789089.

Dar, M.A., Ahsanulhaq, Q., Kim, Y.S., Sohn, J.M., Kim, W.B., Shin, H.S., 2009. Versatile synthesis of rectangular shaped nanobat-like CuO nanostructures by hydrothermal method; structural properties and growth mechanism. Appl. Surf. Sci. 255 (12), 6279–6284. https://doi.org/10.1016/j.apsusc.2009.02.002.

Dar, M.A., Nam, S.H., Kim, Y.S., Kim, W.B., 2010. Synthesis, characterization, and electrochemical properties of self-assembled leaf-like CuO nanostructures. J. Solid State. Electr. 14 (9), 1719–1726. https://doi.org/10.1007/s10008-010-1022-z.

Darvishi, M., Mohseni-Asgerani, G., Seyed-Yazdi, J., 2017. Simple microwave irradiation procedure for the synthesis of CuO/Graphene hybrid composite with significant photocatalytic enhancement. J. Surf. 7, 69–73. https://doi.org/10.1016/j.surfin.2017.02.007.

Das, S., Srivastava, V.C., 2016. Synthesis and characterization of copper succinate and copper oxide nanoparticles by electrochemical treatment: Optimization by Taguchi robust analysis. Canadian J. Chem. Eng. 94 (7), 1322–1327. https://doi.org/10.1002/cjce.22478.

Devi, L.V., Sellaiyan, S., Selvalakshmi, T., Zhang, H.J., Uedono, A., Sivaji, K., Sankar, S., 2017. Synthesis, defect characterization and photocatalytic degradation efficiency of Tb doped CuO nanoparticles. Adv. Powder Technol. 28 (11), 3026–3038. https://doi.org/10.1016/j.apt.2017.09.013.

Ding, J., Liu, L., Xue, J., Zhou, Z., He, G., Chen, H., 2016. Low-temperature preparation of magnetically separable Fe$_3$O$_4$@CuO-RGO core-shell heterojunctions for high-performance removal of organic dye under visible light. J. Alloys Compd. 688, 649–656. https://doi.org/10.1016/j.jallcom.2016.07.001.

Do, H.-T., Phan Thi, L.-A., Dao Nguyen, N.H., Huang, C.-W., Le, Q.V., Nguyen, V.-H., 2020. Tailoring photocatalysts and elucidating mechanisms of photocatalytic degradation of perfluorocarboxylic acids (PFCAs) in water: a comparative overview. J. Chem. Technol. Biotechnol. https://doi.org/10.1002/jctb.6333.

Duan, Y., 2018. Facile preparation of CuO/g-C$_3$N$_4$ with enhanced photocatalytic degradation of salicylic acid. J. Mater. Res. 105, 68–74. https://doi.org/10.1016/j.materresbull.2018.04.038.

Dutta, V., Sharma, S., Raizada, P., Hosseini-Bandegharaei, A., Gupta, V.K., Singh, P., 2019a. Review on augmentation in photocatalytic activity of CoFe$_2$O$_4$ via heterojunction formation for photocatalysis of organic pollutants in water. J. Saudi. Chem. Soc. https://doi.org/10.1016/j.jscs.2019.07.003.

Dutta, V., Singh, P., Shandilya, P., Sharma, S., Raizada, P., Saini, A.K., Rahmani-Sani, A., 2019b. Review on advances in photocatalytic water disinfection utilizing graphene and graphene derivatives-based nanocomposites. J. Environ. Chem. Eng. 7, 103–132. https://doi.org/10.1016/j.jece.2019.103132.

Ekuma, C.E., Anisimov, V.I., Moreno, J., Jarrell, M., 2014. Electronic structure and spectra of CuO. Eur. Phys. J. B 87 (1). https://doi.org/10.1140/epjb/e2013-40949-5.

Eltarahony, M., Zaki, S., Abd-El-Haleem, D., 2018. Concurrent synthesis of zero-and one-dimensional, spherical, rod-, needle-, and wire-shaped CuO nanoparticles by Proteus mirabilis 10B. J. Nanomater. 2018. https://doi.org/10.1155/2018/1849616.

Figueroa, M.G., Gana, R.E., Cooper, W.C., Ji, J., 1993. Electro-chemical production of cuprous oxide using the anode-support system. J. Appl. Electrochem. 23 (4), 308–315. https://doi.org/10.1007/BF00296685.

Filipič, G., Cvelbar, U., 2012. Copper oxide nanowires: a review of growth. Nanotechnology 23, (19). https://doi.org/10.1088/0957-4484/23/19/194001 194001.

Fu, J., Yu, J., Jiang, C., Cheng, B., 2018. g-C$_3$N$_4$-based heterostructured photocatalysts. J. Adv. Energ. Mat. 8 (3), 170–1503. https://doi.org/10.1002/aenm.201701503.

Fujishima, A., Honda, K., 1972. Electrochemical photolysis of water at a semiconductor electrode. Nature 238 (5358), 37–38. https://doi.org/10.1038/238037a0.

Gautam, S., Shandilya, P., Priya, B., Singh, V.P., Raizada, P., Rai, R., Valente, M.A., Singh, P., 2017. Superparamagnetic MnFe$_2$O$_4$ dispersed over graphitic carbon sand composite and bentonite as magnetically recoverable photocatalyst for antibiotic mineralization. Sep. Purif. Technol. 172, 498–511. https://doi.org/10.1016/j.seppur.2016.09.006.

Glaze, W.H., 1987. Drinking-water treatment with ozone. J. Environ. Sci. Technol. 21 (3), 224–230. https://doi.org/10.1021/es00157a001.

Gusain, R., Khatri, O.P., 2013. Ultrasound assisted shape regulation of CuO nanorods in ionic liquids and their use as energy efficient lubricant additives. J. Mater. Chem. A 1 (18), 5612–5619. https://doi.org/10.1039/C3TA10248C.

Hasija, V., Raizada, P., Sudhaik, A., Sharma, K., Kumar, A., Singh, P., Thakur, V.K., 2019a. Recent advances in noble metal free doped graphitic carbon nitride based nanohybrids for photocatalysis of organic contaminants in water: a review. J. Appl. Mater. Today 15, 494–524. https://doi.org/10.1016/j.jphotochem.2004.05.008.

Hasija, V., Raizada, P., Sudhaik, A., Singh, P., Thakur, V.K., Khan, A.A.P., 2020. Fabrication of Ag/AgI/WO$_3$ heterojunction anchored P and S co-doped graphitic carbon nitride as a dual Z scheme photocatalyst for efficient dye degradation. Solid State Sci. 100, 106095.

Hasija, V., Sudhaik, A., Raizada, P., Hosseini-Bandegharaei, A., Singh, P., 2019b. Carbon quantum dots supported AgI/ZnO/phosphorus doped graphitic carbon nitride as Z-scheme photocatalyst for efficient photodegradation of 2, 4-dinitrophenol. J. Environ. Chem. Eng. 7 (4), 103–272. https://doi.org/10.1016/j.jece.2019.103272.

Herrmann, J.M., 1999. Heterogeneous photocatalysis: fundamentals and applications to the removal of various types of aqueous pollutants. J. Catal. Today 53 (1), 115–129. https://doi.org/10.1016/S0920-5861(99)00107-8.

Hoffmann, M.R., Martin, S.T., Choi, W., Bahnemann, D.W., 1995. Environmental applications of semiconductor photocatalysis. Chem. Rev. 95 (1), 69–96. https://doi.org/10.1021/cr00033a004.

Honary, S., Barabadi, H., Gharaei-Fathabad, E., Naghibi, F., 2012. Green synthesis of copper oxide nanoparticles using Penicillium aurantiogriseum, Penicillium citrinum and Penicillium waksmanii. Dig. J. Nanomater. Bios. 7 (3), 999–1005.

Hong, S., Yu, Y., Yi, Z., Zhu, H., Wu, W., Ma, P., 2016. Highly efficient and recyclable g-C$_3$N$_4$/CuO hybrid nanocomposite towards enhanced visible-light photocatalytic performance. Nano 11 (11), 1650121. https://doi.org/10.1142/S1793292016501216.

Jana, R., Dey, A., Das, M., Datta, J., Das, P., Ray, P.P., 2018. Improving performance of device made up of CuO nanoparticles synthesized by hydrothermal over the reflux method. Appl. Surf. Sci. 452, 155–164. https://doi.org/10.1016/j.apsusc.2018.04.262.

Jiang, D., Xue, J., Wu, L., Zhou, W., Zhang, Y., Li, X., 2017. Photocatalytic performance enhancement of CuO/Cu$_2$O heterostructures for photodegradation of organic dyes: effects of CuO morphology. J. Appl. Catal. B. Environ. 211, 199–204. https://doi.org/10.1016/j.apcatb.2017.04.034.

Kabra, K., Chaudhary, R., Sawhney, R.L., 2004. Treatment of hazardous organic and inorganic compounds through aqueous-phase photocatalysis: a review. Ind. Eng. Chem. Res. 43 (24), 7683–7696. https://doi.org/10.1021/ie0498551.

Kamaraj, E., Somasundaram, S., Balasubramani, K., Eswaran, M.P., Muthuramalingam, R., Park, S., 2018. Facile fabrication of CuO-

Pb$_2$O$_3$ nanophotocatalyst for efficient degradation of Rose Bengal dye under visible light irradiation. Appl. Surf. Sci. 433, 206–212. https://doi.org/10.1016/j.apsusc.2017.09.139.

Kanigaridou, Y., Petala, A., Frontistis, Z., Antonopoulou, M., Solakidou, M., Konstantinou, I., Kondarides, D.I., 2017. Solar photocatalytic degradation of bisphenol A with CuOx/BiVO$_4$: insights into the unexpectedly favorable effect of bicarbonates. Chem. Eng. 318, 39–49. https://doi.org/10.1016/j.cej.2016.04.145.

Karami, H., Afshari, B., 2017. Square Pulse Galvanostatic Synthesis and Characterization of Nano-Copper Oxide. Int. J. Electrochem. Sci 12 (2), 1492–1505. https://doi.org/10.20964/2017.02.50.

Kerour, A., Boudjadar, S., Bourzami, R., Allouche, B., 2018. Eco-friendly synthesis of cuprous oxide (Cu$_2$O) nanoparticles and improvement of their solar photocatalytic activities. J. Solid State Chem. 263, 79–83. https://doi.org/10.1016/j.jssc.2018.04.010.

Khusnun, N.F., Jalil, A.A., Triwahyono, S., Hitam, C.N.C., Hassan, N.S., Jamian, F., Hartanto, D., 2018. Directing the amount of CNTs in CuO–CNT catalysts for enhanced adsorption-oriented visible-light-responsive photodegradation of p-chloroaniline. Powder technol. 327, 170–178. https://doi.org/10.1016/j.powtec.2017.12.052.

Konstantinou, I.K., Albanis, T.A., 2004. TiO$_2$-assisted photocatalytic degradation of azo dyes in aqueous solution: kinetic and mechanistic investigations: a review. J. Appl. Catal. B. Environ. 49 (1), 1–14. https://doi.org/10.1016/j.apcatb.2003.11.010.

Koohestani, H., Sadrnezhaad, S.K., 2016. Photocatalytic degradation of methyl orange and cyanide by using TiO$_2$/CuO composite. J. Desalin. Water Treat. 57 (46), 22029–22038. https://doi.org/10.1080/19443994.2015.1132395.

Kum, J.M., Yoo, S.H., Ali, G., Cho, S.O., 2013. Photocatalytic hydrogen production over CuO and TiO$_2$ nanoparticles mixture. Int. J. Energy 38 (31), 13541–13546. https://doi.org/10.1016/j.ijhydene.2013.08.004.

Kumar, A., Raizada, P., Singh, P., Saini, R., Saini, A., Hosseini-Bandegharaei, A., 2019a. Perspective and status of polymeric graphitic carbon nitride based Z-scheme photocatalytic systems for sustainable photocatalytic water purification. J. Energy. Chem. 123–496. https://doi.org/10.1016/j.cej.2019.123496.

Kumar, A., Saxena, A., De, A., Shankar, R., Mozumdar, S., 2013. Facile synthesis of size-tunable copper and copper oxide nanoparticles using reverse microemulsions. RSC Adv. 3 (15), 5015–5021. https://doi.org/10.1039/C3RA23455J.

Kumar, K.Y., Muralidhara, H.B., Nayaka, Y.A., Hanumanthappa, H., Veena, M.S., Kumar, S.K., 2014. Hydrothermal synthesis of hierarchical copper oxide nanoparticles and its potential application as adsorbent for Pb (II) with high removal capacity. Sep. Sci. Technol. 49 (15), 2389–2399. https://doi.org/10.1080/01496395.2014.922101.

Kumar, S., Pal, S., Kuntail, J., Sinha, I., 2019b. Curcumin functionalized CuO/Ag nanocomposite: Efficient visible light Z-scheme photocatalyst for methyl orange degradation. Environ. Nanotechnol. Monit. Manag. 12, 100–236. https://doi.org/10.1016/j.enmm.2019.100236.

Kumaravel, V., Mathew, S., Bartlett, J., Pillai, S.C., 2019. Photocatalytic hydrogen production using metal doped TiO$_2$: a review of recent advances. J. Appl. Catal. B: Environ. 244, 1021–1064. https://doi.org/10.1016/j.apcatb.2018.11.080.

Kumaresan, N., Sinthiya, M.M.A., Ramamurthi, K., Babu, R.R., Sethuraman, K., 2020. Visible light driven photocatalytic activity of ZnO/CuO nanocomposites coupled with rGO heterostructures synthesized by solid-state method for RhB dye degradation. Arab. J. Chem. 13, 3910–3928. https://doi.org/10.1016/j.arabjc.2019.03.002.

Lee, G.J., Wu, J.J., 2017. Recent developments in ZnS photocatalysts from synthesis to photocatalytic applications-a review. Powder Technol. 318, 8–22. https://doi.org/10.1016/j.powtec.2017.05.022.

Li, A., Song, H., Wan, W., Zhou, J., Chen, X., 2014. Copper oxide nanowire arrays synthesized by in-situ thermal oxidation as an anode material for lithium-ion batteries. Electrochim. Acta 132, 42–48. https://doi.org/10.1016/j.electacta.2014.03.123.

Li, D., Yu, J.-C.-C., Nguyen, V.-H., Wu, J.C.S., Wang, X., 2018. A dual-function photocatalytic system for simultaneous separating hydrogen from water splitting and photocatalytic degradation of phenol in a twin-reactor. Appl. Catal. B 239, 268–279. https://doi.org/10.1016/j.apcatb.2018.08.010.

Li, H., Yu, K., Lei, X., Guo, B., Li, C., Fu, H., Zhu, Z., 2015. Synthesis of the MoS$_2$@CuO heterogeneous structure with improved photocatalysis performance and H$_2$O adsorption analysis. Dalton T. 44 (22), 10438–10447. https://doi.org/10.1039/C5DT01125F.

Li, Y., Wang, F., Zhou, G., Ni, Y., 2003. Aniline degradation by electrocatalytic oxidation. Chemosphere 53 (10), 1229–1234. https://doi.org/10.1016/S0045-6535(03)00590-3.

Li, Y., Yang, X.Y., Feng, Y., Yuan, Z.Y., Su, B.L., 2012. One-dimensional metal oxide nanotubes, nanowires, nanoribbons, and nanorods: synthesis, characterizations, properties and applications. Crit. Rev. Solid. State. Mater. Sci. 37 (1), 1–74. https://doi.org/10.1080/10408436.2011.606512.

Li, Z., Liu, D., Huang, W., Sun, Y., Li, S., Wei, X., 2019. Applying facilely synthesized CuO/CeO$_2$ photocatalyst to accelerate methylene blue degradation in hypersaline wastewater. J. Surf. Interface Anal. 51 (3), 336–344. https://doi.org/10.1002/sia.6585.

Liang, S., Zhou, Y., Wu, W., Zhang, Y., Cai, Z., Pan, J., 2017. Preparation of porous CuO nanosheet-liked structure (CuO-NS) using C$_3$N$_4$ template with enhanced visible-light photoactivity in degradation of chlortetracycline. J. Photoch. 168–176. https://doi.org/10.1016/j.jphotochem.2017.06.005.

Lingaraju, K., Naika, H.R., Manjunath, K., Nagaraju, G., Suresh, D., Nagabhushana, H., 2015. Rauvolfia serpentina-mediated green synthesis of CuO nanoparticles and its multidisciplinary studies. Acta Metall. Sinica (English Letters) 28 (9), 1134–1140. https://doi.org/10.1007/s40195-015-0304-y.

Liu, F., Leung, Y.H., Djurisic, A.B., Ng, A.M.C., Chan, W.K., 2013. Native defects in ZnO: effect on dye adsorption and photocatalytic degradation. J. Phys. Chem. C 117 (23), 12218–12228. https://doi.org/10.1021/jp403478q.

Liu, J., Chen, Q., Li, J., Xiong, Q., Yue, G., Zhang, X., Yang, S., Liu, Q.H., 2016a. Facile synthesis of cuprous oxide nanoparticles by plasma electrochemistry. J. Phys. D: Appl. Phys. 49, (27). https://doi.org/10.1088/0022-3727/49/27/275201 275201.

Liu, J., He, B., Chen, Q., Liu, H., Li, J., Xiong, Q., Zhang, X., Yang, S., Yue, G., Liu, Q.H., 2016b. Plasma electrochemical synthesis of cuprous oxide nanoparticles and their visible-light photocatalytic effect. Electrochim. Acta 222, 1677–1681. https://doi.org/10.1016/j.electacta.2016.11.158.

Liu, J., Jin, J., Deng, Z., Huang, S.Z., Hu, Z.Y., Wang, L., Su, B.L., 2012. Tailoring CuO nanostructures for enhanced photocatalytic property. J. Colloid Interface Sci. 384 (1), 1–9. https://doi.org/10.3389/fchem.2018.00428.

Liu, Y., Chu, Y., Zhuo, Y., Li, M., Li, L., Dong, L., 2007. Anion-controlled construction of CuO honeycombs and flowerlike assemblies on copper foils. J. Cryst. Growth Des 7 (3), 467–470. https://doi.org/10.1021/cg060480r.

Lu, C., Qi, L., Yang, J., Zhang, D., Wu, N., Ma, J., 2004. Simple template-free solution route for the controlled synthesis of Cu (OH)$_2$ and CuO nanostructures. J. Phys. Chem. B 108 (46), 17825–17831. https://doi.org/10.1021/jp046772p.

Lu, K.-T., Nguyen, V.-H., Yu, Y.-H., Yu, C.-C., Wu, J.C.S., Chang, L.-M., Lin, A.-Y.-C., 2016. An internal-illuminated monolith photoreactor towards efficient photocatalytic degradation of ppb-level isopropyl alcohol. Chem. Eng. J. 296, 11–18. https://doi.org/10.1016/j.cej.2016.03.097.

Lu, Y., Liu, X., Qiu, K., Cheng, J., Wang, W., Yan, H., Tang, C., Kim, J.K., Luo, Y., 2015. Facile synthesis of graphene-like copper

oxide nanofilms with enhanced electrochemical and photocatalytic properties in energy and environmental applications. ACS Appl. Mater. Interfaces 7 (18), 9682–9690. https://doi.org/10.1021/acsami.5b01451.

Luna, A.L., Dragoe, D., Wang, K., Beaunier, P., Kowalska, E., Ohtani, B., Colbeau-Justin, C., 2017. Photocatalytic hydrogen evolution using Ni–Pd/TiO2: correlation of light absorption, charge-carrier dynamics, and quantum efficiency. J. Phys. Chem. 121 (26), 14302–14311. https://doi.org/10.1021/acs.jpcc.7b01167.

Ma, D., Shi, J.-W., Sun, D., Zou, Y., Cheng, L., He, C., Wang, H., Niu, C., Wang, L., 2019. Au decorated hollow ZnO@ZnS heterostructure for enhanced photocatalytic hydrogen evolution: the insight into the roles of hollow channel and Au nanoparticles. Appl. Catal. B: Environ. 244, 748–757. https://doi.org/10.1016/j.apcatb.2018.12.016.

Ma, P., Yu, Y., Xie, J., Fu, Z., 2017. Ag3PO4/CuO composites utilizing the synergistic effect of photocatalysis and Fenton-like catalysis to dispose organic pollutants. Adv. Powder Technol. 28 (11), 2797–2804. https://doi.org/10.1016/j.apt.2017.08.004.

Mageshwari, K., Sathyamoorthy, R., Lee, J.Y., Park, J., 2015. Novel CuCr2O4 embedded CuO nanocomposites for efficient photodegradation of organic dyes. Appl. Surf. Sci. 353, 95–102. https://doi.org/10.1016/j.apsusc.2015.06.027.

Mancier, V., Daltin, A.L., Leclercq, D., 2008. Synthesis and characterization of copper oxide (I) nanoparticles produced by pulsed sonoelectrochemistry. Ultrason. Sonochem. 15 (3), 157–163. https://doi.org/10.1016/j.ultsonch.2007.02.007.

Maruthupandy, M., Zuo, Y., Chen, J.S., Song, J.M., Niu, H.L., Mao, C.J., Zhang, S.Y., Shen, Y.H., 2017. Synthesis of metal oxide nanoparticles (CuO and ZnO NPs) via biological template and their optical sensor applications. Appl. Surf. Sci. 397, 167–174. https://doi.org/10.1016/j.apsusc.2016.11.118.

Mittal, A.K., Chisti, Y., Banerjee, U.C., 2013. Synthesis of metallic nanoparticles using plant extracts. Biotechnol. Adv. 31 (2), 346–356. https://doi.org/10.1016/j.biotechadv.2013.01.003.

Mosleh, S., Rahimi, M.R., Ghaedi, M., Dashtian, K., Hajati, S., 2018. Sonochemical-assisted synthesis of CuO/Cu2O/Cu nanoparticles as efficient photocatalyst for simultaneous degradation of pollutant dyes in rotating packed bed reactor: LED illumination and central composite design optimization. J. Ultrason. Sonochem. 40, 601–610. https://doi.org/10.1016/j.ultsonch.2017.08.007.

Mureseanu, M., Radu, T., Andrei, R.D., Darie, M., Carja, G., 2017. Green synthesis of g-C3N4/CuONP/LDH composites and derived g-C3N4/MMO and their photocatalytic performance for phenol reduction from aqueous solutions. Appl. Clay. Sci. 141, 1–12. https://doi.org/10.1016/j.clay.2017.02.012.

Nair, M.T.S., Guerrero, L., Arenas, O.L., Nair, P.K., 1999. Chemically deposited copper oxide thin films: structural, optical and electrical characteristics. Appl. Surf. Sci. 150, 143–151. https://doi.org/10.1016/S0169-4332(99)00239-1.

Narayanan, R., El-Sayed, M.A., 2005. Catalysis with transition metal nanoparticles in colloidal solution: nanoparticle shape dependence and stability. https://doi.org/10.1021/jp051066p.

Nasrollahzadeh, M., Sajadi, S.M., Maham, M., 2015a. Tamarix gallica leaf extract mediated novel route for green synthesis of CuO nanoparticles and their application for N-arylation of nitrogen-containing heterocycles under ligand-free conditions. RSC Adv. 5 (51), 40628–40635. https://doi.org/10.1039/C5RA04012D.

Nasrollahzadeh, M., Sajadi, S.M., Rostami-Vartooni, A., Bagherzadeh, M., 2015b. Green synthesis of Pd/CuO nanoparticles by Theobroma cacao L. seeds extract and their catalytic performance for the reduction of 4-nitrophenol and phosphine-free Heck coupling reaction under aerobic conditions. J. Colloid Interface Sci. 448, 106–113. https://doi.org/10.1016/j.jcis.2015.02.009.

Nasrollahzadeh, M., Sajadi, S.M., Rostami-Vartooni, A., Hussin, S.M., 2016. Green synthesis of CuO nanoparticles using aqueous extract of Thymus vulgaris L. leaves and their catalytic perfor-

mance for N-arylation of indoles and amines. J. Colloid Interface Sci. 466, 113–119. https://doi.org/10.1016/j.jcis.2015.12.018.

Nesa, M., Momin, M.A., Sharmin, M., Bhuiyan, A.H., 2020. Structural, optical and electronic properties of CuO and Zn doped CuO: DFT based First-principles calculations. Chem. Phys. 528,. https://doi.org/10.1016/j.chemphys.2019.110536 110536.

Nguyen, V.-H., Nguyen, B.-S., Huang, C.-W., Le, T.-T., Nguyen, C.C., Nhi Le, T.T., Heo, D., Ly, Q.V., Trinh, Q.T., Shokouhimehr, M., Xia, C., Lam, S.S., Vo, D.-V.-N., Kim, S.Y., Le, Q.V., 2020a. Photocatalytic NOx abatement: Recent advances and emerging trends in the development of photocatalysts. J. Clean. Prod. 270,. https://doi.org/10.1016/j.jclepro.2020.121912 121912.

Nguyen, V.-H., Smith, S.M., Wantala, K., Kajitvichyanukul, P., 2020b. Photocatalytic remediation of persistent organic pollutants (POPs): a review. Arab. J. Chem. 13, 8309–8337. https://doi.org/10.1016/j.arabjc.2020.04.028.

Nguyen, V.-H., Tran, Q.B., Nguyen, X.C., Le, T.H., Ho, T.T.T., Shokouhimehr, M., Vo, D.-V.-N., Lam, S.S., Nguyen, H.P., Hoang, C.T., Ly, Q.V., Peng, W., Kim, S.Y., Tra, V.T., Van Le, Q., 2020c. Submerged photocatalytic membrane reactor with suspended and immobilized N-doped TiO2 under visible irradiation for diclofenac removal from wastewater. Process Saf. Environ. Prot. https://doi.org/10.1016/j.psep.2020.05.041.

Nogueira, A.C., Gomes, L.E., Ferencz, J.A., Rodrigues, J.E., Gonçalves, R.V., Wender, H., 2019. Improved visible light photoactivity of CuBi2O4/CuO heterojunctions for photodegradation of methylene blue and metronidazole. J. Phys. Chem. 42, 25680–25690. https://doi.org/10.1021/acs.jpcc.9b06907.

Norzaee, S., Djahed, B., Khaksefidi, R., Mostafapour, F.K., 2017. Photocatalytic degradation of aniline in water using CuO nanoparticles. J. Water Supply: Res. Technol. Aqua 66 (3), 178–185. https://doi.org/10.2166/aqua.2017.104.

Ong, C.B., Ng, L.Y., Mohammad, A.W., 2018. A review of ZnO nanoparticles as solar photocatalysts: synthesis, mechanisms and applications. Renew. Sust. Energy Rev. 81, 536–551. https://doi.org/10.1016/j.rser.2017.08.020.

Ouyang, W., Munoz-Batista, M.J., Kubacka, A., Luque, R., Fernández-García, M., 2018. Enhancing photocatalytic performance of TiO2 in H2 evolution via Ru co-catalyst deposition. J. Appl. Catal. B: Environ 238, 434–443. https://doi.org/10.1016/j.apcatb.2018.07.046.

Pal, J., Ganguly, M., Mondal, C., Roy, A., Negishi, Y., Pal, T., 2013. Crystal-plane-dependent etching of cuprous oxide nanoparticles of varied shapes and their application in visible light photocatalysis. J. Phys. Chem. C 117 (46), 24640–24653. https://doi.org/10.1021/jp409271r.

Patial, S., Hasija, V., Raizada, P., Singh, P., Parwaz, A.A., Singh, K., Asiri, A.M., in press. Tunable photocatalytic activity of SrTiO3 for water splitting: Strategies and Future scenario. J. Environ. Chem. Eng. https://doi.org/10.1016/j.jece.2020.103791 (in press).

Praburaman, L., Jang, J.S., Muthusamy, G., Arumugam, S., Manoharan, K., Cho, K.M., Min, C., Kamala-Kannan, S., Byung-Taek, O., 2016. Piper betle-mediated synthesis, characterization, antibacterial and rat splenocyte cytotoxic effects of copper oxide nanoparticles. Artif. Cells, Nanomed. Biotechnol. 44 (6), 1400–1405. https://doi.org/10.3109/21691401.2015.1029630.

Priya, B., Shandilya, P., Raizada, P., Thakur, P., Singh, N., Singh, P., 2016. Photocatalytic mineralization and degradation kinetics of ampicillin and oxytetracycline antibiotics using graphene sand composite and chitosan supported BiOCl. J. Mol. Catal. A. Chem. 423, 400–413. https://doi.org/10.1016/j.molcata.2016.07.043.

Qin, J., Huo, J., Zhang, P., Zeng, J., Wang, T., Zeng, H., 2016. Improving the photocatalytic hydrogen production of Ag/gC3N4 nanocomposites by dye-sensitization under visible light irradiation. Nanoscale 8 (4), 2249–2259. https://doi.org/10.1039/C5NR06346A.

Raizada, P., Sudhaik, A., Singh, P., Shandilya, P., Thakur, P., Jung, H., 2020. Visible light assisted photodegradation of 2, 4-dinitrophenol using Ag2CO3 loaded phosphorus and sulphur co-doped

graphitic carbon nitride nanosheets in simulated wastewater. Arab. J. Chem. 13 (1), 3196–3209. https://doi.org/10.1016/j.arabjc.2018.10.004.

Raizada, P., Kumari, J., Shandilya, P., Singh, P., 2017a. Kinetics of photocatalytic mineralization of oxytetracycline and ampicillin using activated carbon supported ZnO/ZnWO₄. J. Desalin. Water. Treat. 79, 204–213. https://doi.org/10.5004/dwt.2017.20831.

Raizada, P., Shandilya, P., Singh, P., Thakur, P., 2017b. Solar light-facilitated oxytetracycline removal from the aqueous phase utilizing a H₂O₂/ZnWO₄/CaO catalytic system. J. Taibah. Univ. Sci. 11, 689–699. https://doi.org/10.1016/j.jtusci.2016.06.004.

Raizada, P., Singh, P., Kumar, A., Pare, B., Jonnalagadda, S.B., 2014a. Zero valent iron-brick grain nanocomposite for enhanced solar-Fenton removal of malachite green. Sep. Purif. Technol. 133, 42937. https://doi.org/10.1016/j.seppur.2014.07.012.

Raizada, P., Singh, P., Kumar, A., Sharma, G., Pare, B., Jonnalagadda, S.B., Thakur, P., 2014b. Solar photocatalytic activity of nano-ZnO supported on activated carbon or brick grain particles: role of adsorption in dye degradation. Appl. Catal. A. Gen. 486, 159–169. https://doi.org/10.1016/j.apcata.2014.08.043.

Raizada, P., Sudhaik, A., Singh, P., 2019a. Photocatalytic water decontamination using graphene and ZnO coupled photocatalyst: a review. J. Mater. Sci. Energy, C. 2, 509–525. https://doi.org/10.1016/j.mset.2019.04.007.

Raizada, P., Sudhaik, A., Singh, P., Hosseini-Bandegharaei, A., Thakur, P., 2019b. Converting type II AgBr/VO into ternary Z scheme photocatalyst via coupling with phosphorus doped g-C₃N₄ for enhanced photocatalytic activity. J. Sep. Purif. Technol. 115–692. https://doi.org/10.1016/j.seppur.2019.115692.

Raizada, P., Sudhaik, A., Singh, P., Shandilya, P., Gupta, V.K., Hosseini-Bandegharaei, A., Agrawal, S., 2019c. Ag₃PO₄ modified phosphorus and sulphur co-doped graphitic carbon nitride as a direct Z-scheme photocatalyst for 2, 4-dimethyl phenol degradation. J. Photochem. Photobiol A. 374, 22–35. https://doi.org/10.1016/j.jphotochem.2019.01.015.

Raizada, P., Sudhaik, A., Singh, P., Shandilya, P., Saini, A.K., Gupta, V.K., Hosseini-Bandegharaei, A., 2019d. Fabrication of Ag₃VO₄ decorated phosphorus and sulphur co-doped graphitic carbon nitride as a high-dispersed photocatalyst for phenol mineralization and E. coli disinfection. Sep. Purif. Technol. 212, 887–900. https://doi.org/10.1016/j.seppur.2018.12.007.

Rakibuddin, M., Mandal, S., Ananthakrishnan, R., 2017. A novel ternary CuO decorated Ag₃AsO₄/GO hybrid as a Z-Scheme photocatalyst for enhanced degradation of phenol under visible light. New J. Chem. 41 (3), 1380–1389. https://doi.org/10.1039/C6NJ02366E.

Ran, J., Chen, H., Bai, X., Bi, S., Jiang, H., Cai, G., Wang, X., 2019. Immobilizing CuO/BiVO₄ nanocomposite on PDA-templated cotton fabric for visible light photocatalysis, antimicrobial activity and UV protection. Appl. Surf. 493, 1167–1176. https://doi.org/10.1016/j.apsusc.2019.07.137.

Ranjeh, M., Beshkar, F., Amiri, O., Salavati-Niasari, M., Moayedi, H., 2020. Pechini sol-gel synthesis of Cu₂O/Li₃BO₃ and CuO/Li₃-BO₃ nanocomposites for visible light-driven photocatalytic degradation of dye pollutant. J. Alloys Compd. 152451. https://doi.org/10.1016/j.jallcom.2019.152451.

Ray, S.C., 2001. Preparations of copper oxide thin film by the sol–gel-like dip technique and study of their structural and optical properties. Sol. Energy. Mater. Sol. Cells 68 (3–4), 307–312. https://doi.org/10.1016/S0927-0248(00)00364-0.

Rodney, J.D., Deepapriya, S., Vinosha, P.A., Krishnan, S., Priscilla, S.J., Daniel, R., Das, S.J., 2018. Photo-Fenton degradation of nano-structured La doped CuO nanoparticles synthesized by combustion technique. Optik 161, 204–216. https://doi.org/10.1016/j.ijleo.2018.01.125.

Ruan, S., Huang, W., Zhao, M., Song, H., Gao, Z., 2020. A Z-scheme mechanism of the novel ZnO/CuO nn heterojunction for photocatalytic degradation of Acid Orange 7. J. Mat. Sci.

Semicon. Proc. 104835. https://doi.org/10.1016/j.mssp.2019.104835.

Rubilar, O., Rai, M., Tortella, G., Diez, M.C., Seabra, A.B., Durán, N., 2013. Biogenic nanoparticles: copper, copper oxides, copper sulphides, complex copper nanostructures and their applications. Biotechnol. Lett. 35 (9), 1365–1375. https://doi.org/10.1007/s10529-013-1239-x.

Safarifard, V., Morsali, A., 2014. Sonochemical syntheses of a new fibrous-like nano-scale manganese (II) coordination supramolecular compound; precursor for the fabrication of octahedral-like Mn₃O₄ nano-structure. Ultrason. Sonochem. 21 (1), 253–261. https://doi.org/10.1016/j.ultsonch.2013.05.015.

Salari, H., Sadeghinia, M., 2019. MOF-templated synthesis of nano Ag₂O/ZnO/CuO heterostructure for photocatalysis. J. Photoch. Photobio A. 376, 279–287. https://doi.org/10.1016/j.jphotochem.2019.03.010.

Salehi, K., Bahmani, A., Shahmoradi, B., Pordel, M.A., Kohzadi, S., Gong, Y., Lee, S.M., 2017. Response surface methodology (RSM) optimization approach for degradation of Direct Blue 71 dye using CuO–ZnO nanocomposite. Int. J. Environ. Sci. Te. 14 (10), 2067–2076. https://doi.org/10.1007/s13762-017-1308-0.

Sankar, R., Manikandan, P., Malarvizhi, V., Fathima, T., Shivashangari, K.S., Ravikumar, V., 2014. Green synthesis of colloidal copper oxide nanoparticles using Carica papaya and its application in photocatalytic dye degradation. Spectrochim. Acta Part A- Mol. Biomol. Spectros. 121, 746–750. https://doi.org/10.1016/j.saa.2013.12.020.

Saratale, R.G., Ghodake, G.S., Shinde, S.K., Cho, S.K., Saratale, G.D., Pugazhendhi, A., Bharagava, R.N., 2018. Photocatalytic activity of CuO/Cu(OH)₂ nanostructures in the degradation of Reactive Green 19A and textile effluent, phytotoxicity studies and their biogenic properties (antibacterial and anticancer). J. Environ. Manage. 223, 1086–1097. https://doi.org/10.1016/j.jenvman.2018.04.072.

Saravanan, R., Joicy, S., Gupta, V.K., Narayanan, V., Stephen, A.J.M.S., 2013. Visible light induced degradation of methylene blue using CeO₂/V₂O₅ and CeO₂/CuO catalysts. J. Mater. Sci. Eng. C 33 (8), 4725–4731. https://doi.org/10.1016/j.msec.2013.07.034.

Saravanan, S., Sivasankar, T., 2016. Effect of ultrasound power and calcination temperature on the sonochemical synthesis of copper oxide nanoparticles for textile dyes treatment. Environ. Prog. Sust. Energy 35 (3), 669–679. https://doi.org/10.1002/ep.12271.

Sathiya, S.M., Okram, G.S., Jothi Rajan, M.A., 2017. Structural, optical and electrical properties of copper oxide nanoparticles prepared through microwave assistance. Adv. Mater. Proceed. 2, 2215–2219. https://doi.org/10.5185/amp.2017/605.

Serpone, N., Emeline, A.V., 2012. Semiconductor Photocatalysis Past, Present, and Future Outlook, 673–677. https://doi.org/10.1021/jz300071j.

Sethuraman, R.G., Venkatachalam, T., Kirupha, S.D., 2018. Fabrication and characterization of Zn doped CuO nanofiber using newly designed nanofiber generator for the photodegradation of methylene blue from textile effluent. Mater. Sci. 36 (3), 520–529. https://doi.org/10.2478/msp-2018-0056.

Shaghaghi, Z., Amani-Ghadim, A.R., Seraji, M., 2020. Structural properties and photocatalytic degradation efficiency of CuO and Erbium doped CuO nanostructures prepared by thermal decomposition of some Cu-salophen type complexes as precursors. J. Mater. Chem. Phys. https://doi.org/10.1016/j.matchemphys.2020.122635 122635.

Shandilya, P., Mittal, D., Soni, M., Raizada, P., Hosseini-Bandegharaei, A., Saini, A.K., Singh, P., 2018a. Fabrication of fluorine doped graphene and SmVO₄ based dispersed and adsorptive photocatalyst for abatement of phenolic compounds from water and bacterial disinfection. J. Clean. Prod. 203, 386–399. https://doi.org/10.1016/j.jclepro.2018.08.271.

Shandilya, P., Mittal, D., Soni, M., Raizada, P., Lim, J.H., Jeong, D.Y., Singh, P., 2018b. Islanding of EuVO₄ on high-dispersed fluorine

doped few layered graphene sheets for efficient photocatalytic mineralization of phenolic compounds and bacterial disinfection. J. Taiwan Inst. Chem. E. 93, 528–542. https://doi.org/10.1016/j.jtice.2018.08.034.

Shandilya, P., Mittal, D., Sudhaik, A., Soni, M., Raizada, P., Saini, A.K., Singh, P., 2019. GdVO4 modified fluorine doped graphene nanosheets as dispersed photocatalyst for mitigation of phenolic compounds in aqueous environment and bacterial disinfection. Sep. Purif. Technol. 210, 804–816. https://doi.org/10.1016/j.seppur.2018.08.077.

Sharma, A., Lee, B.K., 2016a. Integrated ternary nanocomposite of TiO2/NiO/reduced graphene oxide as a visible light photocatalyst for efficient degradation of o-chlorophenol. J. Environ. Manage. 181, 563–573. https://doi.org/10.1016/j.jenvman.2016.07.016.

Sharma, A., Lee, B.K., 2016b. Structure and activity of TiO2/FeO co-doped carbon spheres for adsorptive-photocatalytic performance of complete toluene removal from aquatic environment. Appl. Catal. A: Gen. 523, 272–282. https://doi.org/10.1016/j.apcata.2016.06.018.

Sharma, A., Lee, B.K., 2016c. Rapid photo-degradation of 2-chlorophenol under visible light irradiation using cobalt oxide-loaded TiO2/reduced graphene oxide nanocomposite from aqueous media. J. Environ. Manage. 165, 1–10. https://doi.org/10.1016/j.jenvman.2015.09.013.

Sharma, A., Lee, B.K., 2017a. Photocatalytic reduction of carbon dioxide to methanol using nickel-loaded TiO2 supported on activated carbon fiber. Catal. Today 298, 158–167. https://doi.org/10.1016/j.cattod.2017.05.003.

Sharma, A., Lee, B.K., 2017b. Growth of TiO2 nano-wall on activated carbon fibers for enhancing the photocatalytic oxidation of benzene in aqueous phase. Catal. Today 287, 113–121. https://doi.org/10.1016/j.cattod.2016.11.019.

Sharma, J.K., Akhtar, M.S., Ameen, S., Srivastava, P., Singh, G., 2015. Green synthesis of CuO nanoparticles with leaf extract of Calotropis gigantea and its dye-sensitized solar cells applications. J. Alloys Compd. 632, 321–325. https://doi.org/10.1016/j.jallcom.2015.01.172.

Sharma, K., Dutta, V., Sharma, S., Raizada, P., Hosseini-Bandegharaei, A., Thakur, P., Singh, P., 2019a. Recent advances in enhanced photocatalytic activity of bismuth oxyhalides for efficient photocatalysis of organic pollutants in water: a review. J. Ind. Eng. Chem. 78 (25), 1–20. https://doi.org/10.1016/j.jiec.2019.06.022.

Sharma, S., Dutta, V., Singh, P., Raizada, P., Rahmani-Sani, A., Hosseini-Bandegharaei, A., Thakur, V.K., 2019b. Carbon quantum dot supported semiconductor photocatalysts for efficient degradation of organic pollutants in water: a review. J. Clean. Prod. https://doi.org/10.1016/j.jclepro.2019.04.292.

Shen, P., Lofaro Jr, J.C., Woerner, W.R., White, M.G., Su, D., Orlov, A., 2013. Photocatalytic activity of hydrogen evolution over Rh doped SrTiO3 prepared by polymerizable complex method. Chem. Eng. 223, 200–208. https://doi.org/10.1016/j.cej.2013.03.030.

Sherly, E.D., Vijaya, J.J., Kennedy, L.J., 2015. Visible-light-induced photocatalytic performances of ZnO–CuO nanocomposites for degradation of 2,4-dichlorophenol. J. Chinese J. Catal. 36 (8), 1263–1272. https://doi.org/10.1016/S1872-2067(15)60886-5.

Shi, W., Chopra, N., 2012. Controlled fabrication of photoactive copper oxide–cobalt oxide nanowire heterostructures for efficient phenol photodegradation. ACS Appl. Mater. Interfaces 4 (10), 5590–5607. https://doi.org/10.1021/am301488c.

Shinde, S.K., Dubal, D.P., Ghodake, G.S., Fulari, V.J., 2015. Hierarchical 3D-flower-like CuO nanostructure on copper foil for supercapacitors. RSC Adv. 5 (6), 4443–4447. https://doi.org/10.1039/C4RA11164H.

Siddiqui, H., Qureshi, M.S., Haque, F.Z., 2016. Effect of copper precursor salts: facile and sustainable synthesis of controlled shaped copper oxide nanoparticles. Optik 127 (11), 4726–4730. https://doi.org/10.1016/j.ijleo.2016.01.118.

Simamora, A.J., Hsiung, T.L., Chang, F.C., Yang, T.C., Liao, C.Y., Wang, H.P., 2012. Photocatalytic splitting of seawater and degradation of methylene blue on CuO/nano TiO2. J. Hydrogen Energ. 37 (18), 13855–13858. https://doi.org/10.1016/j.ijhydene.2012.04.091.

Singh, P., Gautam, S., Shandilya, P., Priya, B., Singh, V.P., Raizada, P., 2017a. Graphene bentonite supported ZnFe2O4 as superparamagnetic photocatalyst for antibiotic degradation. Adv. Mater. Lett. 8 (3), 229–238. https://doi.org/10.5185/amlett.2017.1467.

Singh, P., Priya, B., Shandilya, P., Raizada, P., Singh, N., Pare, B., Jonnalagadda, S.B., 2019. Photocatalytic mineralization of antibiotics using 60% WO3/BiOCl stacked to graphene sand composite and chitosan. Arab. J. Chem. 12 (8), 4627–4645. https://doi.org/10.1016/j.arabjc.2016.08.005 (in press).

Singh, P., Raizada, P., Pathania, D., Sharma, G., Sharma, P., 2013a. Microwave induced KOH activation of guava peel carbon as an adsorbent for Congo red dye removal from aqueous phase. Indian J. Chem. Technol. 20, 305–311 http://nopr.niscair.res.in/handle/123456789/21463.

Singh, P., Raizada, P., Kumari, S., Kumar, A., Pathania, D., Thakur, P., 2014. Solar-Fenton removal of malachite green with novel Fe0-activated carbon nanocomposite. Appl. Catal. A. Gen. 476, 9–18. https://doi.org/10.1016/j.apcata.2014.02.009.

Singh, P., Raizada, P., Sudhaik, A., Shandilya, P., Thakur, P., Gupta, V.K., 2019a. Enhanced photocatalytic activity and stability of AgBr/BiOBr/graphene heterojunction for phenol degradation under visible light. J. Saudi. Chem. Soc. 23, 586–599. https://doi.org/10.1016/j.jscs.2018.10.005.

Singh, P., Sharma, K., Hasija, V., Sharma, V., Sharma, S., Raizada, P., Thakur, V.K., 2019b. Systematic review on applicability of magnetic iron oxides–integrated photocatalysts for degradation of organic pollutants in water. J. Mater. Today Chem. 14, 100–186. https://doi.org/10.1016/j.mtchem.2019.08.005.

Singh, P., Sudhaik, A., Raizada, P., Shandilya, P., Sharma, R., Hosseini-Bandegharaei, A., 2019c. Photocatalytic performance and quick recovery of BiOI/Fe3O4@ graphene oxide ternary photocatalyst for photodegradation of 2, 4-dintirophenol under visible light. J. Mater. Today Chem. 12, 85–95. https://doi.org/10.1016/j.mtchem.2018.12.006.

Singh, S., Kumar, N., Kumar, M., Agarwal, A., Mizaikoff, B., 2017b. Electrochemical sensing and remediation of 4-nitrophenol using bio-synthesized copper oxide nanoparticles. Chem. Eng. J. 313, 283–292. https://doi.org/10.1016/j.cej.2016.12.049.

Singh, V.P., Jasrotia, R., Kumar, R., Raizada, P., Thakur, S., Batoo, K.M., Singh, M., 2018. A current review on the synthesis and magnetic properties of M-Type hexaferrites material. J. World J. Condens. Matter Phys. 8 2, 36. https://doi.org/10.4236/wjcmp.2018.82004.

Singh, P., Raizada, P., Pathania, D., Kumar, A., Thakur, P., 2013b. Preparation of BSA-ZnWO4 nanocomposites with enhanced adsorptional photocatalytic activity for methylene blue degradation. Int. J. Photoenergy. https://doi.org/10.1155/2013/726250.

Sivaraj, R., Rahman, P.K., Rajiv, P., Salam, H.A., Venckatesh, R., 2014. Biogenic copper oxide nanoparticles synthesis using Tabernaemontana divaricate leaf extract and its antibacterial activity against urinary tract pathogen. Spectrochim. Acta, Part A- Mol. Biomol. Spectros. 133, 178–181. https://doi.org/10.1016/j.saa.2014.05.048.

Sonu, Dutta, V., Sharma, S., Raizada, P., Hosseini-Bandegharaei, A., Gupta, V.K., Singh, P., 2019. Review on augmentation in photocatalytic activity of CoFe2O4 via heterojunction formation for photocatalysis of organic pollutants in water. J. Saudi. Chem. Soc. https://doi.org/10.1016/j.jscs.2019.07.003 (in press).

Sudhaik, A., Raizada, P., Shandilya, P., Jeong, D.Y., Lim, J.H., Singh, P., 2018a. Review on fabrication of graphitic carbon nitride based efficient nanocomposites for photodegradation of aqueous phase organic pollutants. J. Ind. Eng. Chem. 67, 28–51. https://doi.org/10.1016/j.jiec.2018.07.007.

Sudhaik, A., Raizada, P., Shandilya, P., Singh, P., 2018b. Magnetically recoverable graphitic carbon nitride and NiFe$_2$O$_4$ based magnetic photocatalyst for degradation of oxytetracycline antibiotic in simulated wastewater under solar light. J. Environ. Chem. Eng. 6 (4), 3874–3883. https://doi.org/10.1016/j.jece.2018.05.039.

Sun, S., Sun, Y., Chen, A., Zhang, X., Yang, Z., 2015. Nanoporous copper oxide ribbon assembly of free-standing nanoneedles as biosensors for glucose. Analyst 140 (15), 5205–5215. https://doi.org/10.1039/C5AN00609K.

Sun, S., Zhang, X., Cui, J., Yang, Q., Liang, S., 2019. Tuning interfacial Cu-O atomic structures for enhanced catalytic applications. Chem. Asian. J. 14 (17), 2912–2924. https://doi.org/10.1002/asia.201900756.

Sun, T., Zhao, Z., Liang, Z., Liu, J., Shi, W., Cui, F., 2018. Efficient degradation of p-arsanilic acid with arsenic adsorption by magnetic CuO-Fe$_3$O$_4$ nanoparticles under visible light irradiation. Chem. Eng. 334, 1527–1536. https://doi.org/10.1016/j.cej.2017.11.052.

Tahir, Dahlang, Tougaard, Sven, 2012. Electronic and optical properties of Cu, CuO and Cu 2 O studied by electron spectroscopy. J. Phys.: Condens. Matter 24 (17), 175002. https://doi.org/10.1088/0953-8984/24/17/175002.

Tongsakul, D., Wongravee, K., Thammacharoen, C., Ekgasit, S., 2012. Enhancement of the reduction efficiency of soluble starch for platinum nanoparticles synthesis. Carbohyd. Res. 357, 90–97. https://doi.org/10.1016/j.carres.2012.04.012.

Tran, T.H., Nguyen, V.T., 2014. Copper oxide nanomaterials prepared by solution methods, some properties, and potential applications: a brief review. Int. Sch. Res. Notices. https://doi.org/10.1155/2014/856592.

Trujillo-Reyes, J., Peralta-Videa, J.R., Gardea-Torresdey, J.L., 2014. Supported and unsupported nanomaterials for water and soil remediation: are they a useful solution for worldwide pollution?. J. Hazard. Mater 280, 487–503. https://doi.org/10.1016/j.jhazmat.2014.08.029.

Upadhyay, L.S.B., Verma, N., 2015. Recent developments and applications in plant-extract mediated synthesis of silver nanoparticles. Anal. Lett. 48 (17), 2676–2692. https://doi.org/10.1080/00032719.2015.1048350.

Vaidehi, D., Bhuvaneshwari, V., Bharathi, D., Sheetal, B.P., 2018. Antibacterial and photocatalytic activity of copper oxide nanoparticles synthesized using Solanum lycopersicum leaf extract. Mater. Res. Express 5, (8). https://doi.org/10.1088/2053-1591/aad426 085403.

Vaseem, M., Umar, A., Kim, S.H., Hahn, Y.B., 2008. Low-temperature synthesis of flower-shaped CuO nanostructures by solution process: formation mechanism and structural properties. J. Phys. Chem. C 112 (15), 5729–5735. https://doi.org/10.1021/jp710358j.

Verma, N., Kumar, N., 2019. Synthesis and biomedical applications of copper oxide nanoparticles: an expanding horizon. ACS Biomater. Sci. Eng. 5 (3), 1170–1188. https://doi.org/10.1021/acsbiomaterials.8b01092.

Vijaya Kumar, R., Elgamiel, R., Diamant, Y., Gedanken, A., Norwig, J., 2001. Sonochemical preparation and characterization of nanocrystalline copper oxide embedded in poly (vinyl alcohol) and its effect on crystal growth of copper oxide. Langmuir 17 (5), 1406–1410. https://doi.org/10.1021/la001331s.

Vomáčka, P., Štengl, V., Henych, J., Kormunda, M., 2016. Shape-controlled synthesis of Sn-doped CuO nanoparticles for catalytic degradation of Rhodamine B. J. Colloid Interf. Sci. 28–38. https://doi.org/10.1016/j.jcis.2016.07.026.

Vu, C.M., Nguyen, V.-H., Thi, H.V., Jin, C.W., Nguyen, D.D., 2020. Hybrid material based on TiO2, CuBTC, and magnetic particles as a novel photocatalyst for MB removal. J. Chem. Technol. Biotechnol. https://doi.org/10.1002/jctb.6450.

Wang, D., Liu, J., Zhang, M., Song, Y., Zhang, Z., Wang, J., 2019. Construction of ternary annular 2 Z-scheme + 1Heterojunction CuO/WO$_3$/CdS/photocatalytic system for methylene blue degradation with simultaneous hydrogen production. Appl. Surf. Sci. 498,. https://doi.org/10.1016/j.apsusc.2019.143843 143843.

Wang, J., Xu, H., Qian, X., Dong, Y., Gao, J., Qian, G., Yao, J., 2015. Direct synthesis of porous nanorod-type graphitic carbon nitride/CuO composite from Cu–melamine supramolecular framework towards enhanced photocatalytic performance. Chem. Asian. J. 6, 1276–1280. https://doi.org/10.1002/asia.201500131.

Wang, Z., Li, F., Wang, H., Wang, A., Wu, S., 2018. An enhanced ultra-fast responding ethanol gas sensor based on Ag functionalized CuO nanoribbons at room-temperature. J. Mater. Sci.: Mater. Electron. 29 (19), 16654–16659. https://doi.org/10.1007/s10854-018-9758-9.

Wu, C., Sun, Y., Cui, Z., Song, F., Wang, J., 2020. Fabrication of CuS/CuO nanowire heterostructures on copper mesh with improved visible light photocatalytic properties. J. Phys. Chem. Solids 109355. https://doi.org/10.1016/j.jpcs.2020.109355.

Wu, D., Zhang, Q., Tao, M. 2006. LSDA+ U study of cupric oxide: Electronic structure and native point defects. Phys. Rev. B. 73(23), 235206. https://doi.org/10.1103/PhysRevB.73.235206.

Xiao, P., Wu, D., Fang, W.H., Cui, G., 2017. Mechanistic insights into the light-driven hydrogen evolution reaction from formic acid mediated by an iridium photocatalyst. J. Catal. Sci. 7 (13), 2763–2771. https://doi.org/10.1039/C7CY00785J.

Xu, K., Wu, J., Tan, C.F., Ho, G.W., Wei, A., Hong, M., 2017. Ag–CuO–ZnO metal–semiconductor multiconcentric nanotubes for achieving superior and perdurable photodegradation. Nanoscale 9 (32), 11574–11583. https://doi.org/10.1039/C7NR03279J.

Xu, Y., Schoonen, M.A., 2000. The absolute energy positions of conduction and valence bands of selected semiconducting minerals. Am. Mineral. 85 (3–4), 543–556. https://doi.org/10.2138/am-2000-0416.

Yang, H., Ouyang, J., Tang, A., Xiao, Y., Li, X., Dong, X., Yu, Y., 2006. Electrochemical synthesis and photocatalytic property of cuprous oxide nanoparticles. Mater. Res. Bull. 41 (7), 1310–1318. https://doi.org/10.1016/j.materresbull.2006.01.004.

Yang, J., Li, Z., Zhao, W., Zhao, C., Wang, Y., Liu, X., 2014. Controllable synthesis of Ag–CuO composite nanosheets with enhanced photocatalytic property. J. Mater. Lett. 120, 16–19. https://doi.org/10.1016/j.matlet.2014.01.026.

Yang, M., He, J., Hu, M., Hu, X., Yan, C., Cheng, Z., 2015. Synthesis of copper oxide nanoparticles and their sensing property to hydrogen cyanide under varied humidity conditions. Sens. Actuators B: Chem. 213, 59–64. https://doi.org/10.1016/j.snb.2015.02.055.

Yang, M., He, J., Hu, X., Yan, C., Cheng, Z., 2011. CuO nanostructures as quartz crystal microbalance sensing layers for detection of trace hydrogen cyanide gas. Environ. Sci. Technol. 45, 6088–6094. https://doi.org/10.1021/es201121w.

Yu, J.C.-C., Nguyen, V.-H., Lasek, J., Li, D.X., Wu, J.C.S., 2016. Competitive reaction pathway for photo and thermal catalytic removal of NO with hydrocarbon in flue gas under elevated temperatures. Catal. Commun. 84, 40–43. https://doi.org/10.1016/j.catcom.2016.05.020.

Yu, J.C.-C., Nguyen, V.-H., Lasek, J., Wu, J.C.S., 2017. Titania nanosheet photocatalysts with dominantly exposed (001) reactive facets for photocatalytic NOx abatement. Appl. Catal. B 219, 391–400. https://doi.org/10.1016/j.apcatb.2017.07.077.

Yu, Z., Moussa, H., Liu, M., Schneider, R., Moliere, M., Liao, H., 2019. Heterostructured metal oxides-ZnO nanorods films prepared by SPPS route for photodegradation applications. J. Surf. Coat., 670–680 https://doi.org/10.1016/j.surfcoat.2019.07.061.

Yuan, G.Q., Jiang, H.F., Lin, C., Liao, S.J., 2007. Shape-and size-controlled electrochemical synthesis of cupric oxide nanocrystals. J. Cryst. Growth 303 (2), 400–406. https://doi.org/10.1016/j.jcrysgro.2006.12.047.

Yugandhar, P., Vasavi, T., Devi, P.U.M., Savithramma, N., 2017. Bioinspired green synthesis of copper oxide nanoparticles from

Syzygium alternifolium (Wt.) Walp: characterization and evaluation of its synergistic antimicrobial and anticancer activity. Appl. Nanosci. 7 (7), 417–427. https://doi.org/10.1007/s13204-017-0584-9.

Zangeneh, H., Farhadian, M., Zinatizadeh, A.A., 2020. N (Urea) and CN (L-Asparagine) doped TiO$_2$-CuO nanocomposites: fabrication, characterization and photodegradation of direct red 16. J. Environ. Chem. Eng. 8 (1), 103–639. https://doi.org/10.1016/j.jece.2019.103639.

Zeng, Q.X., Xu, G.C., Zhang, L., Lin, H., Lv, Y., Jia, D.Z., 2018. Porous CuO nanofibers derived from a Cu-based coordination polymer as a photocatalyst for the degradation of rhodamine B. New J. Chem. 42 (9), 7016–7024. https://doi.org/10.1039/C8NJ00608C.

Zhang, F., Zhu, A., Luo, Y., Tian, Y., Yang, J., Qin, Y., 2010. CuO nanosheets for sensitive and selective determination of H$_2$S with high recovery ability. J. Phys. Chem. C 114 (45), 19214–19219. https://doi.org/10.1021/jp106098z.

Zhang, H., Li, S., Ma, X., Yang, D., 2008. Controllable growth of dendrite-like CuO nanostructures by ethylene glycol assisted hydrothermal process. Mater. Res. 43 (5), 1291–1296. https://doi.org/10.1016/j.materresbull.2007.05.017.

Zhang, H., Wang, X., Chen, C., An, C., Xu, Y., Dong, Y., Yuan, H., 2016. Facile synthesis of diverse transition metal oxide nanoparticles and electrochemical properties. J. Inorg. Chem. Front. 3 (8), 1048–1057. https://doi.org/10.1039/C6QI00096G.

Zhang, L., Fu, X., Meng, S., Jiang, X., Wang, J., Chen, S., 2015. Ultra-low content of Pt modified CdS nanorods: one-pot synthesis and high photocatalytic activity for H$_2$ production under visible light. J. Mat. Chem. A 3 (47), 23732–23742. https://doi.org/10.1039/C5TA07459B.

Zhang, Q., Zhang, K., Xu, D., Yang, G., Huang, H., Nie, F., Yang, S., 2014. CuO nanostructures: synthesis, characterization, growth mechanisms, fundamental properties, and applications. J. Prog. Mater 60, 208–337. https://doi.org/10.1016/j.pmatsci.2013.09.003.

Zhang, Y., Or, S.W., Wang, X., Cui, T., Cui, W., Zhang, Y., Zhang, Z., 2009. Hydrothermal synthesis of three-dimensional hierarchical CuO butterfly-like architectures. Eur. J. Inorg. Chem. 2009 (1), 168–173. https://doi.org/10.1002/ejic.200800911.